EPFL

Thèse n° 10 007

Human-friendly solutions for last centimeter drone delivery

Présentée le 31 janvier 2020

à la Faculté des sciences et techniques de l'ingénieur
Laboratoire de systèmes intelligents
Programme doctoral en robotique, contrôle et systèmes intelligents

pour l'obtention du grade de Docteur ès Sciences

par

Przemyslaw Mariusz KORNATOWSKI

Acceptée sur proposition du jury

Prof. A. Ijspeert, président du jury
Prof. D. Floreano, directeur de thèse
Prof. A. Ollero, rapporteur
Prof. L. Gambardella, rapporteur
Prof. P. Reis, rapporteur

École polytechnique fédérale de Lausanne

2020

I believe that air delivery of items from person-to-person
will be as easy as sending messages by WhatsApp
– D.F.

To my family…

Acknowledgements

The achievement of this thesis would not have been possible without the help and contributions of a significant number of people around me.

First and foremost, I want to thank my supervisor Dario for guiding me in my transition from an engineer to a scientist. Dario introduced me to his idea of using foldable drones for easier storage and transportation. He provided me with an active and motivating environment in which I could explore different directions of development. The amazing infrastructure and equipment in the lab allowed me to easily and quickly design, build and test different types of drones. Dario gave me a lot of freedom in my project and provided many chances to take part in various events where I could present my work. I enjoyed all the years that I spent in his lab.

I would like to thank the members of my jury: Prof. A. Ijspeert, Prof. D. Floreano, Prof. A. Ollero, Prof. L. Gambardella and Prof. P. Reis, who took the time to read my thesis and travel to Lausanne for my thesis defense.

I also thank the Swiss National Science Foundation through the National Centre of Competence in Research Robotics, whose funding made this research possible.

I would like to thank the post-docs in the lab and friends: Stefano Mintchev, Mir Feroskhan, William Stewert and Fabrizio Schiano, who helped me during my Ph.D. I would like to thank them for the time spent together brainstorming on different topics and facing various problems. I would like to express gratitude for their patience in revising my scientific documents. Finally, I would like to thank them for their motivation and support. It has been a great pleasure to work with them the whole time.

I would like to express my gratitude to Anand Bhaskaran, Greg Heitz and Hauke Maack who helped to organize and perform flight tests on the EPFL campus: helping with administrative procedures, supervising flights as observers and safety pilots, building new drones and constantly debugging the code of the software. Without their help, these tests would not have been possible. I would like to express particular thanks to Anand who developed the code of the Web Application. Anand worked with me for the last three years, starting as my Master's student and continuing as an intern and an engineer. During this time, he was able to find quick solutions in cases of urgent fixes. In addition, I would like to thank him for his graphic skills that allowed us to create many promotional materials and finally, for proposing the name of the project, *Dronistics* and the software, *SimplyFly*.

Over the years of this project, I had the pleasure of supervising and working with many interns, engineers and students doing semester and Master's projects. Much of their work contributed directly or indirectly to this thesis: Cameron Dowd, Guillermo Legarda Herranz, Nicolas Feppon Georg, Alfredo Retamal.

I would also like to thank various people in different departments of the EPFL and in Switzerland whom I worked with closely during my Ph.D. I thank Mauro Lattuada and Isabel Casado (TTO), Marc Gruber (Vice-Presidency for Innovation) and Olivier Kuttel (Head of International affairs), Frederic Steinbruchel and Maureen Décosterd (Mediacom), Nicolas Bideau and Anita Clerc (Presence Switzerland), Roland Dupuis (AFA workshop), Mayra Lirot and Jan Kerschgens (NCCR Robotics), Bettina Buechel and Jim Pulcrano (IMD). Special thanks to Michelle Waelti, who could always find a solution served with advice.

I would like to thank the organization WeRobotics and the Dominican Republic flying labs, especially Patrick and Orland, for organizing the mission in the Dominica Republic. Flight tests in a real-life environment to validate proof of the concept of medical delivery was a fantastic experience and taught me how challenging a remote and rural environment can be.

I would like to express big gratitude to all of my colleagues and friends at the LIS that I met over all the years and with whom I spent time outside of the lab, doing all sorts of other activities.

Beyond the lab, a fantastic group of friends with whom I did many activities, such as skiing, sailing or exploring Switzerland and Europe together supported me. Their presence helped me to get a little break from work. They believed that I would finish this thesis. Thus, I would like to thank Maja, Szymon, Agni, Maciek, Mariusz, Paweł, Konrad, Olga and Michał, Jagoda and Michał, Agnieszka and Rafał. My special thanks go to Sebastian, Aleksandra and Piotr, who supported me all this time.

Then, last but not least, I would like to thank my family, who supported me through the good and bad times of the entire Ph.D. and always believed in me: my parents Elżbieta and Antoni, and my siblings Aleksandra and Krzysztof with their families.

Lausanne, 3rd November 2019 Przemyslaw M. Kornatowski

Abstract

The popularity of delivery drones is constantly increasing due to their ability to deliver packages more rapidly and economically than current transportation methods. Consequently, drones have been employed by logistics companies for delivering payloads to hard-to-reach places and for daily door-to-door deliveries. However, logistic companies focus mainly on large platforms for long-range (<150km) and last-mile delivery (<20km), not designed to deliver directly to individual consumers. The drones suffer four major limitations: limited safety, difficulty for storage and poor portability, poor adaptability to different sized parcels and lack of user-friendliness.

Safety limitations arise from the unshielded spinning propellers. Drone operators have to utilize secure take-off and landing locations, away from people e.g. on runways, rooftops and fenced-off areas. Unshielded propellers and large-sized platforms limit the drone's capability to deliver parcels in crowded urban environments. Moreover, landing in remote locations is challenging due to dense vegetation or inclined surfaces such as mountains. A common solution to shield propellers is to adopt a protective cage to enclose the drone. However, this approach generates a large amount of drag on the drone that reduces its aerodynamic efficiency. Presently, storage and transportation of drones to the deployment area are inconvenient, especially for large flying platforms needed for the delivery of large or heavy parcels. Similarly, the use of large platforms and their software is limited to trained operators. Finally, sizes of delivered parcels vary significantly and the adaptability of current drones is limited; most drones can only deliver parcels of a predefined size.

This thesis focuses on the design process of parcel delivery solutions that addresses the above-mentioned limitations for person-to-person and short-range delivery services. These solutions are integrated into a single aerial delivery system known as Dronistics ("Drone" and "logistics"). This new system consists of the hardware component, which includes two drones code-named *PackDrone* and *GearQuad*, and the software component called *SimplyFly*.

The integrated parcel delivery solution comprises the following features:

- Transportation of parcels of variable sizes
- Enhanced safety for people, the drone and the transported items
- Easier storage and transportation of the drone
- Usability of the delivery drone - software interface for inexperienced users
- An energy-efficient system

Transporting parcels of variable size was realized using a new design approach of placing the parcel above the propellers in both drone platforms. This allows transportation of super-sized parcels larger than the drone while maintaining the vehicle's small footprint. Moreover, *PackDrone* addresses the safety, storage and transportation concerns by integrating a quadcopter

within an origami-inspired foldable cage. The cage separates the propellers from the external environment, which includes people, obstacles and the parcel as well. For easier storage and transportation, *PackDrone* folds in a single hand movement, reducing storage volume by 92%. *GearQuad* on the other hand, overcomes the above limitations and improves safety and aerodynamic efficiency. The very dense cage of *GearQuad* allows it to fly near children and land in the hands of the consumer (last-centimeter delivery) or in hard-to-land environments. Its morphing arm mechanism ensures high aerodynamic efficiency by deploying the propellers outside the cage during flight. *SimplyFly* was designed with an easy-to-use and intuitive user-interface, regardless of the user's experience and is compatible with other drone designs. Overall, the system demonstrates very high versatility and usability compared to actual delivery drones in several proof-of-concept test flights and public demonstrations.

Keywords

Flying robots; Intelligent Transportation Systems; Unmanned Aerial Vehicles; Foldable structures; Human-robot interaction; Last-mile delivery; Last-cm delivery; Efficiency; Variable-sized parcels.

Résumé

La popularité des drones de livraison ne cesse d'augmenter en raison de leur capacité à livrer des colis de façon plus rapide et économique que les méthodes actuelles. En conséquence, certaines entreprises de logistique utilisent déjà des drones pour acheminer des objets dans les endroits difficiles d'accès et pour des livraisons porte-à-porte quotidiennes. Ces entreprises s'intéressent principalement aux appareils de livraison pour les longue distance (<150 km) et pour les derniers kilomètres (<20 km). Néanmoins, ces plate-forme ne sont pas conçues pour faire des livraisons au contact direct des clients. En effet, elles souffrent de quatre limitations majeures: une faible adaptabilité à des colis de tailles différentes, un manque de sécurité, un stockage avec une transportabilité difficile, et un manque de convivialité.

Le manque de sécurité est principalement dû aux hélices des drones qui ne sont pas protégées. De ce fait, les opérateurs de drones doivent utiliser des lieux de décollage et d'atterrissage sécurisés et éloignés de la population comme des pistes d'atterrissage officielles, des grands toits ou des zones clôturées. Les hélices non protégées et les grands appareils limitent ainsi la capacité du drone à livrer des colis dans des environnements urbains densément peuplés. De plus, leur atterrissage dans des endroits reculés est complexe en raison d'une végétation dense ou de terrains inclinées comme en montagnes. Une solution courante pour protéger les hélices consiste à ajouter une cage de protection entourant le drone. Cependant, cette approche génère une traînée importante sur le drone réduisant de fait son efficacité aérodynamique. À l'heure actuelle, le stockage et le déplacement des drones vers la zone de déploiement sont peu pratiques, en particulier pour les grandes plates-formes utilisées pour livrer des colis lourds et volumineux. De même, l'emploi de ces grandes plates-formes et de leurs logiciels est limité à des opérateurs qualifiés. Enfin, la taille des colis livrés varie considérablement et l'adaptabilité des drones actuels est limitée car la plupart ne peuvent livrer que des colis d'une taille prédéfinie.

Cette thèse se concentre sur le processus de conception de solutions de livraison de colis qui aborde les limitations susmentionnées pour les services de livraison de personne à personne et sur des courtes distances. Ces solutions sont intégrées dans un système de livraison aérien unique appelé *Dronistics* («Drone» et «logistics»). Ce nouveau système est composé de deux drones nommés *PackDrone* et *GearQuad* et d'un logiciel appelé *SimplyFly*.

Le système comprend les fonctionnalités suivantes:
• Transport de colis de tailles variables
• Sécurité accrue pour les utilisateurs, le drone et les objets transportés
• Facilité de stockage et de transport du drone
• Facilité d'utilisation du drone de livraison - interface logicielle pour les utilisateurs inexpérimentés
• Un système économe en énergie

Le transport de colis de taille variable a été réalisé en utilisant une nouvelle façon de positionner le colis - au-dessus des hélices. Cela permet de transporter des colis de très grande taille, y compris ceux étant plus gros que le drone, tout en maintenant le faible encombrement du véhicule. De plus, *PackDrone* résout les problèmes de sécurité, de stockage et de transport en intégrant un quadricoptère dans une cage pliable inspirée de l'origami. La cage sépare les hélices de l'environnement extérieur, des gens, des obstacles mais aussi du colis. Pour faciliter le stockage et le transport, *PackDrone* se plie en utilisant une seule main, réduisant ainsi le volume de stockage de 92%. *GearQuad* quant à lui, surmonte les limitations mentionnées ci-dessus et améliore la sécurité et l'efficacité aérodynamique. Sa cage très dense permet de voler à proximité d'enfants et d'atterrir directement dans les mains de l'utilisateur ou dans des environnements difficiles. Les bras mobiles du quadricoptère garantissent une efficacité aérodynamique élevée lorsqu'ils sont déployés à l'extérieur de la cage. De plus, le logiciel a été conçu pour une utilisation facile et est compatible avec d'autres modèles de drones. Globalement, le système fait preuve d'une très grande polyvalence et d'une grande facilité d'utilisation par rapport aux drones actuels, ce qui a été démontré lors de multiples vols d'essais et démonstrations publiques.

Mots-clés:

Robots volants; Systèmes de transport intelligents; Véhicules aériens sans pilote; Structures pliables; Interaction homme-robot; Livraison du dernier-kilomètre; Livraison du dernier-centimètre; Efficacité; Colis de taille variable.

Contents

List of Figures

List of Tables

Chapter 1 **Introduction**

DELIVERY drones can transport objects fast and efficiently. They can even deliver to places previously considered too hard to reach. However, unshielded propellers pose a serious threat, especially to inexperienced users. Additionally, the large size of current delivery platforms limits their capability to be stored or easily transported. Software to control and navigate drones is designed mainly for trained operators. As a result, drone usage has not been extended to the layperson. In this chapter, an analysis of drones currently used for delivery is presented, followed by a state-of-the-art review of existing protective structures for propellers, current foldable designs for vehicles and available software to program drones for autonomous flight. Finally, the main contributions of this thesis are described.

1.1 Motivation and Challenges

Drones are able to fly rapidly from one point to another. They can traverse densely populated environments and reach remote locations with limited road infrastructures. For these reasons and due to their low cost of manufacture and operation [1], drones are effective solutions for cargo transportation and delivery [4]. Last mile delivery is the most challenging part of the logistic chain and is also the most expensive (more than 53%)[7]. That is why major companies have developed various flying platforms (Section 1.2.1). However, they are affected by issues that limit their full exploitation, which includes delivering parcels directly to people.

For example, safety of people is compromised due to the unshielded spinning propellers that can cause severe injuries when flying close to people [9]. In addition, the malfunction of the propulsion mechanism due to battery or motor failure can cause the drone to crash. The cargo has no protection in the event of a crash, which hampers the transportation of fragile packages [10]. One of the most common solutions to protect people against the rotating propellers is the use of a protective cage. The cage separates people and obstacles from the propellers and protects the payload, which is placed inside the cage, during a crash. However, this approach does not provide sufficient protection or efficiency; dense cages reduce aerodynamic efficiency while less dense structures do not provide enough protection. Drone storage and transportation to deployment locations are often difficult, particularly in the case of bulky flying platforms for delivering large and heavy cargos [10]. The transportability issue is even more problematic for operators who need to deploy several drones at the same time. Furthermore, the adaptability of current platforms to transport different sized cargos is poor. Currently, available platforms carry packages of predefined sizes with logistic companies delivering boxes of 2kg weight on average [12]. However, package dimensions can vary enormously [14]. Adopting a fleet of heterogeneous drones to deliver parcels of various sizes is inefficient; small drones cannot be used for heavy parcels while large drones are oversized and require high costs for delivering small packages. Therefore, presently, logistic companies need cargo-specific drones, which are expensive and time-consuming to operate. In addition, the software used to control and navigate large delivery drones with unsecured dangerous propellers are designed for trained operators and are not appropriate for laypeople, preventing the possibility of person-to-person drone delivery.

These limitations show that the drones used by logistics companies are catered for last mile-delivery (<20km) from secured places-to-places (e.g. between warehouses, hospitals, businesses), rather than person-to-person. To the best of the author's knowledge, a drone delivery system that can be used safely and easily by laypeople to deliver objects over short distances has never been developed.

The purpose of this work is to establish a safe, fully integrated system for delivery of variable sized parcels with valuable loads directly from person-to-person over short distances (<5km). The author of the thesis has defined a 5 km distance limit for last-centimeter (cm) delivery. The 'last-centimeter' description was selected to distinguish between the large, heavy platforms and the smaller drones used specifically for lightweight payloads and shorter ranges. The 'last-centimeter' description also explains the requirement of high-precision delivery needed for congested environments. This thesis presents the design process of developing a last-cm drone delivery system for inexperienced users, in which the transportation and delivery of goods are needed (e.g. door-to-door delivery, search and rescue operations, delivery to remote areas, etc.). The final system

should be safe for people, robots and cargos. It should be convenient to store, transport and utilize while still enabling the delivery of payloads of various sizes. Thus, the drone delivery system solves the above-mentioned limitations and problems.

The safety concerns of the delivery drone will be addressed by an innovative platform design, which includes protective structures integrated into the drone's frame (e.g. a surrounding cage that can be opened for cargo loading and unloading and secured during flight) to insulate the cargo and the motors from the environment. The ease-of-storage and transportation limitation will be addressed by developing a foldable structure: a foldable frame and cage that undergoes remarkable volume reduction when folded. Concerns about the malfunctioning of the propulsion system will be addressed using multiple redundant batteries and motors. The demands of competing requirements, safety versus efficiency, will be solved by designing a dense cage and a morphing quadcopter structure. The drone's versatility and usability will be enhanced by placing the parcel carrying above the propellers that will allow carrying different sized parcels, including supersized parcels, clearly bigger than the drone's footprint. Finally, an easy-to-use software for navigation will be developed as a WebApplication that can be used on any operating systems and any portable devices, without the need of installing the software on the device. An intuitive, user-friendly Graphic User Interface and photo tutorials will allow inexperienced users not familiar with drone technology to operate the system comfortably, sending parcels between people rather than places.

The highlights of such a next generation drone system include its usage in multiple application scenarios. During search and rescue operations, rescuers in the field could easily transport a foldable drone. Moreover, if an uneven terrain or the lack of landing space hampers the landing of big drones, our small-sized drones can resolve these issues, as they require a very small landing area and can land via grasping of the shielded drone by the consumer for safe landing. During delivery in public premises, the shielding cage will protect inexperienced users from injury when close to the drone or when loading it. The drone's foldability would reduce the platform volumes, resulting in significantly reduced space and storage costs for logistics companies (especially in the case of multiple platforms). In addition, the capacity to deliver super-sized parcels would allow companies to use a single drone size (based only on package weight).

1.2 State of the Art

The state of the art is presented relative to flying platforms used for transportation (Section 1.2.1), safety mechanisms for drones (Section 1.2.2), foldable structures and drones (section s 1.2.3), and existing software to control and navigate drones (Section 1.2.4). This is followed by (Section 1.3) the main contributions and the thesis organization.

1.2.1 Existing drone delivery solutions

Current drones used for cargo delivery can be classified into three main categories: fixed-wing (Fig. 1.1E), rotary (Fig. 1.1A, C, D, G, H, J) and hybrid aircrafts (Fig. 1.1B, F, I).

The fixed-wing drones can efficiently and quickly transport large payloads over long distances (e.g. 10 kg payload for 50 km range in [15]), but they require special infrastructure to take-off and land such as long runways, inflatable mattresses to land [16] or catapults to take-off. Rotary drones have complementary features with respect to fixed-wing drones. They can take-off and land vertically and are very maneuverable at the expense of payload, efficiency and velocity.

Because of this, they are the ideal choice to deliver parcels precisely in cluttered environments within a small range (e.g. 1 kg payload for 20 km in [17]). A subset of rotorcrafts are multi-rotors, which are the most used solution by companies interested in transporting parcels to cities. Hybrid aircrafts combine the advantages of both fixed-wing and rotary platforms. On the other hand, they require complex design [11] and control algorithms; therefore, they are more expensive and prone to failure. This thesis will focus on multi-rotors as the best choice for cluttered environments.

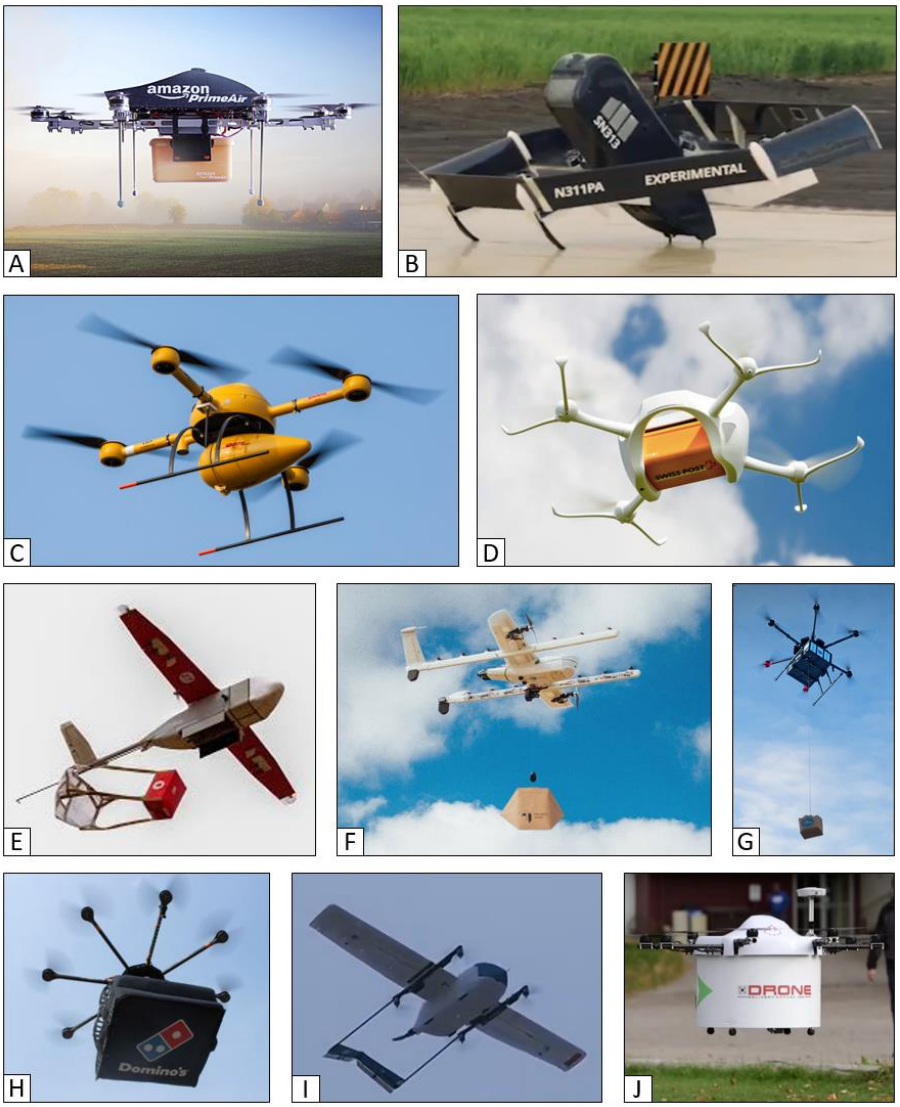

Figure 1.1 Rotary drones tested to deliver packages by logistic companies. (A-B) Amazon [17]. (C) DHL [20]. (D) Matternet [18], (E) ZipLine [16], (F) Google Project Wing [21], (G) FlyTrex [22] , (H) Domino's Pizza [23], (I) RigiTech [24], (J) Delivery Canada Drones[25].

1.2.2 **Safety**

Dangerous propellers - caged drones. The majority of commercially available flying platforms provide only limited protection. As illustrated in Fig. 1.2, the most popular approach is to add lightweight hulls or small plastic elements around the propellers [40-41]. This solution only protects the propellers from side collisions while it is ineffective in protecting the user from the spinning propellers.

Figure 1.2 Quadcopters with protection around propellers. (A) EPP hull around propellers of AR.Drone 2.0 [26]. (B) Lightweight plastic propellers' guards fixed to motors of Phantom 3 [27].

A safer approach is to enclose the entire drone in a cage. In fact, protective cages are well suited for avoiding harmful injuries to users and absorbing collisions from relatively low falls. An example is given by the rotorcraft *AirBurr* [28], which is protected by tetrahedral structures distributed in multiple directions (Fig. 1.3A). Each structure is composed of pultruded carbon rods that act as Euler springs to absorb energy during collisions [28]. This solution allows the robot to survive falls from up to one meter high and collisions with obstacles during flight. *HyTAQ* [28] is equipped with a rotating cage that allows the robot to roll on the ground in order to save energy (Fig. 1.3B).

None of these platforms are directly suited for cargo transportation due to the limited space inside the cage. The *GimBall* [30] has a rigid spherical cage decoupled by a gimbal system from the inner frame, which consists of a control unit and a propulsion unit (Fig. 1.3C). In cases of collision, the cage rotates as a reaction to contact but the inner frame remains stable, thus preventing falls. The *GimBall* is suited for reconnaissance and inspection of cluttered environments, but its use in cargo delivery would not be possible because any additional payload could change the center of mass of the robot and affect its capability to exploit gyroscopic effects for stabilization.

The successor of the *GimBall* drone, *Elios 2* from the company *Flyability* has a surrounding protective cage also but rigidly fixed to the propulsion system. Complex algorithms and the ability to change rapidly the direction of rotation of the propellers enables stability on collision with obstacles. Unfortunately, added payload would change the position of the CG of the drone that would change the stabilizing capability of the algorithms. Another caged drone proposed by [31] shields each propeller individually. The cages around the propellers can rotate freely during contact with obstacles. However, the overall added weight of the added mechanisms required to rotate each cage decreases the payload capacity for delivery. On the market, numerous platforms are available, equipped with different protective structures but these platforms are not optimized for cargo delivery and due to the fixed structure of the cage, it is difficult to load the payload.

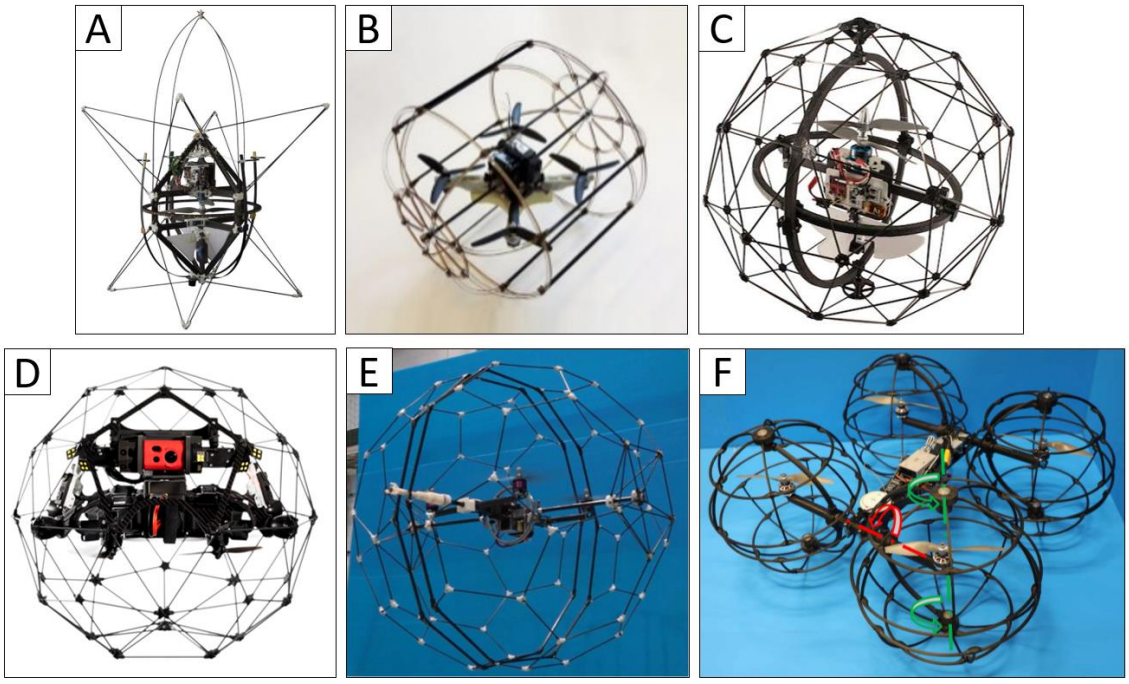

Figure 1.3 Robots with different protective structures surrounding the platform on each side. (A) The AirBurr robot equipped with a protective star-shaped cage and active legs that allow turning the platform upright for take-off after a collision [28]. (B) HyTAQ robot with cylindrical cage with one degree of freedom, which rotates around itself to become upright. The small quadcopter can roll on the ground [29]. (C) GimBall robot with a spherical protective cage decoupled from the inner frame by a three degree of freedom gimbal system. This system stays in the air after collision [30]. (D) Elios 2 - successor of the GimBall drone [32]. (E) A drone with two passive rotating hemispherical shells for physical interaction in cluttered environments [33]. (F) A drone with passive rotating shells on each rotor [31].

Partial malfunction of the propulsion system – control algorithms. For protection of the drone against high falls (e.g. more than 2 m), different protection mechanisms have been implemented. For example, helicopters use a safety procedure called 'autorotation' in case of malfunction of the engine [34]. In this procedure, the main rotor system is rotated by the action of air moving up through the rotor. In order to reduce the falling speed and safely land, the pitch angle of the rotor blades is steered by the control mechanism of the rotorcraft. This procedure requires an additional embedded system, which decouples the main rotor from the engine and allows the free rotation of the rotor. Furthermore, the main rotor has to be already rotating when the procedure starts. These additional requirements make this solution complex and hard to implement in other types of platforms.

Another solution to protect the drone in cases of malfunction of the propulsion system at high altitudes was proposed by Mueller at al. [36]. They presented a solution for a quadcopter to maintain a constant altitude despite having lost a single, two opposing or three propellers. The control strategy consists of the quadcopter spinning about the axis fixed with respect to the vehicle's body. Tilting this axis and changing thrust, the position of the robot can be controlled. However, this platform was not tested with cargo on board, which could modify the expected spinning behavior.

Full malfunction of the propulsion system – parachute. Both of the aforementioned solutions require a still-functioning control system for their operation. In cases of total failure of the system (control and propulsion unit), only an independent mechanism such as a parachute [37] can guarantee safety. Parachutes are cheap, lightweight, passive devices used to decrease the falling speed of different objects (from human bodies to packages). If used as a safety system in flying platforms, the parachute would have the following drawbacks: it would need time to deploy and it could tangle around protruding elements (e.g. propellers).

1.2.3 Storage and transportation – foldable drones

Foldable systems are load-bearing structures that can be reversibly folded in order to reduce their overall size or adapt their shape for different functions [38]. Size reduction has been exploited to facilitate transportation in multiple fields, for instance aerospace equipment [40], civil structures [41] and commercial products [42]. Shape adaptation has been used for the functionalization of roofs of domes and stadiums according to weather conditions [43].

Foldable structures can be classified based on their morphology [45]. This classification includes tensioned membranes [39][46] strut-cable systems [40][44][48], lattice [38] [42] [44] and continuous structures [42] [49]. The tensioned membranes use fabric as the main body component. Thanks to the intrinsic fabric compliance and simple mechanical design, they can be easily stowed, but their potential application in aerial vehicles is not appropriate because these kinds of continuous membranes would affect the airflow. The strut-cable systems use a combination of struts and cables that makes them very lightweight. However, they are complex to manufacture and cables may tangle around the protruding elements of the aircraft (e.g. propellers). Folded plate structures, similar to tensioned membranes, are not suited because they too could affect the airflow from the propellers. From the air vehicle prospective, lattice structures are the most promising group. Their body is mainly composed of struts that would minimally affect the airflow from the propellers. Their main drawback would be the need of multiple joints that induce complexity and fragility.

There are several foldable hovering platforms available on the market (Fig. 1.4) [27][51] . Most of them rely on a very basic design with foldable arms mounted on cylindrical hinges (i.e. lattice foldable structures, according to the above-mentioned classification) [29]. Mintchev et al. [52] (Fig. 1.4F-H) developed another example of a foldable flying robot. Each of these drones use different techniques to fold their arms. However, none of them is integrated with protective structures nor capable of withstanding collisions.

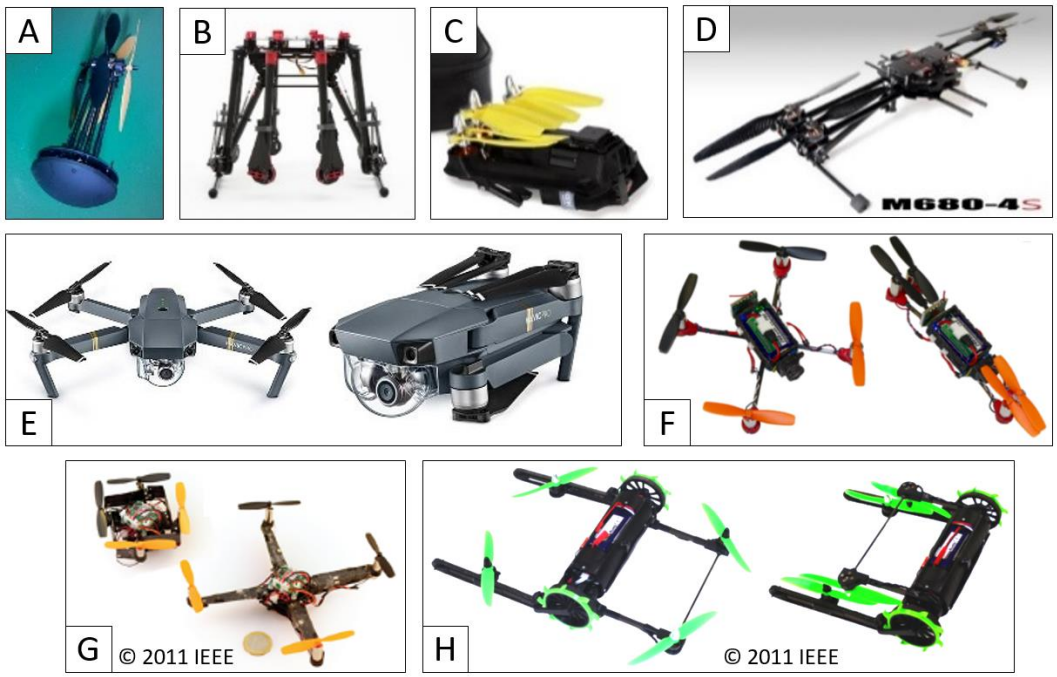

Figure 1.4 Multicopters with different possibilities to fold the arms of the platform. (A) Umbrella type of folding. (B, C, H) Arms folded to the side of the body [27] [51] [53] . (D, F) Arms folded on two sides of the body [53]. (E, G) Arms folded around the body [27][54].

1.2.4 Software to control and navigate delivery drones

Software used by drone delivery companies has been developed for operation by trained users. To the author's knowledge, there is no commercially available software to control and navigate delivery drones available for easy use by inexperienced users and compatible with different platforms. Commercially available drones are currently equipped with software that allows users to define waypoints that the drone follows to reach a destination point. This software is not meant for delivery between people or even fleets of drones.

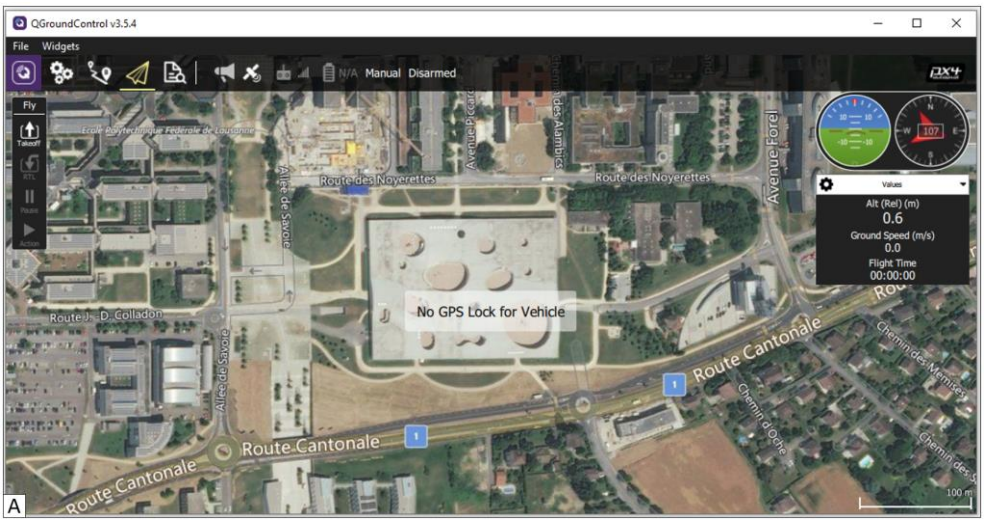

Figure 1.5 QGroundControl - ground stations to configure settings of drones.

Available open source software for controlling and navigating drones such as QGroundControl (Fig. 1.5) [55] or MissionPlanner (Fig. 1.6) [56], provide a large variety of options but with a steep learning curve for inexperienced users, preventing them from easily using them to send a drone to another person and the flight is defined only by the waypoints.

Figure 1.6 Mission Planner - ground stations to configure settings of drones.

1.3 Main Contributions and Thesis Organization

The primary novelty of this thesis is to present a drone delivery platform that integrates all the proposed approaches to the current limitations into a single delivery solution, known as *Dronistics*, that enables person-to-person, last-cm parcel delivery. The design process behind the system's hardware and software combines mechanical design, electronics, Internet of Things (IoT), control theory, aerodynamics and human-drone interactions. All the planned solutions were developed into real prototypes. The prototypes were then tested in many different demonstrations of autonomous flight in order to validate the specific operations of the system.

The thesis is organized around the main challenges it addresses: transportation of parcels of various sizes, safety of people, drones and their transported items, storage and transportation of drones, ease of use of developed drones including convenient software for inexperienced users and system efficiency.

Safety is one of the main challenges in this work. Consequently, several solutions addressing the safety of people, drones and transported parcels are presented throughout most of the chapters.

Chapter 1 above presented the motivation of the thesis and the major challenges faced from the review of the literature.

Chapter 2 presents a new counter-intuitive proposition to place the parcel for transport above the plane of the propellers. This original approach allows delivering parcels of various sizes, including super-sized parcels that are bigger than the multicopter itself.

Chapter 3 presents a new design of a multicopter, integrated into a foldable cage. The cage provides safety for people, the drone and the contained cargo. The foldable design allows reducing

the drone's storage volume by 92%. This enables the folded drone to be stored easily in a drawer, on a shelf, in an office or even transported in a backpack to the deployment location.

Chapter 4 presents the architecture and graphic user interface of the software designed to control and navigate autonomous delivery drones. The software was designed to provide a user-friendly interface for posting parcels from person-to-person using a delivery drone. The author also presents the corresponding flight tests, proof of concepts and future applications of the system. In addition, the chapter includes results of a human-drone interaction study and precision performance of the platform's flight, take-off and landing.

Chapter 5 presents the innovative concept of a morphing drone with a very dense cage that prevents even small children's fingers from accessing the propellers. To recover the aerodynamic efficiency lost through using the dense cage, the arms of the drone can be deployed to extend out of the cage through doors located on the sides of the cage. This is carried out when the drone is in flight, well away from people. During take-off and landing, the propellers are then retracted into the cage and secured, which subsequently enables the vehicle to land in the recipient's hands directly or in an environment that does not have to be a secured, designated landing zone.

Finally, Chapter 6 concludes the thesis. The applications are discussed including the advantages of this work and future research directions.

The appendices present additional calculations, ongoing improvement to the work presented in the chapters and work started during this thesis but not sufficiently final to be included in the main chapters.

Appendix A presents improvement to the cage stiffness of *PackDrone*.

Appendix B presents a new design to enhance the endurance or increase the payload of *PackDrone* while keeping the overall small footprint of the cage. The problem of partial malfunction of the propulsion system was solved by integrating multiple motors, propellers and batteries into the cage. Moreover, the proposed configuration could not reduce the aerodynamic efficiency, which is ongoing work.

Appendix C presents the evolution of the *PackDrone* platform throughout the Ph.D. It discusses goals and limitations of each version alongside the specifications.

Chapter 2 **Transportation of variable-size parcels**

THE conventional approach to parcel placement in most of today's delivery drone designs is to place the parcel centrally beneath the drone's rotor plane. However, if the parcel is too large, this will result in obstruction to the propeller slipstream, incurring significant drag. As such, the parcel's location below the rotor plane limits the size of parcels that can be delivered, specifically super-sized parcels that protrude beyond the bounds of the four rotors. Delivering large parcels therefore requires bigger drone platforms, which consequently consume more energy, necessitate large storage spaces and are less portable. In this work, we propose an alternative design strategy of placing the parcel above the rotor's plane. However, placing a parcel above a quadcopter encounters two main challenges. The first is the optimal position of the CG to maintain stability of the drone. Second is the aerodynamic influence on the lift of the drone with a parcel above the propellers. To address these challenges, aerodynamic characterization experiments were performed and a new drone design proposed. This chapter presents a prototype quadcopter-design solution that places the parcel above the propellers to enable delivery of super-sized parcels, as well as a compact rotor design configuration for lower storage cost and increased portability. The new approach of placing an over-sized parcel above the propellers provides an 82% increase in thrust over putting the parcel below the propellers.

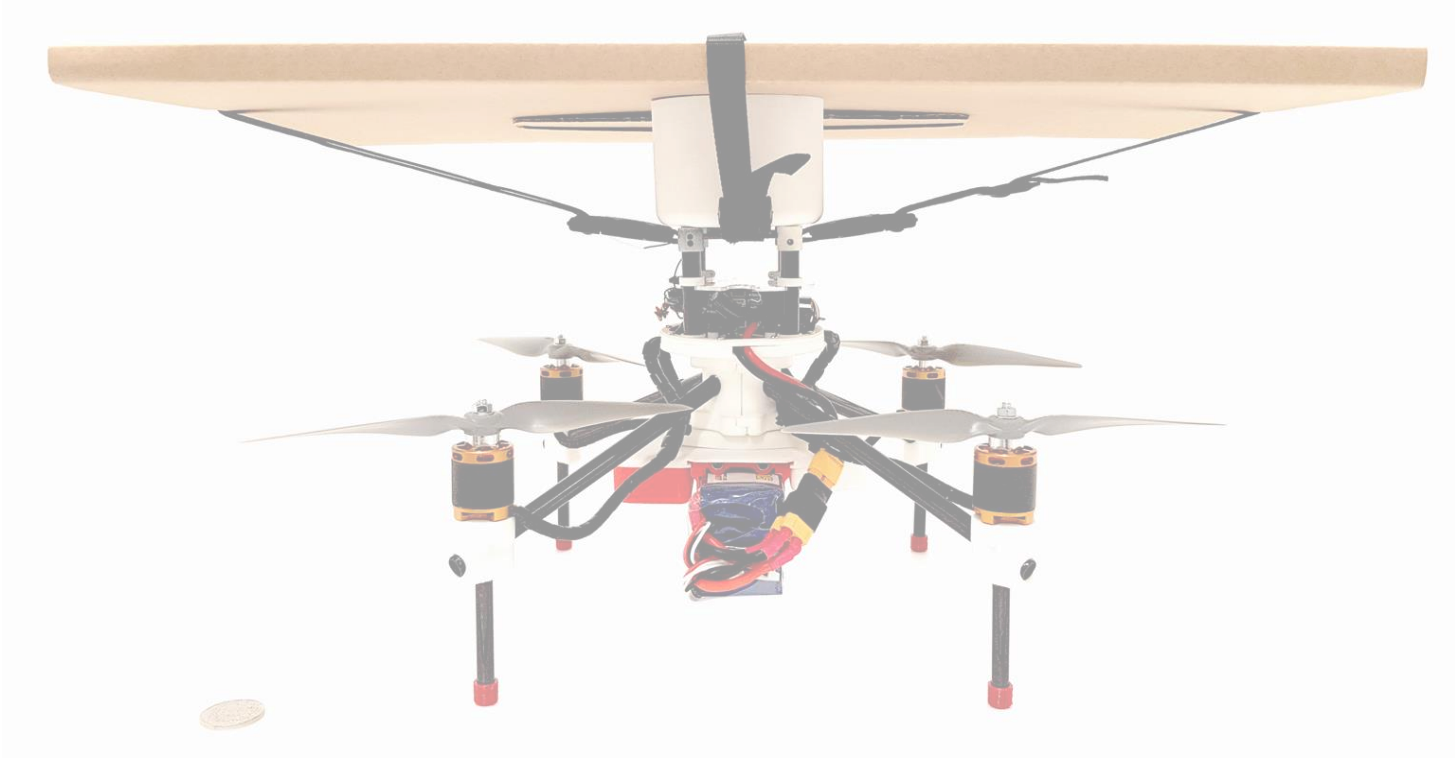

The material presented in this chapter is adapted from:

[57] **P. M. Kornatowski,** M. Feroskhan, W. J. Stewart, and D. Floreano, "Downside Up: Rethinking parcel position for aerial delivery," *Robotics and Automation Letters* in review (2019).

The work presented in this chapter was submitted for patenting:

[58] **P. M. Kornatowski**, Mir Feroskhan, and D. Floreano. "Downside Up: Rethinking parcel position for aerial delivery*,"* patent pending, 2019.

2.1 Introduction

Drones are increasingly becoming a useful tool adopted by logistics companies as a delivery solution that is economical, environmentally friendly and efficient [1]. Threats to urban sustainability such as traffic congestion, living-space constraints and air pollution further propel the need to re-examine conventional dispatch services amidst the growing expectations of e-commerce patrons [6]. Several notable logistics companies have already begun drone deliveries of commercial goods such as Amazon.com, Alibaba, Dominos and DHL. Most of these deliveries tend to employ bulky drone platforms designed for long-range dispatch and require designated take-off and landing spaces. Additionally, the delivery drones used by logistics companies have limited capabilities to deliver parcels of different sizes. Specifically, they are unable to deliver super-sized parcels (parcels larger than the drone itself) due to parcel position beneath the propeller plane. Placing any object in the slipstream directly under the propellers of the drone generates significant drag that reduces the lifting capability of the drone. Thus, the standard practice of delivery drones is to place a parcel between and beneath the rotor plane to ensure the slipstream is unblocked. However, this approach limits the dimensions of parcels that can be delivered. To deliver larger parcels, logistics companies require larger vehicles, regardless of parcel weight, which is expensive and inefficient. Large drones incur a high operational cost as their airframes are heavier and generate more drag, which significantly reduces the drone's endurance and payload capabilities. Additional major drawbacks include occupying large storage spaces, reduced portability, reduced functionality in cluttered environments, and the need for designated take-off and landing spaces. A portable, small-sized drone capable of carrying packages larger than its propeller footprint would reduce the need for larger drones.

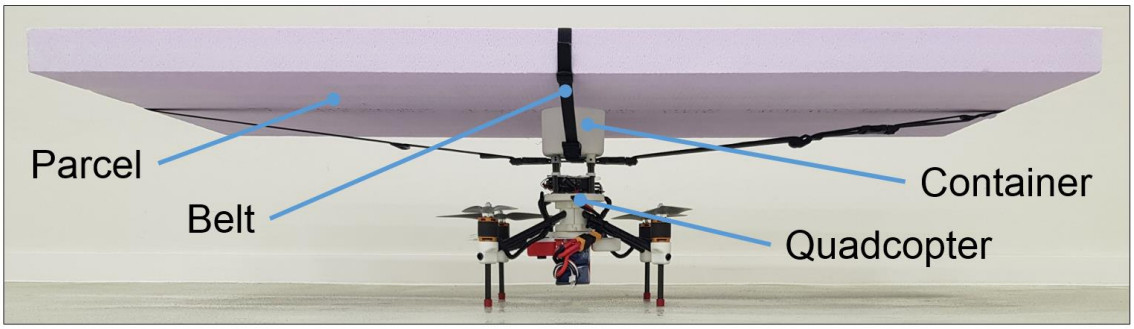

Figure 2.1 Quadcopter with a small footprint to deliver parcels of varying sizes. The parcel, a Styrofoam block (100 x 50 x 5.5 cm), is placed 15 cm above the propeller plane and is secured to the platform using polyester belts.

A possible approach to delivering super-sized parcels is to use drones with adaptive morphology [59]. The foldable scissor-like mechanisms presented in [60], which varies the size of the quadcopter, could be used for accommodating different parcel sizes. However, using adaptive morphology will still not completely remove the restriction on the maximum parcel size. Another approach is to suspend the parcel from the drone with a very long cable [62], which would not interfere with the propeller slipstream because the parcel is far from the downwash of the propellers. However, this approach has two drawbacks: the first is that the cable may become entangled with obstacles, which would prevent the drone from operating in cluttered environments; the second is that the swinging motion of the parcel induced by wind gusts or abrupt maneuvers could destabilize the vehicle and lead to energetically expensive flight adjustments or even a crash.

Furthermore, the complexity in the control algorithms to prevent cargo swinging [64] make cable-suspended load delivery difficult.

We present a novel approach to delivering super-sized parcels, where the parcel is positioned above and within proximity of the propellers (Fig. 2.1). The approach capitalizes on the different airflow dynamics below (Fig. 2.2A) and above (Fig. 2.2B) the propellers, which eliminates slip-stream drag (Fig. 2.2A and 2.2B). However, placing a parcel above a quadcopter encounters two main challenges. The first is CG placement. The CG should be located as close as possible to the propeller plane to reduce control effort of the drone. This is true whether there is a parcel on-board or not and regardless of parcel weight. The vehicle design needs to cover this wide range of mass distributions. The second challenge is to minimize the distance between the propeller plane and the parcel to minimize the aerodynamic influence of the parcel. In this chapter, we developed and validated a quadcopter design that allows its CG to be located near its propellers and the parcel placed at an optimal position above the propellers, determined through physical experiments. In this approach, the propellers can be positioned closer to one another as they do not need to extend beyond the parcel edges (Fig. 2.2C). Having the propellers closer to one another results in smaller sized quadcopters that are properly sized for the package weight resulting in better portability and storage. This new approach of re-positioning the parcel above the propellers (Fig. 2.2B) eliminates the limitation on parcel size, while maintaining low storage requirements and high portability of the drone (Fig. 2.1). By placing the parcel above the propellers, a wider variety of parcel sizes can be delivered, increasing the vehicles utility [14]. The small drone size also allows delivery to cluttered and hard to reach areas that are not accessible for larger drones that carry parcels placed between the propellers. Finally, this approach contains all the vehicle structure in a small space, limiting the risk of entanglement and complex control algorithms encountered by cable-suspended methods.

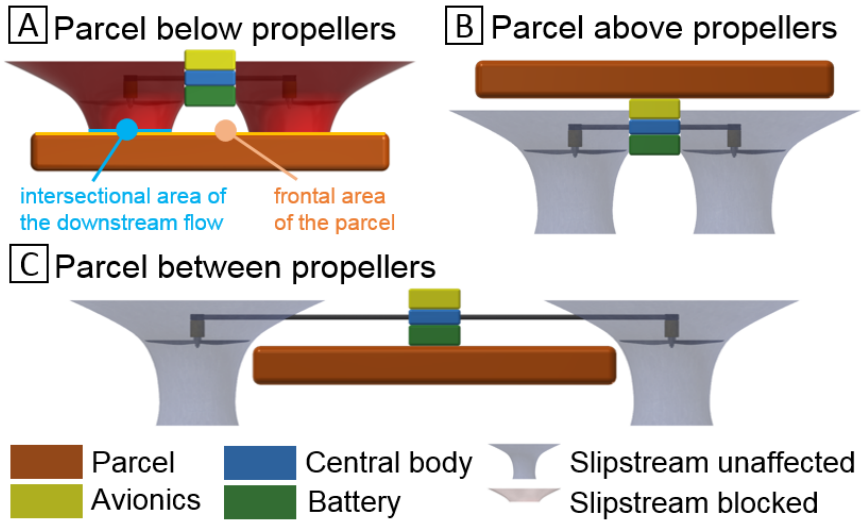

Figure 2.2 Side views of quadcopters with parcels placed in different positions. The propeller slipstreams are depicted in grey (the unaffected slipstream) and red (the blocked propeller slipstream). (A) A super-sized parcel placed below propellers creates slipstream drag, which limits lift and flight capability. (B) A parcel placed above, but close to the propellers does not reduce lift as much compared to the parcel placed beneath propellers. (C) A parcel placed between the propellers does not affect lift but restricts the size of a parcel.

2.2 Benefits of placing a parcel above the propellers

Placing a parcel above a quadcopter allows using a drone with smaller footprint, which brings a number of advantages, described in this section.

2.2.1 Space saving

A small sized quadcopter is desirable for easier storage, transportation and maneuvering in cluttered environments. The footprint size of any quadcopter is a function of propeller size. However, when placing a parcel between the propellers, footprint size is also a function of parcel size. The proposed approach of placing the parcel above the propellers decouples arm length from parcel size, which in turn enables significant reduction of the drone's size by ensuring that footprint size is only limited by propeller size. This is because the propellers can be placed in closer proximity to one another to form a compact configuration. Propeller size is useful to compare the parcel placement approaches because the relations presented here are independent of payload mass.

To study this space reduction, a simple geometric correlation between the propeller size (light blue circles in Fig. 2.3A) and the region enclosed by the four propellers is used (dark blue circle in Fig. 2.3A). The propeller disks are equally distributed around the exterior of the enclosed region. The diameter d of this region is the same as the radius of the propeller disk, r. This configuration includes a small gap e (12% of r) between the propellers tips to prevent contact between the propellers, representing a practical lower limit to vehicle size. A square (brown in Fig. 2.3A) inscribed in the reference circle represents the maximum size of a deliverable square parcel using the conventional approach of placing the parcel between the propellers.

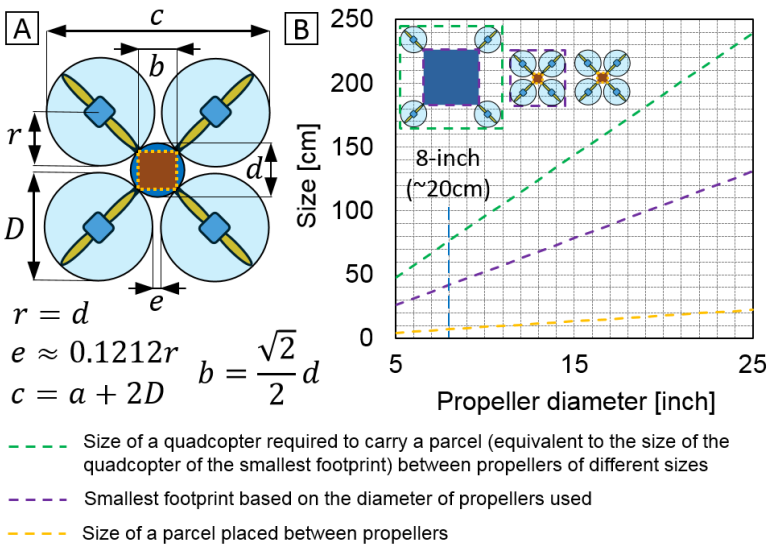

Figure 2.3 (A) The schematic representation of the geometric relationship between the radius of the propeller disk r, diameter d of the central free space (dark blue circle) between propellers and the space between propellers' tips e. (B) A plot presenting the relationship between propeller diameter and the size of a parcel or quadcopters.

Following these geometric relations, we first identify the largest sized parcel that can be delivered by a vehicle between its propellers (yellow line in Fig. 2.3B). For example, a quadcopter with 8-inch (20.32 cm) propellers has a minimum footprint of 42 x 42 cm (intersection of blue and purple

lines in Fig. 2.3B). The maximum square-shaped parcel size that can be placed between the propellers measures only 7 x 7 cm (intersection of blue and yellow lines in Fig. 2.3B), regardless of parcel weight. By comparison, a parcel placed above the propeller plane has no restrictions on parcel size. Therefore, the propellers can be placed closer together, resulting in a smaller vehicle footprint (purple line in Fig. 2.3B) for a given propeller size. As a second example, take a parcel with a size of 42 x 42 cm (the threshold of super-sized parcels in the previous example) delivered by placing it between the propellers. The minimum required size of the quadcopter will be 76.5 x 76.5 cm (intersection of blue and green lines in Fig. 2.3B). When compared to the minimum vehicle size for this propeller, there is a volume saving of 70% when placing the parcel above the propellers.

2.2.2 **Weight and drag saving**

A rigid and stable positioning of the propulsion systems is required for efficient flight. Big parcels placed between the propellers requires big quadcopter airframes that increase vehicle mass and aerodynamic drag. Instead, when the parcel is located above the propellers, the smaller vehicle footprint has comparatively lower mass and drag.

To compare the weight and drag between the two approaches, we adopted a simple drone design framework using tube structures that has been utilized by several drone manufacturers, such as DJI, Tarot and Yuneec for building lightweight drones.

The tube structures used for the quadcopter's arms are lengthened accordingly to accommodate the different parcel sizes. However, as the lengths of the arms are increased, the tube's thickness and/or diameter has to be increased to maintain the rigidity of the drone's arms. This leads to an increase in both mass and drag incurred by the airframe.

The mass of the tube arm M_{tube} is computed as

$$M_{tube} = l \cdot \rho_{material} \cdot A_{tube} \tag{2.1}$$

Where l, is the length of the tube arm, $\rho_{material}$ is the density of the material used. The cross-sectional area of the tube arm, A_{tube}, is calculated as

$$A_{tube} = \frac{\pi \cdot (D_{tube\ external}{}^2 - d_{tube\ internal}{}^2)}{4} \tag{2.2}$$

Where $D_{tube\ external}$ is the external diameter of the tube, $d_{tube\ internal}$ is the internal diameter of the tube.

Using the cross-sectional area of the tube, the moment of inertia of the section of the tube I is calculated as

$$I = \frac{A_{tube}}{16} \tag{2.3}$$

The deflection of the arm/tube can then be calculated as

$$y_{arm} = \frac{F_{max.\ thrust} \cdot l^3}{3 \cdot E \cdot I} \tag{2.4}$$

Where $F_{max.\ thrust}$ is the force applied (max thrust generated by the motor and propeller), and E is the Young's modulus. By combining the above expressions, the external diameter of the tube/arm D can be expressed as

$$D = \sqrt{\frac{64 \cdot F_{max.\ thrust} \cdot l^3}{3 \cdot E \cdot \pi \cdot y_{arm}} + d^2} \tag{2.5}$$

By using this expression in equations (2.1) and (2.2), M_{tube} can be described as follows:

$$M_{tube} = \frac{16 \cdot F_{max.\ thrust} \cdot l^4 \cdot \rho}{3 \cdot E \cdot y_{arm}} \tag{2.6}$$

Thus,

$$M_{tube} \propto l^4 \tag{2.7}$$

This indicates that scaling the arm length up sharply increases the weight of the vehicle. Conversely, a small reduction in arm length dramatically reduces the vehicle weight. A similar analysis can be done with the drag force incurred by the airframe,

$$F_{D_{frame}} = \frac{1}{2} \cdot \rho_{air} \cdot A_{arm\ fontal\ area} \cdot C_{D_{tube}} \cdot V_{cruise}{}^2 \tag{2.8}$$

Where ρ_{air} is the density of the air, $C_{D_{tube}}$ is the drag coefficient of a tube, and V_{cruise} is the velocity of the drone in cruise flight. $A_{arm\ fontal\ area}$ is the frontal area of the tube used and can be defined as

$$A_{arm\ frontal\ area} = D \cdot l \tag{2.9}$$

By combining equations (2.5), (2.8), and (2.9), the following expression is obtained

$$F_{D_{frame}} \propto l^{\frac{5}{2}} \tag{2.10}$$

This shows a similar sharp increase in drag of the vehicle as a function of arm length, reinforcing the benefits of using a small vehicle, which can only be achieved by placing the parcel above the propellers.

2.2.3 Power savings

For the drone that delivers parcels between its propellers, the drone can carry a maximum parcel size due to limited arm length. Using large drones designed for lifting large payloads results in higher operating costs when delivering small and/or lightweight parcels.

To illustrate the difference in power consumption of a quadcopter with different payloads, equation (2.11) from [1] is used:

$$Energy(kWh) = \frac{d_{cruise}}{V_{cruise}} \cdot \left(\frac{(m_p + m_v) \cdot V_{cruise}}{\frac{3600}{g} \eta \cdot r} + p \right) \tag{2.11}$$

where d_{cruise} is the distance flown, m_p is the payload mass, m_v is the vehicle mass, V_{cruise} is the cruise speed, g is the gravitational acceleration, η is the motor/propeller power transfer efficiency, r is the lift/drag ratio, and p is the power consumption of electronics. The first term in brackets is the kinetic energy of the vehicle adjusted for inefficiency. The power consumption of the electronics and the energy of the vehicle are multiplied by the mission time for comparing vehicles within a given mission.

TABLE 2.1 VALUES USED FOR EQUATION (11). RESULTS OF CALCULATIONS ARE PRESENTED IN TABLE II.

Parameter	d	v	g	η	$r_{big\ drone}$	$r_{small\ drone}$	p
Value	2	45	9.81	0.5	3	7	0.1
Unit	[km]	[km/h]	N	-	-	-	kW

TABLE 2.2 COMPARISON OF POWER CONSUMPTION OF QUADCOPTERS WITH DIFFERENT PAYLOADS AND MASSES FOR THE 2 KM FLIGHT DISTANCE

Mass of payload [kg]	**Mass of vehicule [kg]**	**P [kWh]**
2	8	**0.041**
0.5	8	**0.035**
0.5	2	**0.008**

An example is presented in Tables 2.1 and 2.2 based on quadcopters from [1][67]. A quadcopter weighing 8 kg that transports a 2 kg payload over a 2 km range consumes 0.041 kWh of energy (the quadcopter in [1]). Based on equation (2.11), the same quadcopter carrying a payload of 0.5 kg consumes only 0.006 kW less energy. However, for the same 0.5 kg payload, a smaller quadcopter (similar to the quadcopter in [67]) weighing 2 kg consumes only 0.008 kWh over the 2 km range, which translates to a 76.4% decrease in energy compared to the larger vehicle. These calculations suggest that using a small drone to transport lightweight yet large parcels is more efficient and economical than using larger sized and heavier drones.

2.3 Degradation of lift force due to parcel placement

In this section, discussion of the aerodynamic challenges associated with different parcel positions are presented.

2.3.1 Super-sized parcels positioned below propellers - standard approach

Placing any object beneath a multicopter's propellers imparts a slipstream drag force that reduces the lift force generated by the propulsion system (Fig. 2.2A). This drag force is a result of the momentum lost by the air encountering the object, for instance, a parcel. When the airflow produced by a propeller affects an object fixed to the same structure as the propulsion system, the slipstream drag force generated by the object opposes the thrust force, thus reducing the multicopter's capability to fly (Fig. 2.4A). In this case, the lift can be calculated from:

$$L = T - F_{SD} \tag{2.12}$$

Where L is the lift force, T is the thrust generated by the propeller, and F_{SD} is the slipstream drag-force acting on the parcel. The slipstream drag-force is dependent on the distance d between propeller and the parcel and can be described as:

$$F_{SD} = f(d, \rho_{air}, A_S, C_{SD}, V_{RPM}) \tag{2.13}$$

Where, A_S is the cross-sectional area of the parcel within the propeller wash as shown in Fig. 4A, C_{SD} is the slipstream drag coefficient of the parcel, and V_{RPM} is the velocity of the airstream at the point of contact with the parcel as a function of rotation speed of propeller.

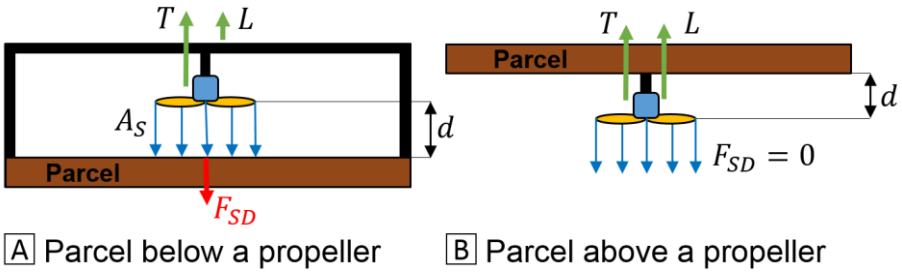

Figure 2.4 Representation of the distribution of forces. (A) Parcel placed below the propeller produces the slipstream drag-force F_{SD} (red arrow) that opposes the thrust force T (left green arrow). Thus, the lift L (right green arrow) is reduced. A_S is the cross-sectional area of the parcel within the propeller wash, d between propeller and the parcel. (B) Parcel placed above the propeller does not generate as much drag, thus does not reduce lift.

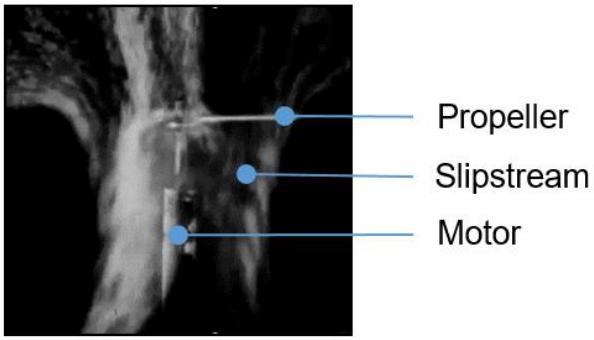

Figure 2.5 Screen shot from an experimental representation video of the flow distribution, adapted from [68].

The slipstream drag-force is not dependent on the entire frontal area of the parcel, but rather the intersectional area of the flow below the propeller and the parcel (Fig. 2.4A). As presented in Fig. 2.5 [69], the slipstream below the propeller is more defined, condensed and narrow than above the propeller. As a result, a parcel placed below the propeller is affected by the propeller slipstream only in the region where the slipstream meets the parcel's surface. Because the slipstream is narrower here, the slipstream drag can be eliminated by placing the parcel between the propellers, as shown in Fig. 2.2C. This is the typical approach to delivering parcels, however, with large parcels; this approach suffers from the aforementioned issues with large vehicles.

2.3.2 Super-sized parcels positioned above propellers - new approach

The reduction in lifting capability of the drone can be significantly reduced without enlarging the vehicle, when the parcel is placed above the propellers. With the parcel placed above the propellers, the slipstream is not blocked and therefore slipstream drag is eliminated. However, a challenge associated with this approach is that an object placed above, but in close proximity to the propellers will hinder airflow into the propellers. According to Froude's momentum theory of

propulsion [70], the air passing through the rotor disc plane receives energy from the propeller, thus generating thrust. However, when there is insufficient airflow to the propeller, a lower amount of energy is transferred to the air, reducing the thrust produced. Instead of blocking the airflow below the propellers, placing the parcel above blocks airflow above the propellers (Fig. 2. 4B). Mathematically, this is written by replacing slipstream drag in equation (2.12) with inflow blockage. To prevent inflow blockage, the parcel placed above the propellers has to be located at a distance that provides sufficient room for airflow to the propellers. Because the airflow above the propeller is wider than below, it is possible to place parcels mounted above the propellers closer to the propellers than if they were mounted below (Fig. 2.2B). Furthermore, because the airflow above the propeller is independent of flow direction, parcels placed above the propellers are not limited in size, unlike parcels placed between the propellers (Fig. 2.2C). The aerodynamic requirements of our approach are validated through physical experiments, comparing slipstream drag and inflow blockage effect, in Sections 2.5 and 2.6.

2.4 Conflicting constraints of CG location and efficient aerodynamics

Multicopters are naturally unstable platforms, thus a quadcopter remains unstable regardless of the location of the center of gravity (CG). For instance, placing the CG below the propeller plane results in an unstable oscillation, while placing the CG above the propeller plane results in pure divergence, but divergence can be easily corrected by an autopilot [71]. Nevertheless, to reduce the quadcopter's control effort, the CG of the entire platform should be as close to the propeller plane as possible [72]. Because of these two findings, some studies have indicated a preference for the CG location to lie slightly above the propeller plane, as concluded in [73]. This advantage in controlling a quadcopter with a CG location above the propellers is further supported in recent work [57] that stated that quadcopters under a proportional–integral–derivative (PID) controller are more stable when the load is placed directly on top of the airframe. Moreover, the PID controller can handle CG offset from the yaw axis more easily when the CG is placed above the propeller plane. This is particularly important for parcel delivery, as the parcel CG may not be centered in the parcel.

It is ideal to place the parcel as close as possible to the propeller plane to keep the CG as close as possible to the propeller plane. However, placing a parcel close to the propellers will block the airflow stream into the propellers, due to inflow blockage effect. Thus, to address the problem of competing constraints it is necessary to find the smallest distance between the parcel and the propellers that does not inhibit adequate airflow. This was studied experimentally in Section 2.5 and 2.6. Additionally, distance of the CG from the propellers' plane can vary significantly with and without a parcel. To keep the smallest distance between the CG and the propellers' plane in both configurations, a quadcopter was designed (Section 2.6) to situate the propeller plane midway between the two CG locations.

2.5 Experimental validation – single propeller

To demonstrate the aerodynamic effects of parcel position on the drone, a series of experiments were performed. These experiments were conducted to demonstrate that slipstream drag reduces lift more than inflow blockage does. During the experiments, lift, slipstream drag and electric

power consumption were measured at different distances d between a parcel and a single propeller (Fig. 2.6A-C).

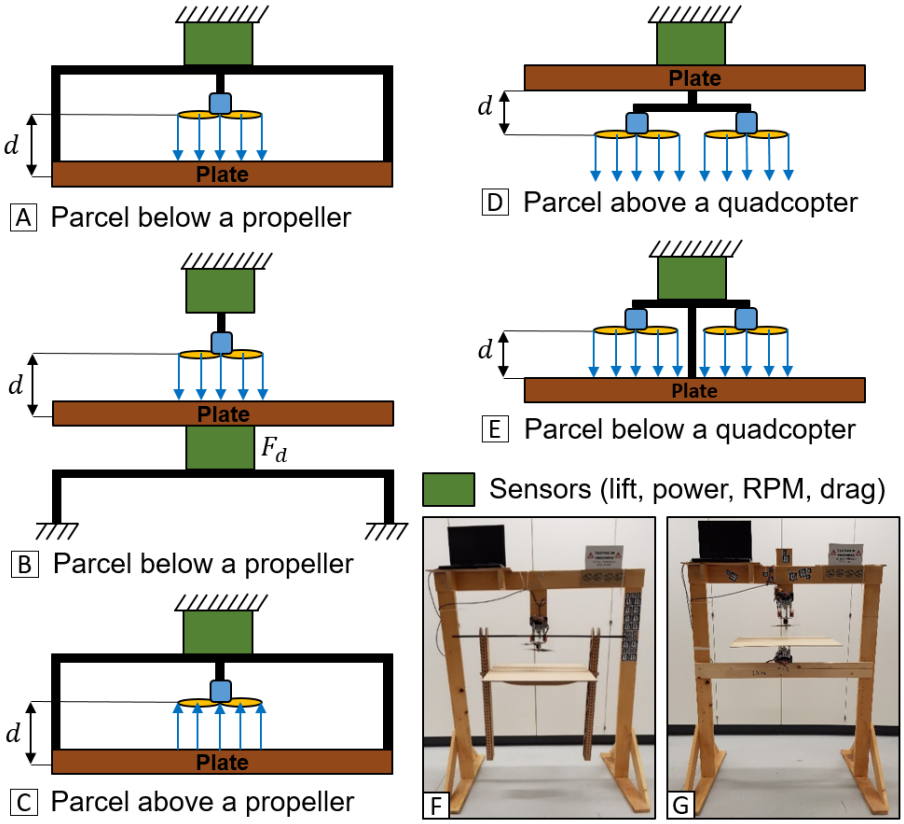

Figure 2.6 (A-C) Schematic representation of the experimental set-up for lift and drag measurements with a single propeller. The blue arrows represent the direction of the airflow. (A) Plate placed below the propeller. (B) Plate placed below the propeller. Different sizes of plates are fixed to the bottom sensor. (C) Plate placed above the propeller. (D-E) The schematic representation of the experimental set-up for lift and drag measurements with a quad configuration. (D) Quadcopter with a plate placed above the propellers. (E) Quadcopter with a plate placed below the propellers. (F) Photograph of the setup with a plate of size 60 x 60 cm. (G) Photograph of the setup to measure the slipstream drag-force when the plate is placed below the propellers.

Two configurations were considered, one with the parcel below the propeller (Fig. 2.6A) and another with the parcel above the propeller (Fig. 2.6C). Additionally, for each configuration, two other factors were considered: (i) dependency of lift on different rotation speeds, (ii) dependency of lift on different propeller diameters. The first experiment was conducted with an APC 8x4.5 propeller and the second at a constant 9000RPM, which is 70% of the maximum rotation speed of the propeller-motor pair used in the first experiment. This value was chosen because multicopters do not cruise at maximum throttle but rather at around 70% (9000 RPM for proposed setup) capability.

To represent the parcel, a flat wooden MDF plate 60 x 60 x 0.5 cm was attached to a force sensor (marked as a green rectangle in Fig. 2.6A) via a vertical wooden structure connected to a horizontal 10 mm carbon tube (both marked as black beams in Fig. 2.6A and 7C). The distance between the MDF plate and the propeller can be varied from 2 cm to 50 cm. A control case was also

run without the MDF plate. The motor is powered by a power supply (Keithley 2260B-30-72) which has a maximum output of 720 W.

The measurements were conducted using the RC Benchmark 1580 Series dynamometer sensor (Fig. 2.6, marked as a green rectangle) [74] attached to a stand. The motor used for the tests was an AXI 2217-16 V2 (1380 KV) with a 40A ESC (Electronic Speed Controller). The voltage was set to 12.6 V, which is equivalent to a fully charged 3S battery. Each measurement was done ten times.

2.5.1 Parcel below the propeller

When the parcel (MDF plate) was positioned directly below the propeller, the slipstream drag significantly reduced the lift as observed in Fig. 2.7-9. Regardless of rotation speed, shown in Fig. 2.7, or propeller diameter, in Fig. 2.8, the observed effect of parcel placement on lift is the same. A plate situated as far as 50 cm beneath the propeller still diminishes the measured lift by 90% compared to when there is no plate at all (marked "w/o" – without, on the farthest right in both plots). This shows that there is no dependency on distance between the propeller and plate regardless of rotation speed or propeller size.

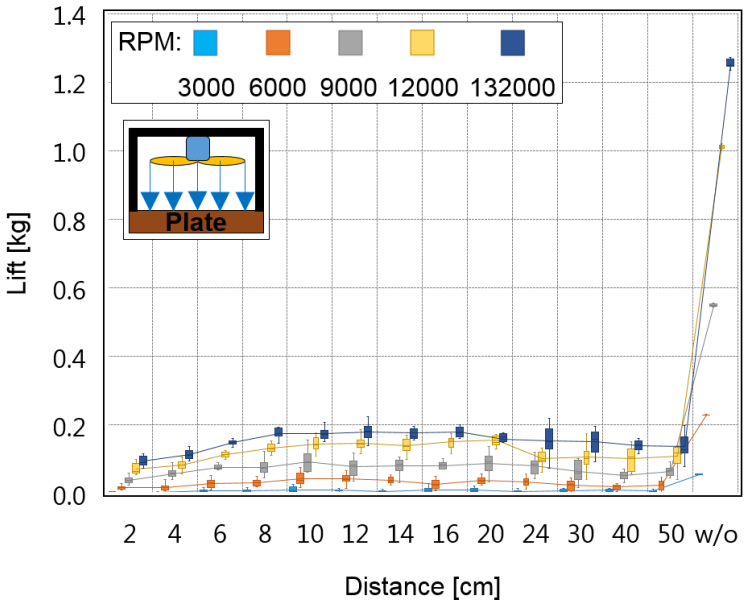

Figure 2.7 Influence of the distance of a plate below the propeller on lift measurements. The plot presents lift measurements of APC MR8x4.5 propeller with a flat plate (the equivalent of a parcel) placed beneath the propellers for different rotation speeds.

Experimental verification that slipstream drag is a function of the area of the parcel in contact with the propeller slipstream A_S was also performed. Different sized square plates were attached to the RC Benchmark 1580 Series dynamometer sensor and were placed 10 cm below the propeller (Figs. 2.6B and G). As expected, plates that are larger (30 cm and above) than the propeller disk have approximately the same drag measurements, regardless of how much larger they are (Fig. 2.9). This is because the cross-sectional area between the slipstream and parcel is constant between runs. When the plate is equivalent or smaller than the propeller disk, the measured drag

force is lower and varies with the size of the plate. These results confirm that the slipstream drag is indeed dependent on the area of the parcel in contact with the propeller slipstream.

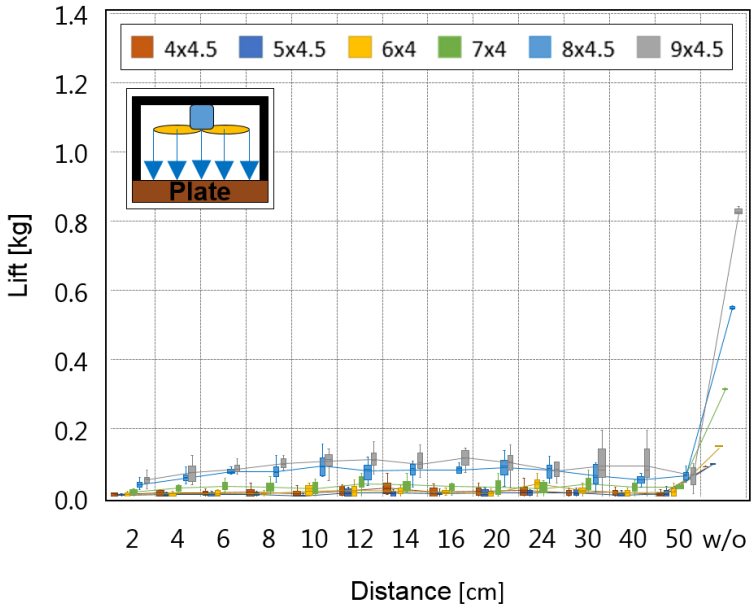

Figure 2.8 Influence of the distance of the plate below the propeller on lift measurements. Measurements are obtained at a constant speed of 9000 RPM. Propellers of various diameters but similar pitches were used.

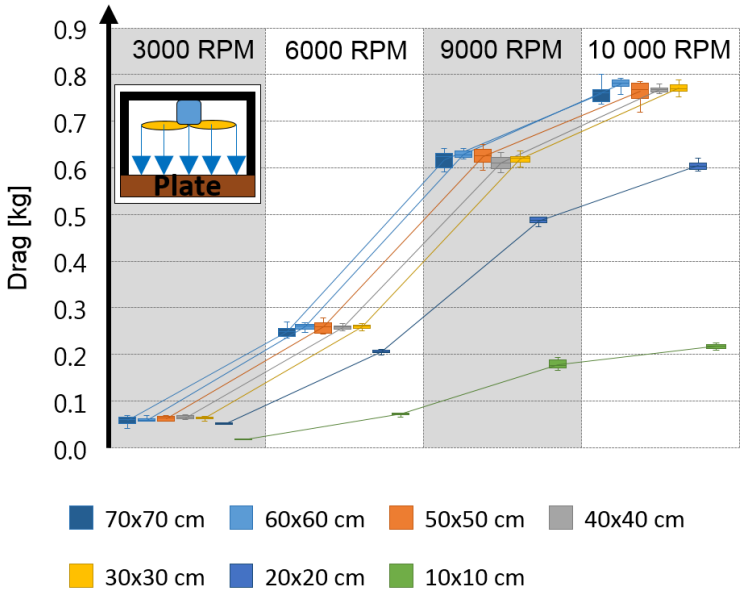

Figure 2.9 Drag measurements of different sized square plates placed 10 cm below a single propeller.

2.5.2 Parcel above the propeller

Conducting the experiment with the parcel above the propellers illustrated that the inflow blockage is most significant when the parcel is within 10 cm of the propeller (Fig. 2.10). Beyond 10 cm, as the distance between the propeller and a parcel increases, the lift levels off and becomes constant, within 10% of its maximum value. Within the 10 cm distance, the most significant

measured impact on the lift is the plate placed 2 cm above the propeller. At 12000 RPM, the lift is affected by 57% while at 13200 RPM; the lift is affected by 66%.

As with the previous experiment, the investigation of different sized propellers (Fig. 2.11) was conducted at 9000 RPM. The lift stabilized at 6 to 11 cm distance between the plate and the propellers for each of the propeller sizes. This matches well with the 10 cm threshold found when varying the RPM. Larger propellers have larger volumes of air inflow, therefore with larger inflow blockage; there is a larger decrease in lift. This is why the initial slopes are steeper for the larger propellers. In the experiments with the plate placed above the propeller (Figs. 2.10 and 2.11), the distance at which the lift begins to converge within 10% of its maximum value for a specific propeller is approximately equivalent to its radius, which is significantly less than 90% when a parcel is placed below the propeller.

Throughout the experiments, the electrical power consumption was measured. Analyzed data suggest that the electric power consumption remained constant as the plate was moved away from a propeller for parcel placements above and below the propeller.

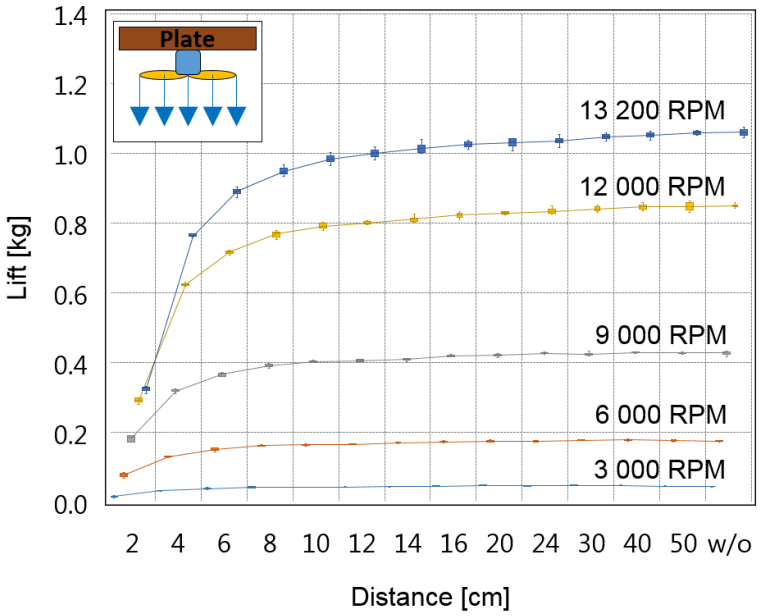

Figure 2.10 Influence of the distance of a plate above the propeller on lift measurements. The plot presents lift measurements of APC MR8x4.5 propeller with a flat plate (the equivalent of a parcel) placed above the propellers for different rotation speeds.

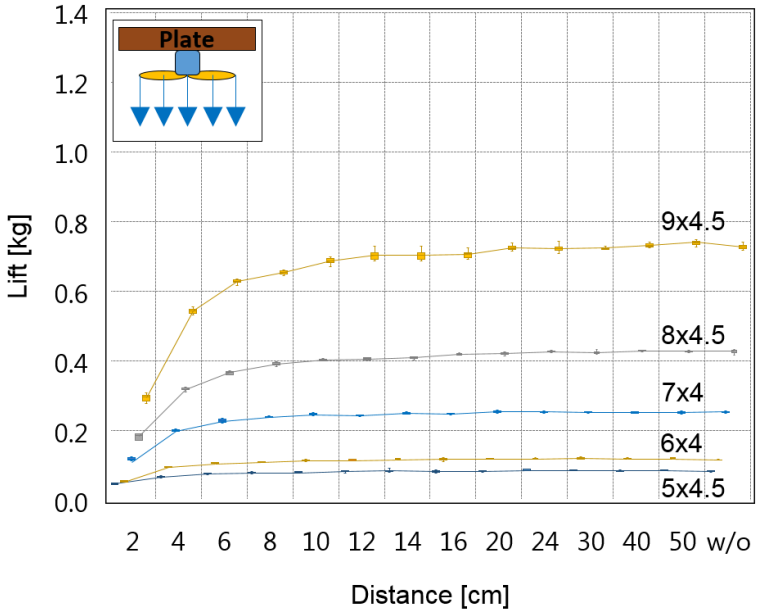

Figure 2.11 Influence of the distance of the plate above the propeller on lift measurements. Measurements are obtained at a constant speed of 9000 RPM. Propellers of various diameters but similar pitches were used.

2.6 Experimental validation – delivery drone

To validate the concept of delivering super-sized parcels, a 50 x 50 cm quadcopter that can carry 0.75 kg worth of payload was designed and manufactured (Fig. 2.1 and 2.12).

2.6.1 Delivery drone description

The proposed design ensures that the CG is positioned as close as possible to the propeller plane with or without the payload. For the configurations with and without the payload, the distance of the CG to the propeller plane should be similar. With the payload, the CG is designed to be above the propellers to ensure that the PID controller handles potential parcel CG offsets from the yaw axis efficiently. Without the payload, the CG will subsequently be located below the propellers. If the payload is lighter than a maximum 0.75 kg, the CG is located above but closer to the propeller plane.

To position the CG close to the propeller plane, batteries are located below the propeller plane while the parcel is placed above the propeller plane. More importantly, to achieve a similar distance between the CG and the propeller plane with and without a parcel, the quadcopter arms are inclined by 68 degrees to the yaw axis (Fig. 2.12). This shifts the propeller plane to the midway point between the extreme CG positions. In the proposed design, the parcel is positioned 15 cm above the propeller plane as this is above the distance that minimally affects the lifting capability of the propulsion system with a margin of safety.

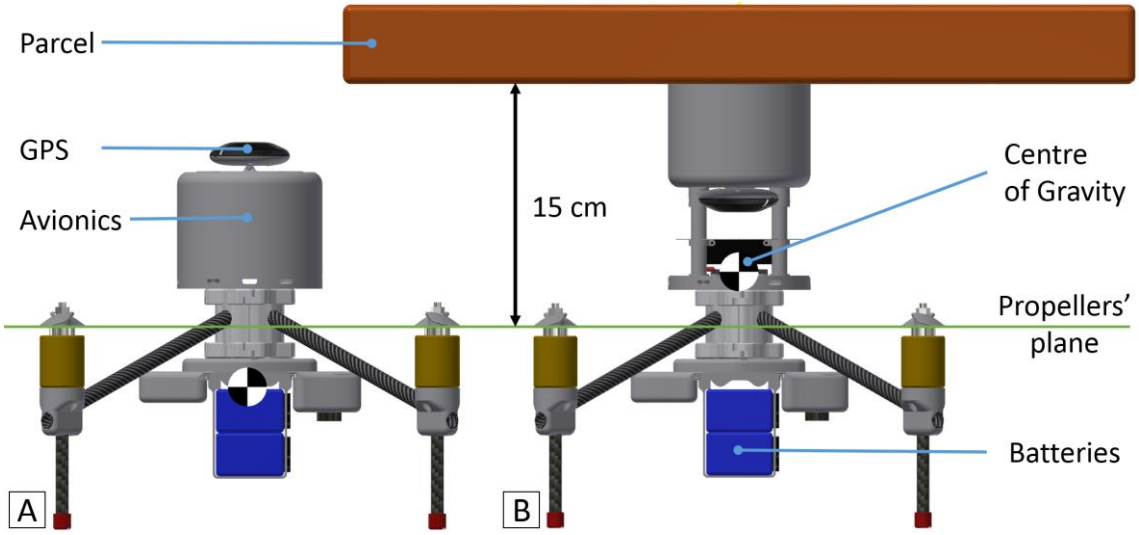

Figure 2.12 Side views of the quadcopter. (A) The quadcopter without a parcel. Center of Gravity placed 36 mm below the plane of the propellers along the yaw axis. (B) The drone with a parcel placed above the propellers. The Center of Gravity was placed 39 mm above the propeller plane along the yaw axis.

The parcel is secured to the top of the drone by two polyester belts crossed perpendicular to each other (Fig. 2.1). The GPS module is connected to one of the belts and when strapped, is situated above the box. This is favorable as GPS readings can be affected by objects, such as parcels, made of or containing metal material (e.g. aluminum foil). The platform is equipped with four AXI 2217-16 V2 (1380 KV) motors with APC8x4.5 propellers and 4in1 ESC. The flight controller used is PixHawk 4 Mini. The drone is equipped with two 3S Li-Po batteries, each 5000 mAh.

2.6.2 Influence of a parcel on a quadcopter propulsion system

The influence of parcel size on the lifting capability of the quadcopter was investigated by attaching different sizes of square plates to the quadcopter as shown in Fig. 2.6D-E. These plates range from 10 x 10 cm to 70 x 70 cm, attached at a 10 cm distance from the propellers, as concluded earlier that the distance between the parcel and the propeller should be equal to the radius of the propeller used.

Two experiments were conducted, the first with the parcel placed above and the second with the parcel placed below the propellers. In both cases, ten measurements of lift affected by the plates were made for four rotation speeds. The lift reduction is presented in Fig. 2.13. It was calculated by subtracting the measured lift with a parcel from the measured lift without the parcel. Thus, plots show directly the amount of lift reduction for each plate.

The schematic representatoin of how the plate was attached below the quacopter is presented in Fig. 2.6E. The results of the experiment are presented in Fig. 2.13A and show that a plate bigger than the enclosed area between the propellers has significant influence on lift reduction. For instance, plates of sizes 70 x 70 cm and 60 x 60 cm encountered up to 96% lift reduction for 10 000 RPM which is the equivalent of 2.4 kg of lift. Also of note is that a higher inflow blockage was measured with a plate of same size as the quadcopter than a larger plate than the quadcopter. This is likely due to vortices at the edge of the plate. Further investigation should be conducted to understand this phenomenon.

In Fig. 2.13B, results of the lift reduction are presented for a parcel placed above the propeller plane. The lift reduction between different sized parcels is very small for small rotation speeds. When the speed increases, the lift reduction increases with increase in size of the propellers. The experiments with a small parcel (10 x 10 cm and 20 x 20 cm) below the propeller plane confirm that a smaller parcel size has smaller influence on the lift. This is not true of larger parcels that confirms that the arms of the multicopter have to be increased to secure unobstructed airflow. The earlier experiment on a single propeller spinning at 9000RPM showed that a 60 x 60 cm parcel placed 10 cm above produces only a 6% lift reduction (Fig. 2.7). However, when the same sized plate is placed 10 cm above the quadopter's propellers, a maximum lift reduction due to inflow blockage of about 23.4% is measured (Fig. 2.13B). This is approximately four times the reduction with a single propeller, suggesting that inflow blockage is additive with the number of propellers. Repositioning the parcel to 15 cm above the quadcopter further decreases the lift reduction to 14%. This is a remarkable improvement compared to the 96% lift reduction due to slipstream drag if the parcel is placed 15 cm below the quadcopter.

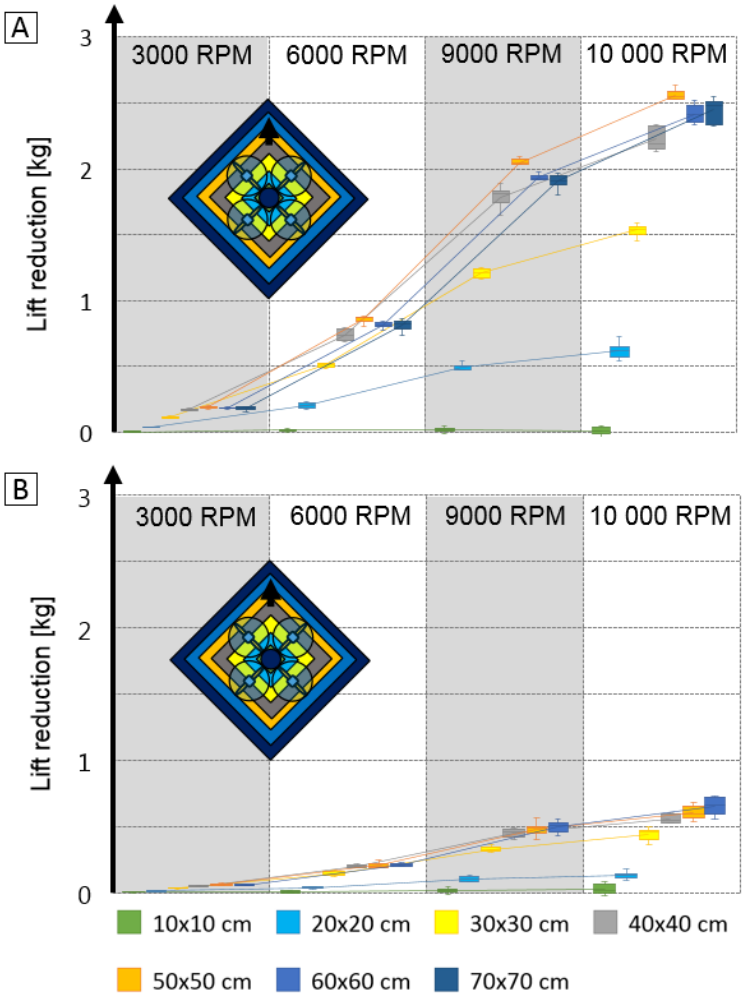

Figure 2.13 (A) Lift measurements based on different sizes of square plates placed 10 cm above a quadcopter. The size of the quadcopter is 50 x 50 cm. (B) Lift measurements based on different sizes of square plates placed 10 cm below a quadcopter. The size of the quadcopter is 50 x 50 cm. Colors of the squares correspond to the different sized plates. The total lift is 0.20 kg, 0.89 kg, 2.11 kg, and 2.66 kg for 3000RPM, 6000RPM, 9000RPM, and 10000RPM respectively.

The phenomena shown in this experiment of positioning a flat object above or below propellers, differs from the ceiling effect or the ground effect described by [75] respectively. This is because unlike the ceiling and ground, the parcel is rigidly connected to the airframe making the slipstream drag-force produced by the parcel internal to the system and hence negatively affecting the lifting capability of the system.

2.6.3 Flight experiments

Flight tests with the quadcopter in hover were performed to validate the approach of placing the parcel above the propeller plane while minimally affecting its lifting capabilities. A flat plate was attached above the propellers at a distance of 15 cm from the propeller plane. During the experiment, the quadcopter employed 55% (550g payload) throttle with an ultrasound sensor to maintain an altitude of 1.5 m above the ground. The drone used a standard PX4 flight stack software for the X-shaped quadcopter, which is much simpler than the complex controllers used when delivering a parcel on a long tether. A pilot kept its position constant. The drone automatically landed after reaching 5% of its battery level. Time of hover was measured for the quadcopter with a super-sized foam plate and smaller box; both placed 15 cm above the propellers. The experiment showed a difference of 2 minutes in the hover flight time (12%) between flight with a super-sized parcel and a smaller parcel of the same weight, both placed above the quadcopter. The foam plate measured 100 x 50 x 5.5 cm and had a mass of 550 g. Its time of hover was 15 minutes 30 seconds. The smaller parcel measured 7 x 7 x 5 cm, also had a mass of 550 grams. Its time of hover was 17 minutes 30 seconds. The experiment was repeated with the parcel placed below the propellers. The time of hover with the smaller parcel (550 g) attached between the propellers was 16 minutes 10 seconds. The super-sized parcel attached 12.5 cm below the propeller plane generated excessive drag, which counteracted all of the thrust generated. As such, the drone was not able to take-off (see attached video). All flight tests were performed three times and the average time of hover was provided. We conclude that placing a big parcel above the propeller plane does not significantly influence the drone's endurance.

2.7 Conclusions

This chapter presented the novel concept of placing a parcel above the propeller plane of a quadcopter. This approach allows the transportation of different sized parcels without limitation, unlike when a parcel is beneath the frame of the quadcopter.

Placing a parcel above the propellers enables a smaller footprint of the quadcopter, reducing the airframe's size, weight and drag and enhancing its storage and transportation capabilities. Moreover, a smaller drone is more feasible for deliveries in cluttered environments. Simply relocating the package brings these benefits without the use of exotic designs or a complex controller: a simple PID can be used.

We validated the proposed approach by developing and testing a quadcopter that allows the transportation of different sized parcels, including super-sized parcels that are larger than the quadcopter itself. Experiments revealed that placing a parcel above the quadcopter at a distance equivalent to the radius of the operating propeller, reduces the drone's lifting capability by 23%, compared to 96% when the parcel is below the quadcopter. When the distance between the quadcopter and parcel placed above it is increased, the lift reduction can be further reduced.

The new approach of placing a parcel above the propeller plane should spur the development of new cargo-delivery drone designs, capitalizing on the compactness, efficiency and functionality of the strategic parcel placement. Future work will explore wind tunnel tests to study the influence of parcel sizes on drag and lift during cruise flight and the design of a compact protective cage around the propellers [77].

Chapter 3
Safety, storage and transportation

CURRENT delivery multicopters can be dangerous for people, require a large amount of storage space and are difficult to transport. Safety issues arise because users are exposed to the unshielded spinning propellers. Transportation to the place of deployment and storage is often complicated by the large size required for lifting heavy objects. This chapter addresses these limitations by proposing the integration of the quadcopter into a foldable protective cage. The cage provides an all-round protective structure that physically separates the propellers from the external environment, ensuring the safety of people and the quadcopter. The drone and the cage can be easily folded in a single movement, significantly reducing its size for easier storage and transportation. The parcel is located inside the cage, attached to the top joint above the plane of the propeller. Placing a parcel above the quadcopter maintains the small footprint of the drone, thus reducing the overall weight and drag of the drone as discussed in Chapter 2. Moreover, the drone was designed to place the Centre of Gravity (CG) close to the plane of the propellers. The design was validated on a quadcopter that can lift parcels up to 500 g and that has a reduced storage volume of 92% when folded.

The material presented in this chapter is adapted from:

[78] **P. M. Kornatowski,** S. Mintchev, and D. Floreano, “An origami-inspired cargo drone,” in IEEE International Conference on Intelligent Robots and Systems, 2017, vol. 2017–September, pp. 6855–6862.

The work presented in this chapter was submitted for patenting and the patent has been granted in the US and Europe:

[79] Patent. **P. M. Kornatowski,** S. Mintchev, and D. Floreano, “Foldable aircraft with protective cage for transportation and transportability” (US10252795, PCT/IB2017/052034).

3.1 Introduction

Drones are rapidly becoming a cost and time effective solution for delivering parcels to densely populated environments as well as to remote locations without suitable road networks [6]. Their capability to navigate above obstacles, along the shortest route is capturing attention from companies seeking affordable solutions for cargo transportation and delivery. Most cargo-drone prototypes are multicopters [4][15][80] that leverage vertical take-off and landing capabilities to deliver parcels precisely, even in cluttered environments. Furthermore, the growing popularity of drones for consumers could pave the way to new e-commerce models where drones could enable peer-to-peer transportation of goods. Both scenarios require hovering platforms that are intrinsically safe and easy to store and transport, requirements not yet fulfilled by the commercially available platforms.

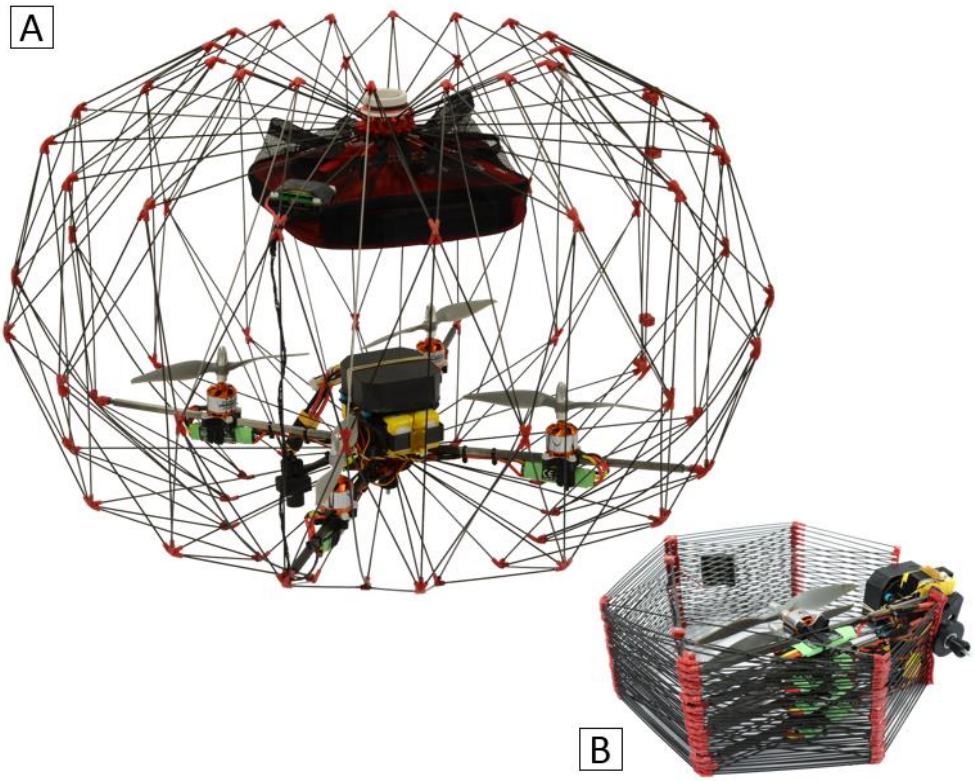

Figure 3.1 A safe and foldable quadcopter for cargo delivery. (A) Deployed configuration with an enclosed first-aid kit held by a net. (B) Folded configuration with a volume reduction of 92%.

Concerning safety, unshielded spinning propellers are a serious threat and can cause injuries or damage when interacting with people or obstacles. Commercially available delivery drones provide only limited protection. Lightweight hulls (such as the Parrot AR.Drone 2.0) or small plastic elements around the drone (such as the DJI Phantom 4) only protect the propellers from side contact with objects and are not very effective for users' safety. A safer approach is to enclose the drone into all-round protective structures. For example, lightweight carbon fiber cages have been shown effective in avoiding injuries to users and averting drone damage on collisions [28] [81]. However, none of the platforms are directly suited for parcel transportation due to the limited space inside the cage. Moreover, the cages are cumbersome structures than cannot be folded for easy storage and transportation.

Concerning size, transportation of heavy payloads requires large aerial surface in order to generate sufficient lift. This means that the drone is much larger than the parcel and thus difficult to store, handle and possibly transport to the deployment location. This is even more problematic when the drone is equipped with all-round protective structures, which further increase its size [30][81]. A possible solution lies in foldable drones that are large enough to carry a useful payload when fully deployed, while being transportable folded and easy to store [54]. Although several commercial foldable hovering platforms are available, such as, DJI Spreading Wings S1000plus, Simtoo Dragonfly, none of them is equipped with all-round protective structures. Indeed, according to our knowledge there are no foldable drones equipped with integrated all-around protective structures that can be simultaneously folded with the drone.

Here we describe a novel design that addresses both the safety and size issues and consists of a foldable protective cage integrated with a multicopter, as presented in Fig. 3.1. The cage encloses the entire multicopter including the parcel. During flight, the cage is closed to protect the users from the spinning propellers. A safety mechanism shuts down the propellers when the cage is open, reducing the risk of injuries while loading the cargo. The cage is inspired by origami that allows the drone to be manually folded with an intuitive operation in order to reduce its volume. With this new design, a recipient can catch easily and safely the approaching drone. During commercial delivery, the all-round cage coupled with the propeller-disengagement system protects inexperienced users from harmful injuries while in close proximity to the drone or while loading it. The foldable structure allows users to easily carry the platform and deploy it within seconds when required. For example, the prototype in Fig. 3.1 fits into a backpack when folded.

3.2 Concept of the safe foldable cage

The cage functions as an all-round protective structure that separates the harmful propellers of the multicopter from the outside environment and people. We resort to an origami design to make the drone foldable with a simple arm movement. Origami structures have been shown to achieve high strength-to-weight ratios [82] and a significant size reduction by folding [84]. Among the possible origami designs [86] (Fig. 3.2A, 3.2B), the drone cage is inspired by the pattern used for foldable shelters [88] (Fig. 3.2C). This pattern can be adapted to obtain a foldable cage, similar to a Chinese lantern (Fig. 3.2A and B).

Traditional origami structures [84] are composed of tiles joined by folds. For the cage, struts connected by flexible joints replace the tiles in order to obtain a spatial structure that does not obstruct the airflow generated by the enclosed propellers. The cage has a modular design composed of repeated multiple foldable segments (Fig. 3.3A). Each segment is the result of a tessellation of congruent isosceles triangles, where the edges are struts and the vertices are flexible joints. The spatial structure of the cage (Fig. 3.3D) is obtained by connecting the free ends of multiple segments forming the top and bottom joints. The cage may be folded by pushing apart the first and last segment from each other (Fig. 3.3F). All the segments fold rotating around the central axis of the cage, marked as a red dot-dashed line (Fig. 3.3F). In doing so, the top and bottom central joints get closer to each other, resulting in the final folded polygonal shape of the cage.

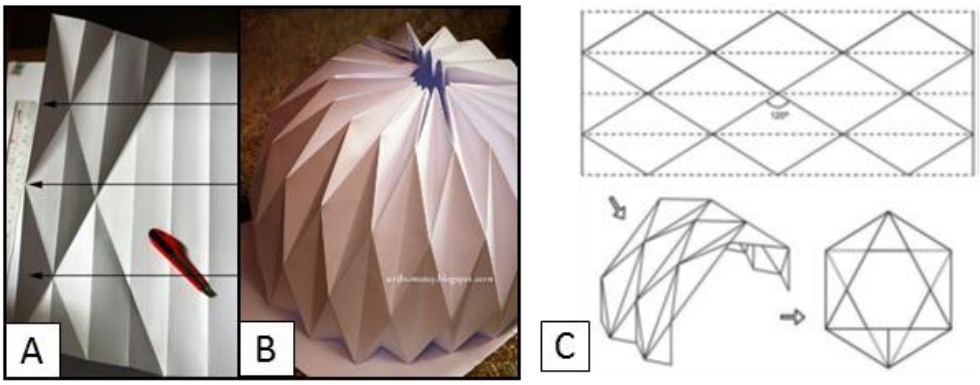

Figure 3.2 A paper origami lantern [86]. (A) the pattern of creases required to create the lantern structure; (B) the deployed structure; (C) the foldable origami-based shelter and the 3 stages of deployment [88].

The dimensions of the cage in the folded and deployed configurations can be described by a small number of parameters, as illustrated in the flat configuration of the segments (Figure 3A). *L* is the length of the longest edge of the triangles (struts marked in red color) and corresponds to radius *R* and height *H* of the internal empty space inside the cage (Fig. 3.3B). Thus, *L* is also the radius of the footprint of the multicopter. β is the apex angle of the triangles, influenced by the number of segments. The value of β defines the distance *h* between the central top and bottom joints (Fig. 3.3C). Together, *R* and *H*, define the internal volume of the cage available for the drone and the cargo. *l* is the length of the shorter arm of the triangle and its distance is a function of *L* and β. In the deployed configuration the angle, α, between *R* and *H*, is 90 degrees.

The design of the cage presents four important features that make it suitable for cargo delivery. Firstly, the folding pattern allows the cage to be rigid in the deployed configuration, thus ensuring stability during flight. Other origami structures, such as the "magic ball" [89], can be squeezed in the deployed configuration. Secondly, the modular structure enables control of the spatial density of the cage. A dense cage with a high number of segments provides more safety at the expense of increased drag, smaller payload and consequently, shorter energetic autonomy of the drone. Thirdly, in the folded configuration the cage offers sufficient free space to encapsulate the components of the multicopter and protect them during transportation.

The cage integrates the multicopter and the cargo (Fig. 3.1). The cargo position was chosen above the multicopter to avoid obstructing the airflow generated by the propeller, which would result in reduced efficiency (Section 3.5). That is why the multicopter is integrated into the bottom part of the cage. The arms of the multicopter replace some struts of the cage, making the two structures seamlessly integrated. This integration has two advantages: weight reduction as structural components can be shared and simplified operation, as a single arm movement folds both the cage and the multicopter structure.

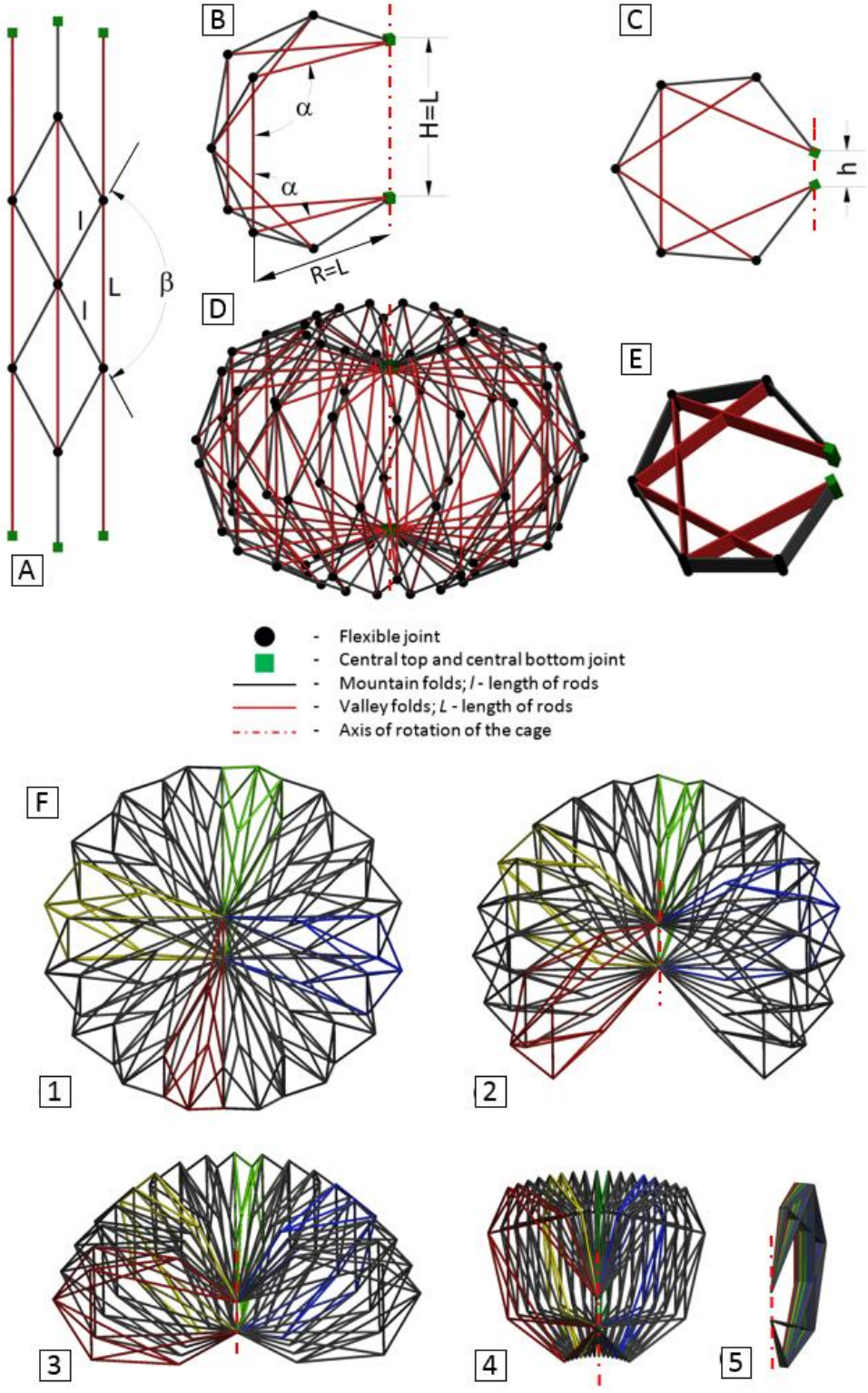

Figure 3.3 (A) Top view of the flat pattern of one basic segment of the cage before assembling. (B) The basic segment presented in the deployed configuration. (C) Shape of the folded basic segment. Colors represent mountain folds (black) and valley folds (red). (D) Example cage in the fully deployed state consisting of 16 basic segments. (E) Fully folded cage in an isometric view. (F) Folding process of the cage. For sake of clarity, every fourth segment is marked with a different color.

3.3 Implementation

In order to validate the design presented in the previous section, we describe the manufacturing of a drone that can carry 0.5 kg parcels (the typical weight of a first-aid kit). Its total take-off weight (with the parcel) is equal to 1.5 kg. The drone has a size of 65 x 65 x 43 cm when deployed, and folds down to a size of 31 x 38 x 12 cm when stowed (Fig. 3.4).

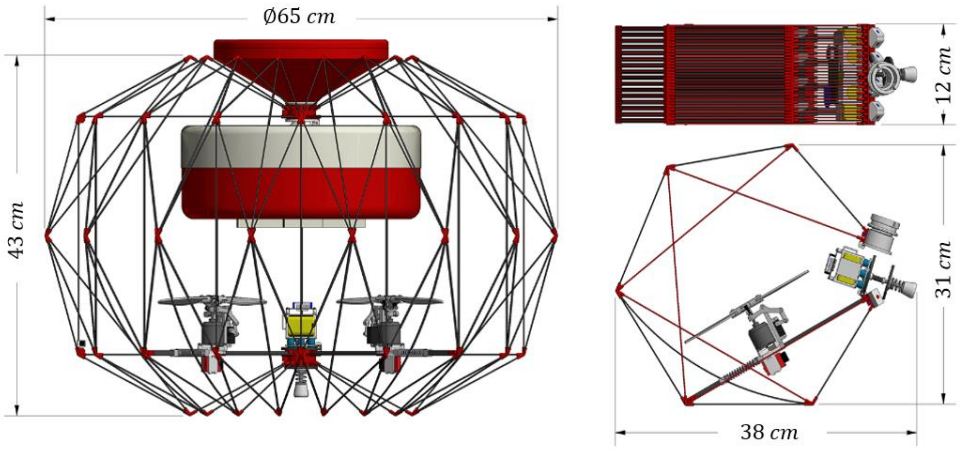

Figure 3.4 3D rendering of the prototype of the foldable flying cage with integrated quadcopter. (On the left) Deployed configuration of the robot with a container for cargo (a white-red box) attached to the top internal part of the cage. A parachute (red cone) is on the top and attached to the external part of the cage. (On the right) Side and top view of the stowed cage with detached cargo box and parachute.

3.3.1 Cage

The cage is manufactured from carbon-fiber tubes connected by soft joints that are 3D printed using a flexible material (NinjaFlex® Flexible 3D Printing Filament). As the cage can be manufactured flat, the joints can also be made using an over-molding technique by locally injecting soft polymers over the tubes. Compared to conventional foldable structures composed of rigid hinged joints, the flexible joints provide smooth folding without affecting the cage rigidity when deployed, which is ensured by the strength of the carbon-fiber tubes. According to the calculations presented in the section 3.4, a 0.5 kg parcel can be hung from the top joint of the cage and cause only minor deformations (Section 3.5) when 1.5 mm carbon tubes are used (wall thickness 0.5 mm). The rigidity of the cage is mandatory to prevent undesired oscillations of the cargo during flight that could destabilize the drone.

As mentioned earlier, the cage can be made of a variable number of segments. The prototype described here is composed of 16 segments, a number that provides enough protection for users (openings in the cage are smaller than a fist of an adult male), without significant loss of aerodynamic thrust (Section 3.5).

The central top and bottom joints of the cage are composed of a 3D printed flexible strip and multiple connections for the tubes. This part takes the shape of a hollowed cylinder when the cage is deployed (Fig. 3.5A) and is flattened when the cage is folded (Fig. 3.5D). This design prevents interference of tubes during folding and allows achieving a flat configuration of the edges of the cage when stowed (Fig. 3.5E). A locking mechanism that prevents opening of the cage during

flight is integrated at the top and bottom joints. This mechanism uses a screw system that is manually operated by the user who tightens the joints before take-off. The cage is also equipped with a side locking mechanism that connects the vertical carbon tubes of the first and last segments of the cage. The side locking mechanism consists of two pairs of cylindrical magnets encapsulated into the flexible joints of the cage (Fig. 3.5C). To open the cage, these segments have to be pushed apart from each other (see opening process in Fig. 3.5F), thus unlocking the mechanism.

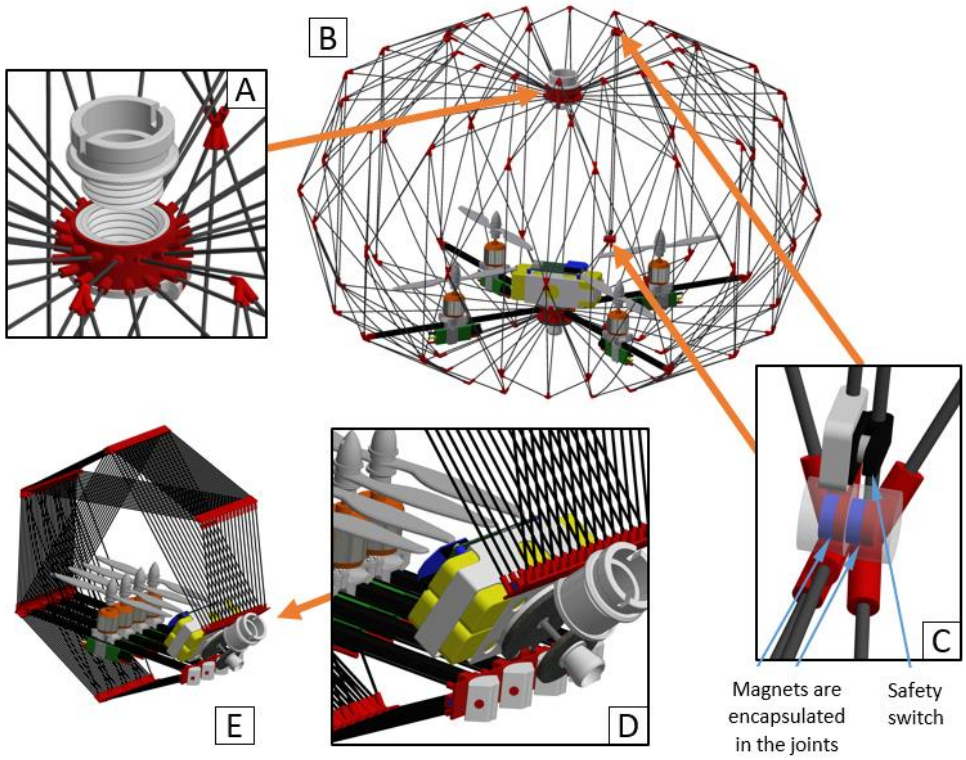

Figure 3.5 (A) The top-locking mechanism. (B) The deployed drone. (C) The side-locking mechanism with the safety switch that disables the propulsion system when the cage is open. (D) A zoom-in of the bottom and top locking mechanisms in the folded state of the cage. (E) The folded state of the drone.

3.3.2 Multicopter integration

Four of the bottom horizontal tubes are replaced by pultruded carbon fiber 6 mm square tubes that hold the motors of the multicopter. These stiffer tubes prevent undesired vibrations and oscillations of the motors that could lead to instability during flight and compromise reactivity and energetic efficiency. Additionally, the arms of the multicopter are merged with the bottom joint of the cage and secured before flight by the locking mechanism of the cage.

The battery and the autopilot are housed in a frame directly connected to the bottom joint of the cage. The autopilot is the PixHawk board with PX4 software framework.

In order to enhance further user safety, the drone is equipped with a mechanism that cuts the power to the propellers as soon as the cage is open for loading/unloading operations. The safety mechanism comprises two switches that are installed next to the side locking mechanism, between the segments of the cage (Fig. 3.5B-C). As soon as the cage is open, they automatically disengage the propulsion system.

3.3.3 **Cargo integration**

The cargo can be manually connected to the top joint of the cage with two alternative interfaces. The first interface is composed of a round-shaped lightweight net and ropes. The edges of the net are attached with ropes to the top central joint while the object is placed in the center of the net. This method is very versatile allowing objects of different shapes to be easily secured rigidly. Although, parcels are subjected to swing oscillations when they do not have a shape that allows them to lay close to the central top joint. The second type of interface – rigid boxes made out of card or thin plastic solves this problem. However, boxes are heavier than the net and many of them are required to deliver objects of different shapes and sizes (Fig. 3.6). These two interfaces are therefore complementary solutions that depend on the transported cargo. The position of Centre of Gravity with the 0.5 kg payload is presented in Fig. 3.7.

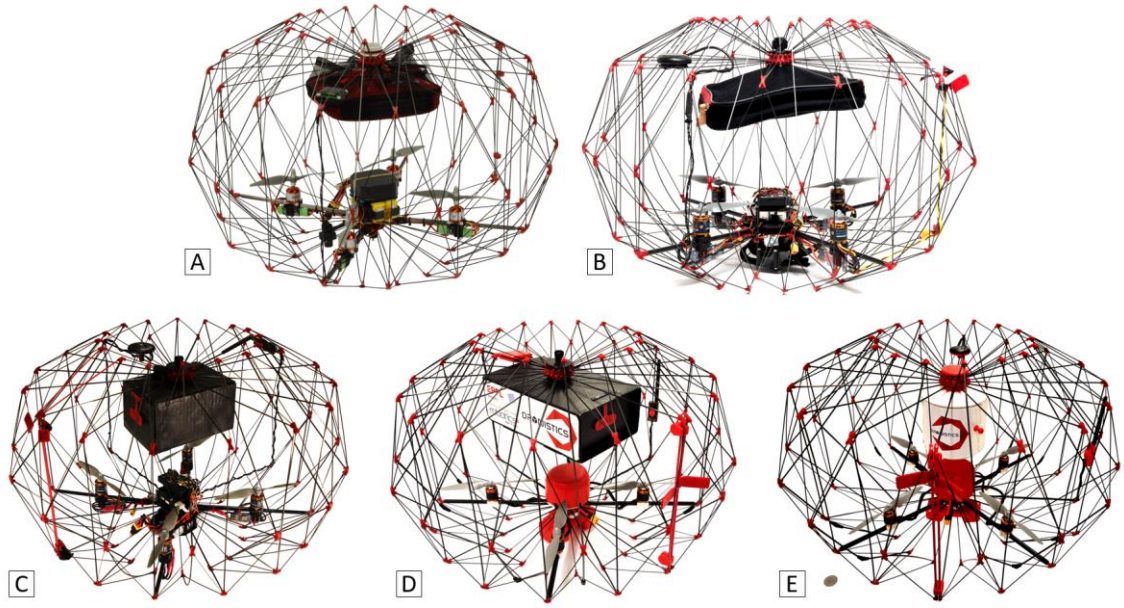

Figure 3.6 Different types of cargo interfaces. (A) A net around a first aid-kit box attached by thin ropes to the top joint. (B) A fabric bag with an integrated interface that allows locking to the top joint. (C) A small carton with thick walls. (D) A big carton with thin walls. (E) A custom-made cylindrical box with thermal insulation for delivery of thermal-sensitive payloads.

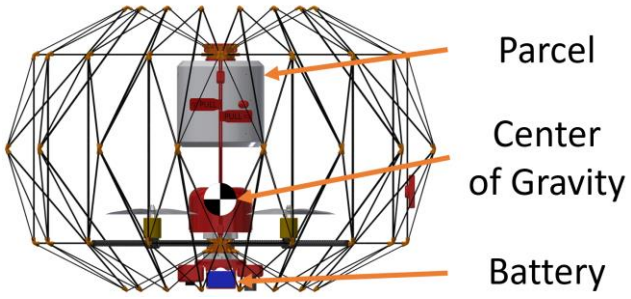

Figure 3.7 Position of the CG in PackDrone. CG is located 3 cm above plane of the propellers. The mass of the payload is 500 grams and the battery (6520mAh) 430 grams.

3.4 Scalability

Here we describe a scalability model to calculate the size of the drone given the payload and the flight time. The model takes the desired flight time and cargo mass as input and generates as output, firstly the dimensions and mass of the multicopter and secondly the dimensions of the tubes and mass of the cage (Fig. 3.8). The model consists of three sub models: mass and power model of the quadcopter, geometrical model of the cage and rigidity model of the cage.

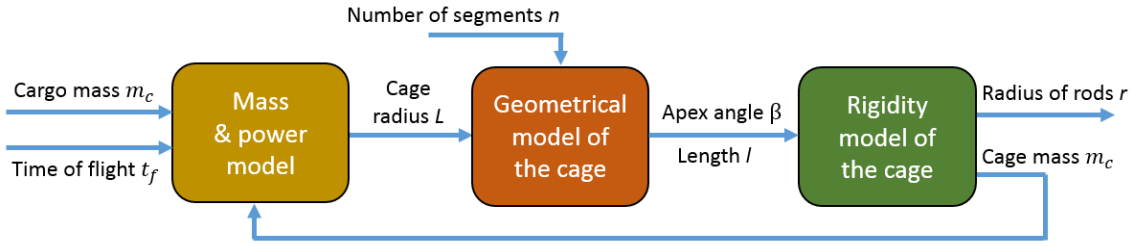

Figure 3.8 The dimensioning and scalability model of the drone composed of a mass and power model, a geometrical and rigidity model of the cage.

In the first step, a mass and power model described in [91] (see also Appendix) is used to compute the footprint of the drone for a given payload and time of flight. The resulting footprint is used to compute the length L of the tubes that correspond to the valley folds of the cage. In the second step, a geometrical model of the cage is used to compute the remaining parameters that define the cage geometry (β and l). β is the apex angle of the triangles and l is the length of the shorter arm of the triangle (Fig. 3.3). In the third step, a rigidity model computes the minimum radius of the tubes that prevents buckling of the cage under the cargo load, thus ensuring flight stability. The same model also computes the total mass of the cage considering the density of the material of the tubes. The resulting cage mass is fed back to the mass and power model where it is added to the total mass of the drone to compute a new and higher value for the footprint. The entire process is iterated until the difference between the L values of two consecutive iterations is less than 5%.

3.4.1 Mass and power model

The first step to design the cage is to define the footprint of the multicopter for a given time of flight and mass of transported cargo. To do that and to discuss scalability of the cage, the mass and power model using propulsion-system momentum theory developed in [91] is used. It is transformed to calculate a propeller diameter of the multicopter:

$$D = \frac{43.45\, t_f \sqrt{m_c}}{R_b\, e_d\, FM \sqrt{\delta\, n\, \pi\, R_c}} \tag{3.1}$$

where t_f is the time of flight, m_c is mass of the cargo, R_b is the ratio between mass of the battery and a take-off weight, e_d is energy density, FM is a figure of merit, δ is air density, n is number of propellers, R_c is the ratio between the mass of the cargo and take-off weight.

Given the radius of the propellers, the radius of the footprint of the quadcopter can be calculated from aerodyanmic considerations. As discussed in [92] the space around the propellers should be around $\sqrt{2}$ times the propeller's radius in order to avoid vortex interferences between the propellers. Moreover, additional clearance (10% of the diameter) arround the perimeter of the

footprint of the multicopter was allowed to provide safety for human fingers during in-hand landing.Thus, the radius of the quadcopter is calculated:

$$R_{quadcopter} = 1.59\ \mathrm{D} \tag{3.2}$$

The values of the mass ratios in [91] adopted for high-payload capabilities are as follows: R_b=22%, $R_c = 50\%$, R_s=28% (ratio between the mass of the structure and the total take-off mass). We kept the ratio R_b=22% and changed the two other ratios, taking into account the additional mass of the cargo. The remaining value is divided equally, thus R_c and R_s are equal to 39%. After each iteration, the added mass of the cage to the total take-off mass changes ratios R_c , and R_s. Values of parameters assumed in the model: *FM*=0.333 (measured for the motor and propeller used in the prototype); the time of flight t_f =10 minutes; the battery energy density e_d=162.5 Wh/kg; the air density δ=1.2 kg/m^3; the number of propellers *n*=4.

3.4.2 Geometrical model of the cage

After calculating the radius of the footprint of the multicopter, which is equal to dimension *L* of the cage, the number of segments is chosen and other dimensions of the cage can be calculated: the apex angle β, and the shorter arm of the triangle *l*.

As stated before, the number of segments of the cage has to be divisible by the number of arms of the multicopter. A relation has to be respected in order to design the foldable cage because β has to fit within a certain range. Details of these relations are presented below.

In the folded state of the cage, the free space between the central top and bottom joints, the dimension *h* (Fig. 3.3C) is left on purpose as a place for components of the central part of the robot (autopilot, battery, etc.):

$$h = L(1 - 2\cos(2\beta - 180°)) \tag{3.3}$$

Equation 3.3 allows us to conclude that β has to be bigger than 120° to leave space for components. As was presented in Section 3.3, the arms of the quadcopter are integrated directly into the structure of the cage. To facilitate this integration, the vertical and horizontal *L* tubes presented in Fig. 3.3B have to be perpendicular (α=90°). To keep this position of tubes β cannot be greater than 135°.

It is important to remember that β changes with the chosen number of segments of the cage and thus, *h* can be changed only by changing *L* for a given number of segments. Table 3.1 presents values of apex angles β for different numbers of segments. The values that are crossed out do not fit in the range discussed above.

l is the length of the shorter arm of the triangle (rod marked with black color in Fig. 3.3A) and it is dependent on the chosen *L* and β angle:

$$l = \frac{L}{2\sin\left(\frac{\beta}{2}\right)} \tag{3.4}$$

TABLE 3.1 EXAMPLE VALUES OF APEX ANGLES FOR DIFFERENT NUMBERS OF SEGMENTS.

Multicopter type	Number of segments 'ns'														
	4	6	8	12	16	18	20	24	28	30	32	36	40	42	44
	Apex angle 'β'														
Quadcopter	~~70,53~~		~~101,57~~		123,86		126,92	129,20	130,65		131,62	132,57	132,80		133,17
Hexacopter		~~88,84~~		~~116,02~~		125,27		129,20		131,18		132,57		133,00	
Octocopter			~~101,57~~		123,86			129,20			131,62		132,80		

3.4.3 Rigidity model of the cage

To calculate the mass and volume of the cage, the radius of the tubes of the cage should be found. The goal is to find the lightest tubes that will not buckle under the load of the cargo, thus will keep the cargo in a stable position during the flight. To do this, we should find the outer radius of the tube knowing its material properties. We assumed constant wall thickness of the tube of 0.5mm in the model (commercially available). The cargo attached to the top central joint of the cage is kept in position due to the rigidity of the tubes AC, marked in red in the single segment (Fig. 3.9). To emphasize the importance of this tube for the rigidity of the cage, we assume that this tube is removed. Thus, the pyramid EFDC at the top part of the cage would just freely rotate around the axis joining the points E and F. This means that the load from the cargo will be applied mainly to the tube AC. Finding the radius of the tube AC is therefore crucial to determine the rigidity of the cage with the cargo attached to the central top joint.

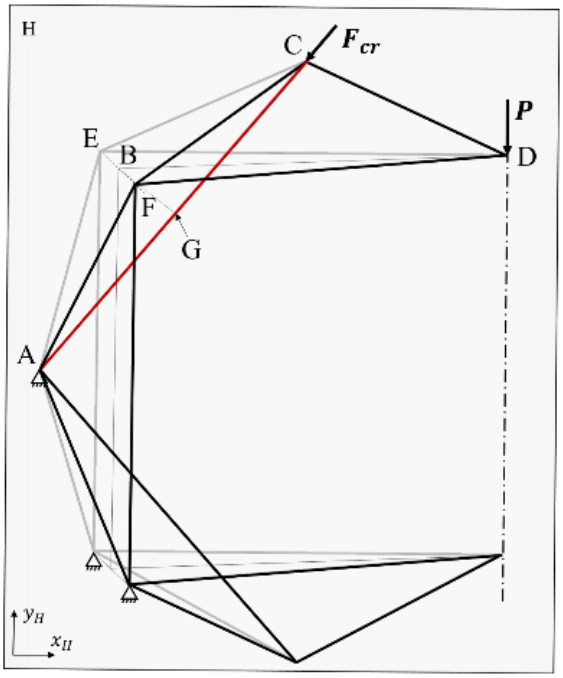

Figure 3.9 The basic segment of the cage. A view with the distribution of forces on the plane *H*. The visible rods are in front of the plane.

To simplify the design, the calculated radius *r* for the tube AC is also used for the other tubes in the cage. Knowing *r*, the mass and the volume of the cage in the folded state can be calculated. A tube under vertical load starts to buckle after reaching a certain force called Euler Buckling load, F_{cr}.

To calculate this force for tubes pinned on both sides, standard beam theory is used [93]:

$$F_{cr} = \frac{\pi^2 E(\frac{\pi(R^4 - r^4}{4})}{L^2} \tag{3.5}$$

Where E is the Young's modulus of the material, $\frac{\pi(R^4 - r^4)}{4}$ is the tube's area moment of inertia (R is outer radius, r is inner radius), L is the length of the tube.

The critical force F_{cr} acting along the rod AC under the desired load of the cargo should be calculated. To simplify calculations, the geometry of a single segment is presented in 2D (Fig. 3.9).

To calculate F_{cr} a simple equilibrium of forces is used:

$$F_{cr} \cdot BG = P \cdot BD \tag{3.6}$$

Where BG and BD are distances from forces F_{cr} and P to rotation point B. The assumption is that the point B is fixed.

P is the force acting on the basic segment of the cage, coming from the weight of the cargo:

$$P = \frac{s_f m_c g}{n_s} \tag{3.7}$$

Where m_c is the mass of the cargo, $n_{s,}$ the number of segments, g, the gravitational acceleration. The rod starts to buckle just after exceeding the critical force. Therefore, to ensure rigidity of the cage during flight maneuvers with the required cargo on board, a safety factor s_f is applied.

Distances BG and BD are found from geometrical relationships in the basic segment of the cage (Fig. 3.9):

$$BD = L\cos(\frac{\pi}{n_s}) \tag{3.8}$$

$$BG = \sqrt{\left(\frac{L}{2\sin\left(\frac{\beta}{2}\right)}\right)^2 - \left(L\sin\left(\frac{\pi}{n_s}\right)\right)^2 - \left(\frac{L}{2}\right)^2} \tag{3.9}$$

Now r can be computed by combining the above presented equations.

Knowing r, the mass of the cage composed of tubes and joints is calculated from:

$$M_{n_s} = n_s\, \varrho\, \pi\, r^2\, (10l + 5L) + (5\, n_s\, m_{joint}) \tag{3.10}$$

Where ϱ is density of the material of the rod and m_{joint} is the mass of one joint.

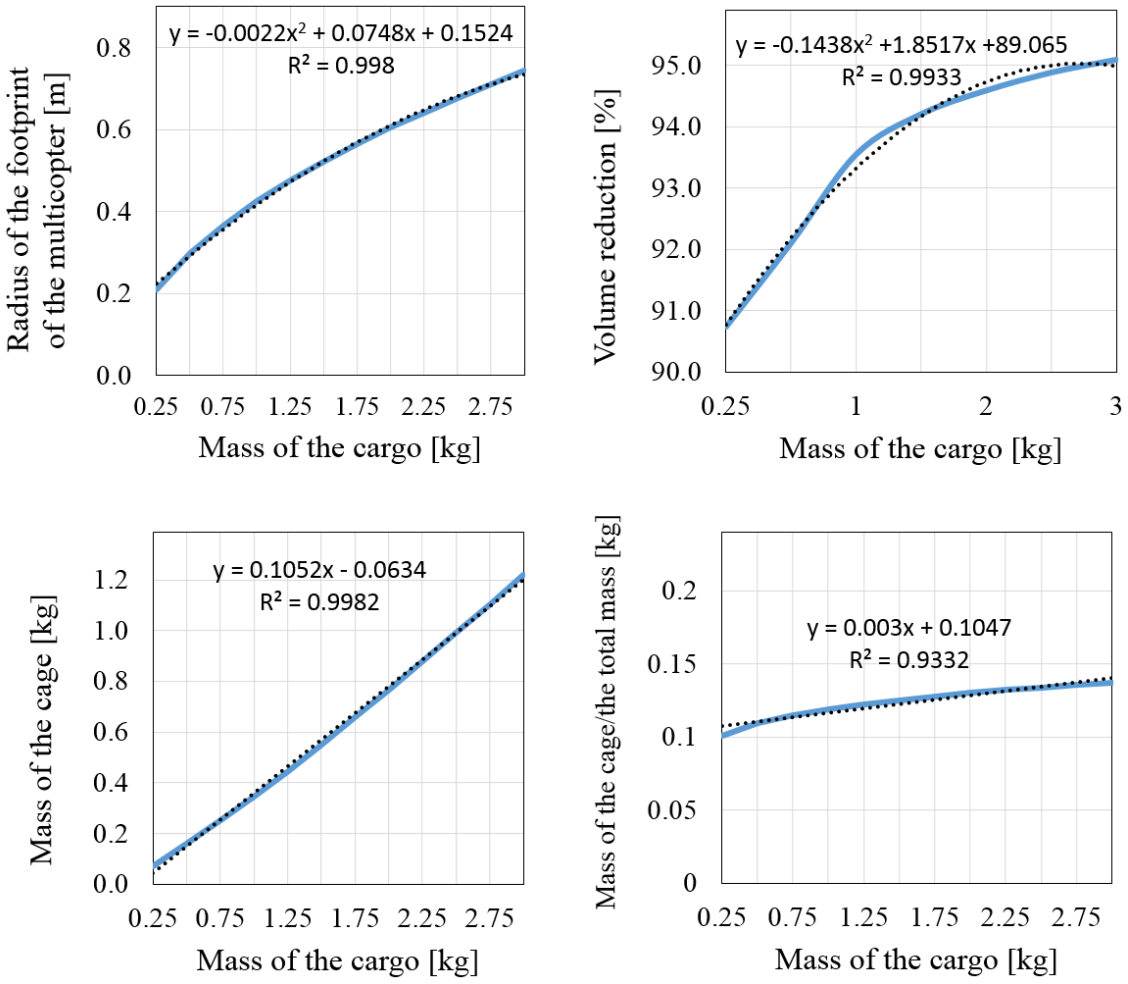

Figure 3.10 The plots present different parameters of the drone as a function of the mass of the cargo. Parameters: (A) Radius of the footprint of the multicopter calculated from equation 3.2. (B) Volume reduction is the ratio between the volume of the deployed and folded drone. (C) The mass of the cage. (D) The ratio between the mass of the cage and the total mass of the drone. The dotted black lines show the trend lines, which are the curves of the best fit.

The model (equation 3.2) predicts that the radius of the footprint of the multicopter grows more slowly than the mass of the cargo (Fig. 3.10A). For example, when the cargo's mass increases 3 times, the radius of the footprint of the multicopter increases less than 2 times. In parallel, the volume reduction of the folded multi-copter decreases with cargo mass (Fig. 3.10B). Both cases reveal that the drone can be scaled up well in terms of size.

The mass of the cage grows linearly with the mass of the cargo (Fig. 3.10C). The model also predicts that the ratio between the mass of the cage to the total mass increases slowly and linearly with the cargo mass (Fig. 3.10D). The plots C and D are plotted by combining equations 3.4-3.7 and 3.10.

The same behavior as presented in Fig. 3.10D can be observed when the time of flight is changed for a given payload. The cage to total mass ratio increases with the time of flight because of the increased dimensions.

These results reveal that the cage can be conveniently scaled up for larger payloads.

3.5 Experimental validation

3.5.1 Cargo integration

The model predictions match the values measured on the prototype designed for 0.5 kg cargo and 10 minutes of flight (Table 3.2). In a series of 15 flight tests (hovering on the spot) with 0.5 kg payload, we measured 10 minutes $\pm 1\%$ minute of hovering time, which is comparable to the 10 minutes predicted by the model.

A 10% difference can be explained by the drag induced by the cage on the airflow generated by the propellers (see next section), which is not considered in the model. Moreover, the test for distance coverage was performed. The drone flew a distance of 2 km with a 0.5 kg parcel. The distance coverage was tested outdoors with 10 degrees-inclination of the multicopter around the pitch axis in the forward flight.

TABLE 3.2 MASS COMPARISON BETWEEN PREDICTED AND OBSERVED VALUES OF THE PROTOTYPE

Component	Mass [kg]		Difference
	Model	Prototype	%
Multicopter w/o battery and cage	0.466	0.564	17.4
cage	0.154	0.150	-1.0
battery	0.316	0.319	0.94
cargo	0.5	0.5	0.0
Total	1.436	1.53	6.14

The largest difference between predicted and measured values (17.4%) concerns the mass of the multicopter (excluding the battery and the cage). However, this difference could be reduced using different materials or an alternative design for the central bottom locking mechanism, the battery holder or by using expensive materials, such as carbon fiber that is stronger and lighter. Nevertheless, the difference between the predicted and observed total mass is only 6.14%.

In order to measure the stiffness of the cage under loading, the top central joint (the place of cargo attachment) has been incrementally loaded up to 1.4 kg while measuring its vertical displacement. The results indicate that the cage remains stiff up to 1.2 kg, but collapses for heavier loads (Fig. 3.11). The vertical displacement is reversible and is due to the buckling of the vertical and oblique top tubes (see yellow dashed lines in Fig. 3.11B). These results indicate that the cage is sufficiently rigid and thus stable in flight, for the desired cargo load of 0.5 kg.

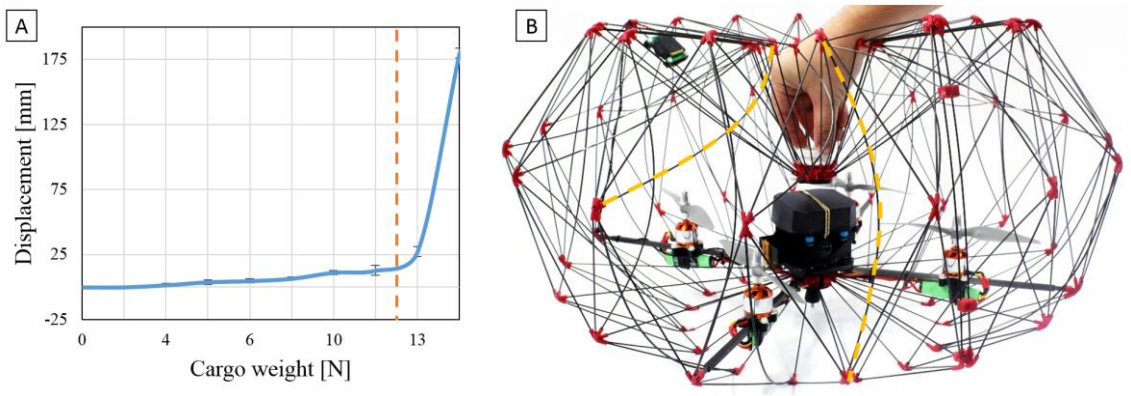

Figure 3.11 (A) The plot presents experimentally measured displacement of the top central joint of the cage under different cargo loads (continuous blue line). The tubes of the cage start to buckle significantly under a load of 1.2 kg (dashed red line). Therefore, the cage can withstand the desired payload of 0.5 kg with a safety factor of 2.4. (B) The cage under a load above of 1.2 kg with displaced central top joint. The yellow dashed curves mark two representative buckled tubes.

3.5.2 **Effect of the cage on drag**

Wind tunnel tests were performed to show how the cage and a parcel (size 28 cm x 28 cm x 6 cm) increase the drag of the drone. We tested the drone in four different configurations: (i) unladen drone without the cage, (ii) unladen drone with the cage, (iii) laden drone without the cage, (iv) laden drone with the cage. The propellers were removed for these tests. Additionally, we compared (Table 3.3) our results with existing values in the literature of similar sized drones tested by [81][94].

The wind tunnel used was an open loop, blower configuration wind tunnel. The drone was mounted on an arm with a load cell. The interface between the arm and the drone could be changed, allowing positioning of the drone at eight different pitch angles, from 0 to 40°. The rotation of the drone was changed by rotating the drone on its mount. The drone was half scale (diameter 33 cm and height 21cm) to fit into the wind tunnel with cross-sectional dimensions of 44.5 x 30 cm. This created a 4.5 cm gap in the vertical direction and a 5.7 cm gap in the horizontal direction between the drone and the wall of the wind tunnel. Due to a high blockage ratio of 28.5% (defined as its frontal area divided by the total area of the wind tunnel), correction factors were applied for all measured results. The blockage correction follows the method outlined in [95] for bluff bodies.

The drag coefficient is nondimensionalised using the motor-to-motor area of the drone as a reference. For a comparison to other results in the literature, the equivalent flat plate area (drag coefficient times reference area of the airframe) is also provided. This is a value often used in rotary wing vehicle literature.

The results show that the cage increases the drag four times compared to the same quadcopter without cage. However, comparing our caged drone to a DJI Phantom 3 or 3DR Solo (without protective mechanisms around propellers) the average drag coefficient is increased only by one and a half times. This is an acceptable value considering the advantage of the cage in terms of user safety.

TABLE 3.3 AVERAGE DRAG COEFFICIENT COMPARISON BETWEEN OUR CAGED DRONE AND OTHER DRONES OF SIMILAR SIZE.

Name	Averaged drag coefficient	Equivalent flat plat area [m^2]
Unladen drone without cage	0.125	0.006
Unladen drone with cage	0.497	0.024
Laden drone without cage	0.723	0.035
Laden drone with cage	1.226	0.060
DJI Phantom 3 [20]	0.326	0.020
3DR Solo [20]	0.353	0.030
3DR Iris + [20]	0.271	0.029
Straight Up Imaging Endurance [20]	0.160	0.042
Caged drone [8][1]	0.847	0.092

[1] For the [81] drone, the motor-to-motor dimensions were estimated from the total diameter of the drone.

The impact of the cage on the drag can be quantified by an averaged difference between the equivalent flat plate areas of the drone, with and without the cage, for both the laden and unladen cases. This is a value of 0.00215m^2, being the average of the difference between the caged and uncaged drone with the package and the difference between the caged and uncaged drone without the package. Taking the average of the difference between the laden and unladen drone with the cage and the laden and unladen drone without the cage gives a value of 0.0325m^2, which is the increase in flat plate area that results from the package. This indicates that the package has a larger effect than the cage. If a similar parcel were to be added to a DJI Phantom 3 or 3DR Solo (without protective mechanisms), they would have similar drag values to the laden drone with the cage.

This allows us to conclude that while the cage has a measurable effect on the drag of the airframe, its impact on the overall aerodynamics is of a similar scale to the impact of a parcel. The overall drag of the airframe with a parcel and the cage is comparable to commercial systems carrying a similar parcel.

3.5.3 Effect of the cage on thrust

The density of the cage structure can be modified to find an optimal trade-off between safety and flight efficiency. The prototype is composed of 16 vertical segments with an inter-tube distance of 7.5 cm. This value ensures that the fist of an adult male cannot be inserted horizontally into the cage. Moreover, the number of tubes placed below the propellers cause drag and turbulences that reduce the total thrust generated by the four propellers from 1.2 kg (without the cage) to 1.06 kg (with the cage). We find this thrust-loss acceptable considering the protection benefits.

3.5.4 **Folding procedure**

Before folding the drone, the top and bottom locking joints of the cage have to be unlocked (Fig. 3.5C), which takes about 10 seconds.

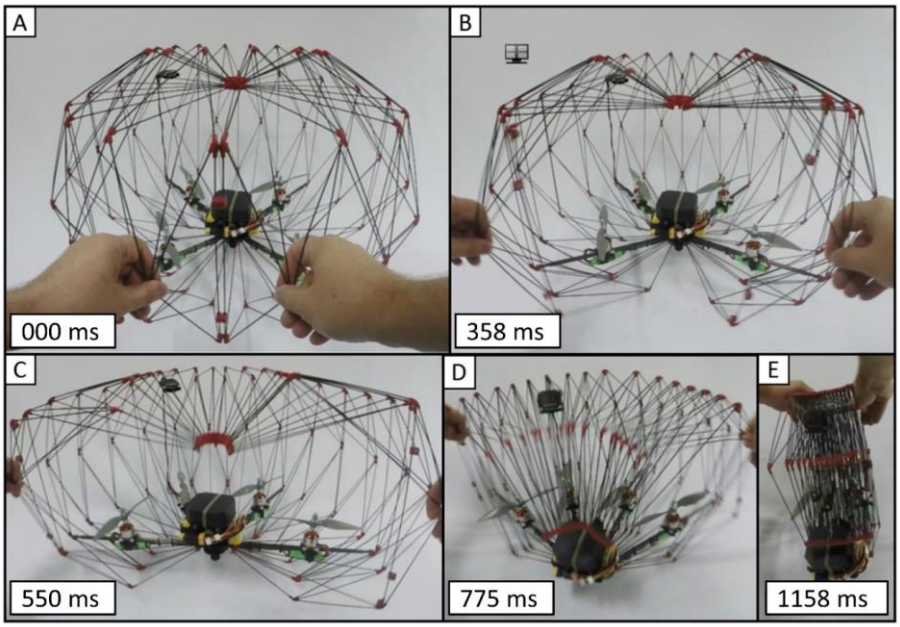

Figure 3.12 Multiple snapshots from a video captured by a GoPro HERO3 (120 fps) showing unlocking of the side locking mechanism and the last folding step of the drone. (A) The drone fully deployed. (B) The drone 25% folded. (C) The drone 50% folded. (D) The drone 75% folded. (E) The drone fully folded.

Afterwards, the folding process is carried out as illustrated in Fig. 3.12 and shown in the attached video. First, the user has to unlock the side locking mechanism while opening the cage. Two adjacent segments of the cage have to be pushed away from each other to fold the cage and integrated quadcopter. The folding procedure takes 1.2 s. The deployment process takes the same amount of time and requires the same steps but in reverse order.

Table 3.4 presents a comparison of the dimensions of the drone in deployed and folded configurations along with those of a deployed airframe of the foldable quadcopter without the cage. The values given in the table are the dimensions of a cuboid box containing the drone. The cuboid shape approximates the encumbrance of the drone during transportation or while stored on a shelf. Thus, the foldable drone can reduce its storage volume by 92%. The deployed quadcopter without the cage has only a 14% smaller volume than the folded configuration with the cage.

TABLE 3.4 SIZE COMPARISON BETWEEN FOLDED AND DEPLOYED DRONE WITH THE CAGE AND A NOT-FOLDABLE QUADCOPTER WITHOUT THE CAGE

	Size [m]	Footprint [m^2]	Volume [m^3]	Weight [g]
Deployed configuration with the cage	0.65 x 0.65 x 0.43	0,423	0,182	1034
Folded configuration with the cage	0.31 x 0.38 x 0.12	0,118	0,014	
Deployed configuration w/o the cage	0.35 x 0.35 x 0.1	0,123	0,012	640

3.6 Conclusions

We have developed a safe foldable drone for cargo transportation. The quadcopter is equipped with an all-around cage that protects people and the drone. The drone can be manually folded for easy storage and transportation. Moreover, in the folded state, the electromechanical components of the quadcopter are protected inside the structure of the folded cage. To ensure safety for people while removing a parcel from the cage, the drone is equipped with security switches that disengage the propulsion system while the cage is open. The wind tunnel tests revealed that the overall drag of the airframe with a parcel and the cage is comparable to unshielded commercial drones carrying a similar parcel. Model-based predictions on the dimensions of the drone match the physical prototype and suggest that the proposed design could scale up to fly 2 kg cargos over 15 km, which would cover 86% of the deliveries made by Amazon.com, Inc. [19].

Future work should investigate other shapes of the cage, adapted for special parcels, such as documents. Delivery of flat documents could allow us to reduce the height of the drone, thus the length of the vertical and oblique tubes in the cage. This could reduce the weight, drag of the cage and increase the time of flight. To protect the drone from damage caused by falls from high altitudes, a parachute should be installed at the top central joint outside of the cage. In order to verify receipt of a package or allow drones to precisely land, additional sensors, such as cameras will be installed on the cage. To facilitate the usage of the drone for less experienced users, the unlocking mechanisms should be redesigned for easier access to the cargo placed inside the drone and for faster folding and deployment of the cage. Our approach with a foldable protective cage has the potential to increase cargo deliveries to people. Furthermore, we believe that our solution could revolutionize person-to-person transportation using drones.

Chapter 4

The software to navigate drones, field deployments and user interaction

DRONES are rapidly becoming an affordable and often faster solution for parcel delivery than terrestrial vehicles. Existing transportation drones and software infrastructures are mainly designed by logistics companies for trained users for use in either long-range (<150km) or last-mile delivery (<20 km). This chapter discusses *Dronistics*, an integrated software and hardware system for last-centimeter (<5 km) person-to-person delivery using cargo drones. The system was conceived to be intuitive and intrinsically safe to enable short distance deliveries between inexperienced users. Dronistics is composed of a safe foldable drone *PackDrone* and a web application software *SimplyFly* to intuitively control and track the drone in real time. In order to assess Dronistics' user acceptance, we conducted 150 deliveries over one month on the EPFL campus in Switzerland. Here we describe the results of these tests by analyzing flight statistics, environmental conditions and user reactions. Moreover, we also describe the technical problems that occurred during flight tests and solutions that could prevent them. At the end, we present additional use cases, demonstrations and future applications.

The material presented in this chapter is adapted from:

[96] **P. M. Kornatowski,** A. Bhaskaran, G. M. Heitz, S. Mintchev, and D. Floreano, “Last-Centimeter Personal Drone Delivery: Field Deployment and User Interaction,” *IEEE Robotics and Automation Letters,* 2018.

4.1 Introduction

Recent years have witnessed an exponential rise in interest in delivery drones and mainly multicopters, due to their capability to effectively overcome obstacles or traffic jams, to rapidly reach remote locations and to take off and land in cluttered environments. Therefore, logistics companies have started to explore the possibility of using aerial delivery as a faster and more cost-effective alternative to terrestrial transportation [1][6]. Examples include Amazon.com's tests of product deliveries to homes directly from warehouses in the United Kingdom [97], DHL's mountain deliveries of emergency medical supplies using its Parcelcopter [98], Alphabet's burrito deliveries to Australian homes with its Project Wing drones [99], Swiss Post's experiments with transportation of lab samples between hospitals in Lugano, Switzerland [100] and Zipline's transportation of blood from central storehouses to remote hospitals in Africa [101].

All these aerial delivery services were developed for trained employees of logistics companies for business-to-business (B2B) or business-to-client (B2C) operations. Consequently, the software framework used to control and navigate delivery drones is proprietary and not designed for inexperienced users. In addition, most of the drones are designed for long-distance delivery (around 150 km) or last-mile delivery (around 20km) [102]. Covering long distances requires bulky platforms that do not allow for personal delivery due to storage and transportation difficulties. Furthermore, take-off and landing spots should be specially prepared and must be located at safe distances from users to prevent contact with dangerous unshielded propellers. Thus, these drones do not deliver directly to people's hands in the way that mail carriers or courier services often do.

Figure 4.1 Three phases of delivery on the EPFL campus (A) The PackDrone just before take-off at the sender location. The sender is operating the software from a tablet. (B) The drone is flying above the EPFL campus (C) The drone in the recipient location. The recipient is unloading a parcel.

In this chapter, we present an integrated hardware and software solution for last-centimeter, short-range delivery by which people can exchange goods safely through the air. Items arrive directly to the recipients' hands without the need of intermediate logistics companies, dedicated infrastructure or trained operators. This approach could be suitable for person-to-person exchanges within private grounds, such as large governmental or industrial campuses, construction sites, hospitals or harbors. Additionally, last-centimeter delivery may be suitable for dispatching parcels vertically, to the top of cranes and scaffoldings or to the bottom of deep opencast mines.

The proposed Dronistics system consists of a safe quadcopter called the *PackDrone* [78] and a customizable software framework called *SimplyFly*. The *PackDrone* has a foldable structure that shields the propellers to ensure people's safety. Additionally, folding the origami-inspired structure significantly reduces its volume, allowing for easy storage and transportation in small containers. In parallel, the web-based software allows recipients and senders to intuitively control parcel exchanges and monitor flight trajectories in real-time while ensuring flight safety.

The literature contains several studies of the societal impact of drones [103], drone use in the context of governance, ethics and privacy [104], growth of the drone market [105], possibilities of using drones in urban environments [106], drone efficiency [1], the economic benefits for last-cm delivery with trucks [107] and the dangers of falling drones [108]. However, no field studies have yet investigated practical aspects of drone delivery such as the behavior of inexperienced users when operating delivery drones, the reliability of the hardware and software and the impact of weather conditions on day-to-day operations.

The goal of this chapter is to present the results of the deployment of Dronistics on the campus of the École Polytechnique Fédérale de Lausanne (EPFL) in Switzerland, focusing on the aforementioned issues of inexperienced user behavior, hardware and software reliability and the effect of changing weather conditions on daily operations. We conducted 150 delivery flights between July and August 2017. This real-life field study was largely successful, but also highlighted critical issues in last cm-delivery that must be addressed in future developments.

4.2 The safe foldable PackDrone used during field test

During the field test on the EPFL campus the *PackDrone* v.1.1 (for more details check Appendix A) presented in Fig. 4.2 was used. The small goods-holding carton was tailored to the delivered items, e.g. PCB, 3D printed parts. The box can be opened on the side to remove the parcel (Fig. 4.5F) or can be entirely removed from the drone.

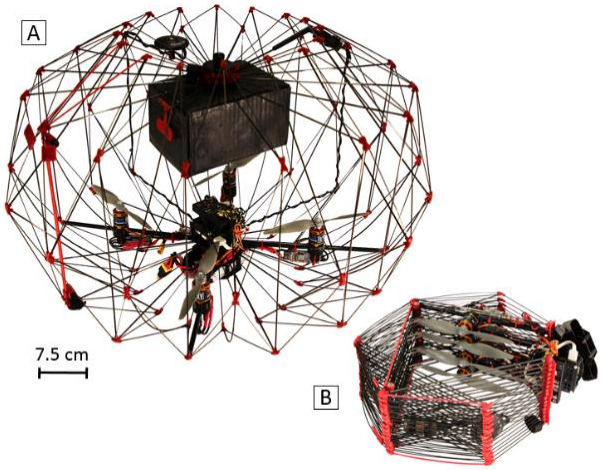

Figure 4.2 The foldable PackDrone for last-cm delivery. (A) Deployed configuration with the enclosed carton containing a parcel. (B) Folded configuration with a volume reduction of 92%.

4.3 The Dronistics software

The Dronistics software framework has three key features to ensure inexperienced users can use delivery drones intuitively. First, it makes the delivery process fully automatic, minimizing the number of operations that users must perform. Second, it is compatible with multiple operating systems and drones in order to facilitate portability and adoption. Third, it ensures safe communication and privacy of a user's personal data. To achieve these key features, the Dronistics software framework is based on a web application [109] and the overall architecture composed of three main parts, a front-end layer composed of the Sender and Recipient Applications; a back-end layer composed of the Dronistics Server and a Drone layer composed of the drone software (Fig. 4.3).

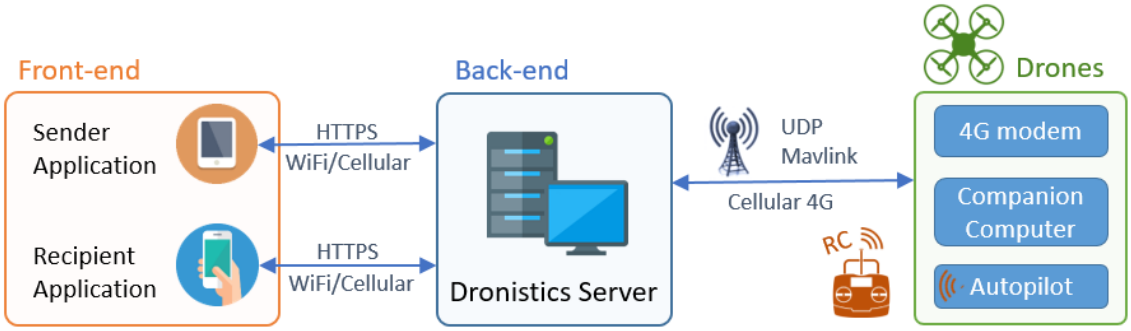

Figure 4.3 The architecture of the Dronistics software framework

The front-end software is hosted on a mobile device, such as a smartphone, tablet or laptop. It has a simple graphic user interface for sending and receiving parcels with a small number of user commands. This interface also displays the position of the drone in real time. The software is compatible with different operating systems such as macOS, Android, Microsoft Windows and Linux. The back-end software is hosted on a secure server and is responsible for automating the whole delivery process. It computes the drone's path, performs safety checks and handles real-time communication between the user and the drone. Moreover, all the personal data of users are stored and processed on this secured server. The drone software is hosted on a companion computer on-board the drone and creates a bridge between the drone's autopilot and the Dronistics server through an internet connection. The companion computer is independent of the specific autopilot software and hardware, ensuring the broadest compatibility. Finally, a connection to the internet via the omnipresent GSM network enables control and real-time tracking of the drone over the whole flight path. The system is easily scalable to multiple drones flying simultaneously, given sufficient access to servers and communication bandwidth. The three software layers and their features are described in detail in the following sections.

4.3.1 Front-end Layer: Sender and Recipient applications

The sender and recipient applications were developed using front-end tools (HTML, CSS, and JavaScript) with a responsive user interface in order to create an accessible and intuitive software with secure communication. This allows the applications to run in any browser on any portable device independently of its operating system. Users can access the corresponding application by navigating through the respective URLs on the Dronistics Website. Asynchronous JavaScript,

XML (AJAX) and is encrypted with SSL certification for enhanced security establishes all communication between the front-end and back-end.

The Sender Application is a web-application that displays all the information and functions in a single window. It is currently designed to allow parallel dispatching of multiple drones to multiple users. To access this application, the user has to register and/or login to the Dronistics system as a sender. The Sender Application is composed of four panels A, B, C, and D (Fig. 4.4). Panel A is a map (interfaced with Google Maps), that shows the real-time position of the drone(s), the location of the user(s) and the paths of active deliveries. Panel B shows the list of active deliveries and all drone control commands are issued from this panel only. This panel also shows the wind speed from various nearby weather stations. Panel C contains the list of drones owned by the sender. A sender can add drones to the application by specifying the drone ID. Each drone can be online or offline. Panel D contains the list of pending requests with the name of the user and the requested item.

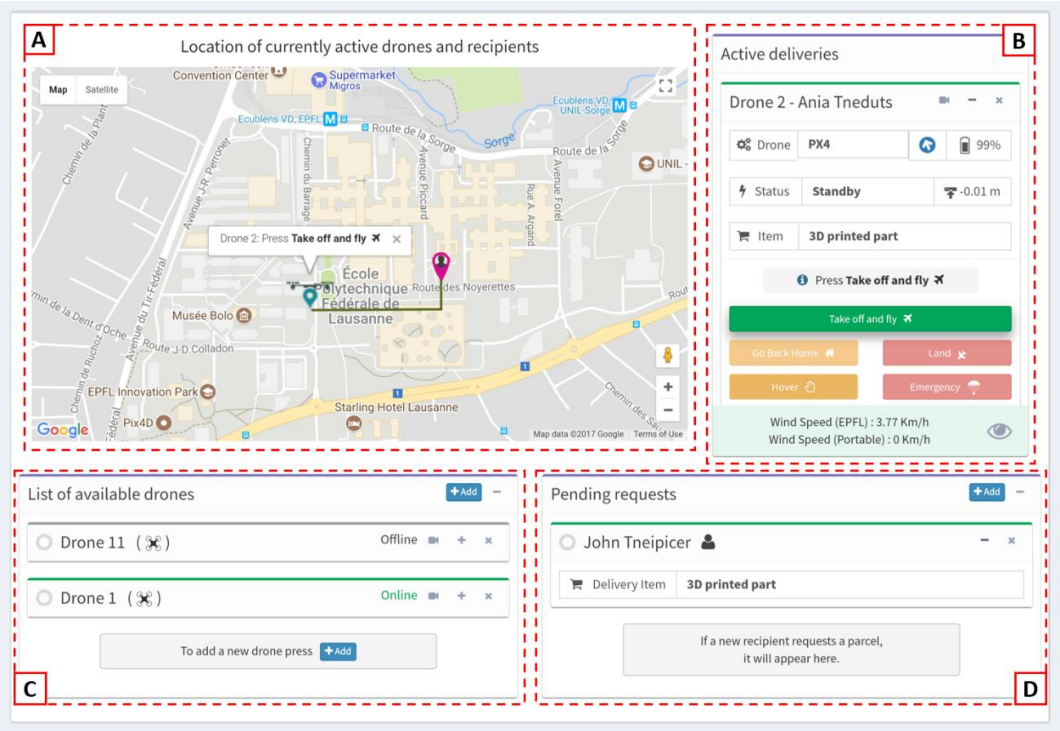

Figure 4.4 The interface of the sender web application with four panels, A to D. (A) A map with the real-time position of drone(s), the location of users and the paths of active deliveries. (B) The list of active deliveries. (C) The list of drones owned by this specific sender. (D) The list of pending requests. The location of the specific recipient is shown on the map as a pink user icon.

The entire delivery process requires only three steps. In the first step, the sender registers and/or logs in to the system. In the second step, the sender receives a request for delivery and assigns a drone to the recipient. Once the assignment is done, the drone and recipient disappear from their respective locations in panel C and D and appear in the active delivery in panel B. For example, in Fig. 4.4B, the sender assigned Drone 2 to recipient Ania Tneduts for delivery of 3D-printed parts. The Active deliveries panel of the Sender Application also shows real-time telemetry data, such as battery status, altitude and delivery status. To ensure reliable delivery even in the event of communication disruption, the back-end server computes the entire flight plan and uploads it

to the drone before take-off. In the third and final step, the sender loads the requested goods into the drone and triggers the mission by clicking on the *Take Off and Fly* button. Additionally, the sender can issue other commands during the mission such as *Go Back Home* (drone returns to the sender's location), *Land* (drone lands in its current position), *Hover* (drone holds its position in the air) and *Emergency* (drone disengages the propulsion system and deploys a parachute, if installed).

The Recipient Application guides a user through the delivery process in three simple steps. The current design allows requesting one delivery at a time. The first step is to register on or login to the recipient web application (Fig. 4.5A). In the second step, the recipient selects the required delivery from the list of senders and deliveries and specifies delivery location using the map. After the recipient completes the second step, the sender receives the request and sends the drone with the specified item. The recipient is informed (Fig. 4.5C) and can monitor the drone in real-time during the onward-flight (Fig. 4.5D and 4.5E). In the field tests reported below, the second step was further simplified by specifying a fixed delivery location due to security constraints (Section 2.4) and then, the application guided the recipient towards the delivery location (Fig. 4.5B). The third step consists of retrieving the parcel and sending the drone back. This step is guided by a short photo tutorial displayed on the screen (Fig. 4.5F and 4.5G). On pressing the *Send the drone back* button, the web application reminds the recipient to ensure a safe space around the drone for take-off and triggers a countdown before the drone takes-off (4.5H and 4.5I). For the purpose of the delivery tests only, an additional anonymous survey form was displayed after the drone took-off in order to gather feedback from recipients.

4.3.2 Back-end Layer: the Dronistics server software

The back-end layer plans the flight path as follows: no-fly zones determined from information on surrounding obstacles (e.g. buildings, trees, or mountains) and from live meteorological data gathered from nearby wind stations are encircled on the map. The shortest path between the sender and recipient, flying tangentially around the edge of any no-fly circles lying on the trajectory is then calculated. The back-end layer also acts as a middleware between the front-end layer and the drone layer. Hence, it not only provides real-time data of the drone to the front-end but also receives operational commands such as *Take-off*, *Land*, and *Hover* from the front-end and forwards them to the drone.

Additionally, the back-end layer receives wind speed data from a wind station mounted on top of a building close to the recipient's location and transfers it to the front-end for visualization. The back-end layer resides on a Java-based Apache Tomcat Server web-server. The relational database (built using PostgreSQL) is an integral part of this layer and allows the storage of all information regarding drones and deliveries. In addition to the web-server that acts as a communication entity of the front-end, the back-end layer runs a User Datagram Protocol (UDP) thread that allows bidirectional communication between the web-server and the drones in real time. As this communication is encapsulated in an independent thread, multiple drones can communicate with the server in parallel, thereby providing scalability of the system for future applications. Additionally, the back-end layer runs on the server with a static IP address (with a public Domain Name Record), to enable back-end communication of front-end devices and drones over the internet.

4.3.3 The Drone Software

The drone software architecture, which reflects the hardware architecture, is composed of three elements: an autopilot, a companion computer and the 4G modem (Fig. 3). The companion computer is designed to be compatible with different autopilots that use the common MAVLink protocol for communication [110]. It hosts the Dronistics software and acts as an interface between the autopilot and the Dronistics server.

The autopilot controls the drone and executes the commands from the Dronistics server. Typical examples of these commands include: *Landing*, *Take off and fly*, *Emergency*, etc. In addition, the autopilot can communicate directly with the remote control of a safety pilot, who can override the Dronistics software at any time and manually control the drone. This feature is a legal requirement, which is useful in emergencies. The autopilot used for this field test is the PixHawk board with PX4 software framework.

The Companion Computer is an on-board lightweight Linux computer that communicates between the autopilot and the Dronistics server. This computer may be used for other features that cannot be handled by the autopilot, such as sensor-based obstacle avoidance or audio and video communication. The companion computer used in the field test is a XU4 Odroid board.

The 4G modem is a USB dongle for hybrid (3G and 4G) internet access of the companion computer to enable bi-directional communication between the drone and the server.

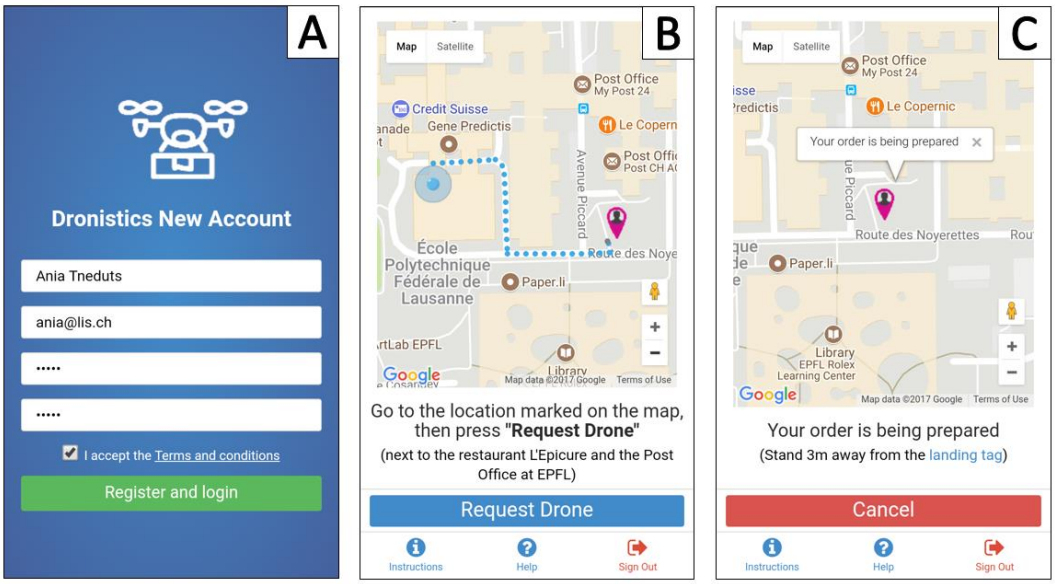

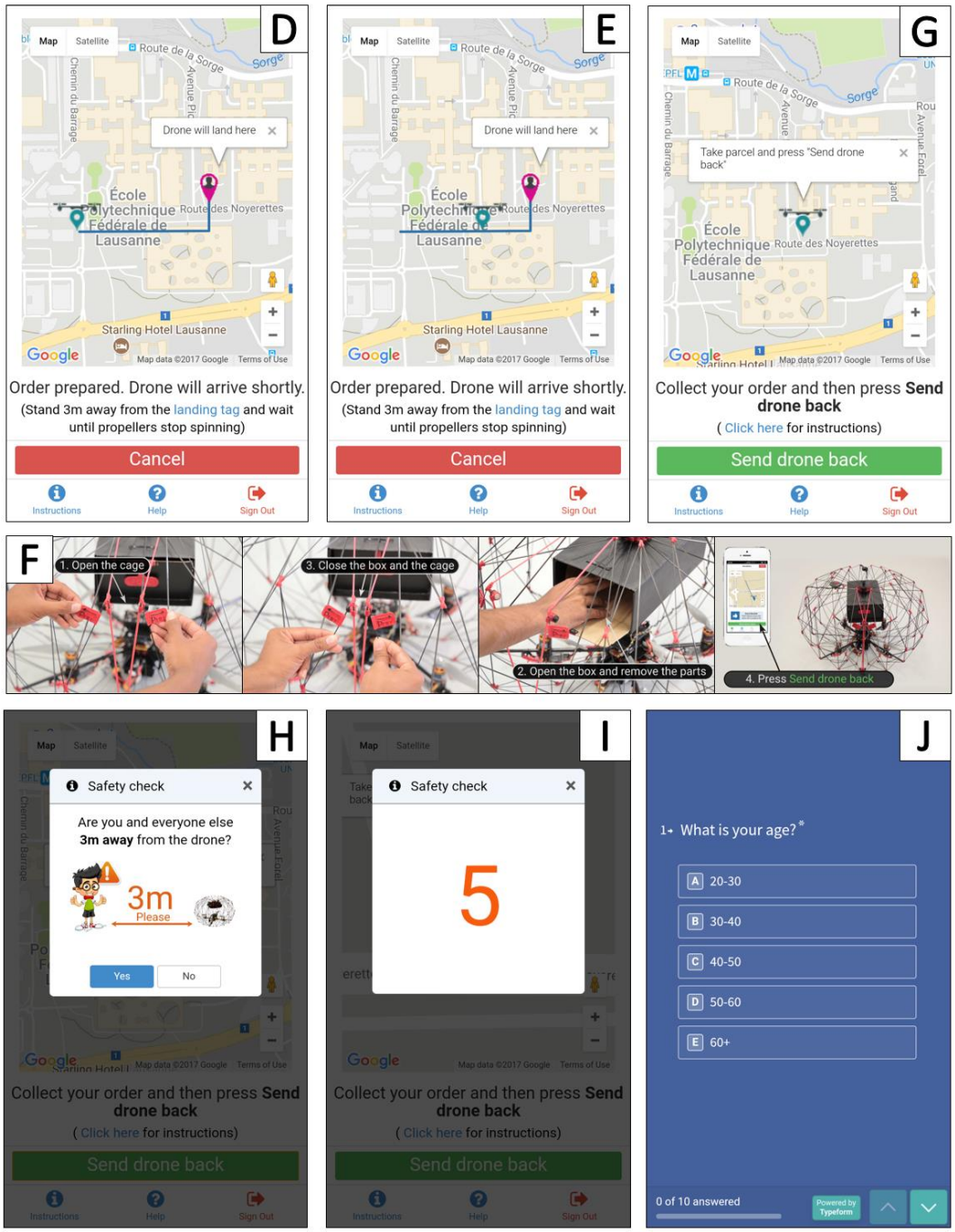

Figure 4.5 Recipient web application with the stages of delivery shown on the screen. (A) The registration screen. (B) The dotted path guides the recipient (big blue dot) to the landing spot (pink icon). (C) The web app informs that a sender is loading a drone. (D) The web app shows that the drone is matched to a recipient and is ready to fly. The flight path appears. (E) The web app shows the real-time position of the drone. (F) After the drone has landed, the web app displays a short photo tutorial explaining how to open the cage and remove the requested item from the drone. (G) The web app shows when ready to send the drone back to the sender. (H) The web app informs on securing space around the drone for take-off. (I) Countdown is launched to inform the recipient when the drone takes off. (J) When the drone takes off, a survey appears on the screen for the recipient. The web app automatically logs the user out after answering all the questions.

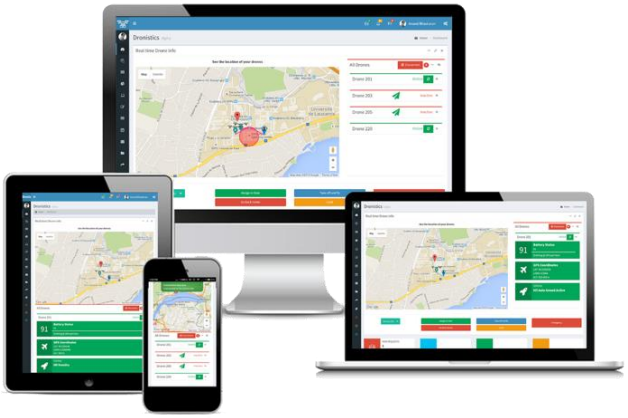

Figure 4.6 The view of the SimplyFly sender application software on different devices.

4.4 Field tests – delivery of 3D-printed parts and PCB on a university campus

The field test consisted of delivering various objects of up to 250 grams between EPFL campus employees and students. The tests were designed to comply with three regulations set by the Swiss Federal Office of Civil Aviation (FOCA) [111] and by the EPFL Security Office [112].

Firstly, drones must always be kept within a Visual Line of Sight (VLOS) and at least one operator must be able to intervene and land the drone in case of emergency. Secondly, the *PackDrone* must be operated at a distance of at least 100 meters from a crowd (defined as a gathering of 24 or more individuals) as its mass exceeds 500 grams when fully loaded. Thirdly, drone operators should have authorization from the nearby Lausanne Airport, as the EPFL campus is within 5 km of the airport grounds. The airport authorities can revoke authorization at any time in case of emergencies to prevent interference with manned aircraft traffic. To comply with the rules, we conducted the autonomous drone delivery tests between two fixed points on the EPFL campus under the supervision of three people: a safety pilot and two observers, one at the sender's location and one at the recipient's location. The green line in Fig. 4 indicates the flight path. The first point (denoted by the drone in Fig. 4.4, panel A) is the sender's location, near the EPFL campus workshops where 3D-printed parts and Printed Circuit Boards (PCB) are fabricated for all campus employees and students. The recipient's point was located near a post office at the EPFL. The flight path between the sender and user locations used a longer trajectory planned to fly over less crowded areas to reduce the risk of accidents. To ensure visual contact with the drone during the entire flight, the pilot stood at the center of the flight path, which was limited to a distance of 300 meters. A failsafe function was included to make the drone land immediately in the event of malfunction of the pilot's remote controller. We also limited the drone's speed to 6 m/s to facilitate a potential manual takeover of its controls. Additionally, we set the flight altitude to 15 meters above the ground (5 meters above the tallest building on the flight path) to allow direct line of sight with the safety pilot on the ground and provide a significant distance between the drone and any manned air traffic from the nearby airport. At the sender location, a person loaded the cargo and attended to different safety procedures. The person could trigger safety procedures from the Sender application, such as hover, land, return home or disengage the propulsion system in case of unexpected behavior. We recruited trained students to act as senders for conducting experiments to verify landing precision in the proximity of buildings, trees and a road for safety purposes. Thus, they

would be able to react quickly if the drone flew too close to obstacles or exhibited undesired behavior due to GPS signal reflections. As the method for loading and unloading the drone are very similar, the users' behavior when operating the drone was analysed at the recipient location.

Drone deliveries were carried out between 9 and 11 AM and 2 and 4 PM only to avoid flying over crowds gathering at breaks. The drone delivery service was announced to the EPFL community and a website was set up (dronistics.epfl.ch/EPFL). Interested users could register by logging their email and delivery time availability. When the requested item was ready, an email specifying the exact delivery time was automatically sent to the recipient. We gave the recipients the possibility to receive 3D-printed parts, printed circuit boards or a surprise package containing sweets. While the average weight of all the delivered items was 150g in experiments, the drone can carry up to 500g of payload. All items were placed into a box (14 x 18 x 11cm) and covered with bubble wrap to prevent items shifting during flight. The participants were free to use their own internet-connected device (smartphone, tablet or laptop). We recorded the behavior of the recipients on video for further analysis. We informed the recipients of this at registration and each person had to read and consent to the Terms and Conditions (Fig. 5A). The recorded videos were only used for internal data analysis. However, a reader could request any additional data recorded during the tests by emailing the authors. As the Recipient application provides all the necessary information, recipients were not given additional help. Nevertheless, the person recording videos acted as the second observer, reporting on dangerous situations to the safety pilot or the first observer at the sender site by walkie-talkie.

4.4.1 Behaviour of the Recipients

We expected that the recipients would follow the instructions provided in the recipient application. To test this hypothesis, we filmed 141 recipients who consented to be recorded and measured the percentage of individuals following each instruction (Table 4.1).

The analysis of the videos revealed that more than 98% of the participants followed four out of the seven instructions in the tutorial. However, only 74% of the participants monitored the flight of the drone in the web application, mainly because they were distracted - taking photographs, recording videos or staring at the drone in flight. 20% of the participants did not follow instructions displayed in the web application for removing items from the drone. Indeed, several users read the instructions in advance to keep both hands free to operate the drone. 48% did not know what to do with their portable device while operating the drone. 8.5% of the participants stopped using the web application and were unable to remove the package from the drone without help from the observer. Finally, only 6% of participants ensured a safe space around the drone before take-off. Moreover, we observed 44 non test-participants walking less than 3 meters away from the drone prior to take off. To achieve flawless unloading of the package and safe take offs, we propose to complement the current visual tutorial with voice instructions that users should find convenient to follow [113].

TABLE 4.1 INSTRUCTIONS PROVIDED IN THE RECIPIENT APPLICATION AND THE PERCENTAGE OF PEOPLE WHO FOLLOWED THE INSTRUCTIONS

Instructions in the recipient application	**Percentage**
Wait 3 metres away from the landing tag	99%
Monitor the drone's flight in the web application	74%
Follow the photo tutorial to unload the parcel	80%
Open the cage	99%
Open and close the box	98%
Step back more than 3 metres from the drone	99%
Ensure a safe space around the drone before take-off	6%

During the tests, we also observed some unexpected behavior, which described in Table 4.2.

TABLE 4.2 UNEXPECTED BEHAVIOR AND PERCENTAGE OF THE PARTICIPANTS WHO REPEATED THE SAME ACTIONS

Unexpected behaviour of the recipients	**Percentage**
Recipients took photos and videos while the drone was in flight	17.7%
People took photos of the drone and with the drone on the ground	7%
Confusion about the procedure after the drone landed	8.5%
Uncertainty on how to handle the mobile device while operating the drone:	
Holding the device in their hand while operating the cage	32%
Placing the device on the ground	48%
Keeping the device in a pocket while opening the cage	20%

The video analysis revealed that 20% of the users lost time because they were not following the instructions correctly, while 7% spent time taking photos of the drone before removing the parcel. The variable ground time at the recipient location highlights the need for some form of audio support to speed up the drone unloading and return process.

4.4.2 Results of the survey

To gather further feedback, recipients were asked to fill in an anonymous survey, which appeared on the portable device after pressing the take-off button. The survey was completed by 84% of the participants and contained nine closed and one open question (Fig. 4.6).

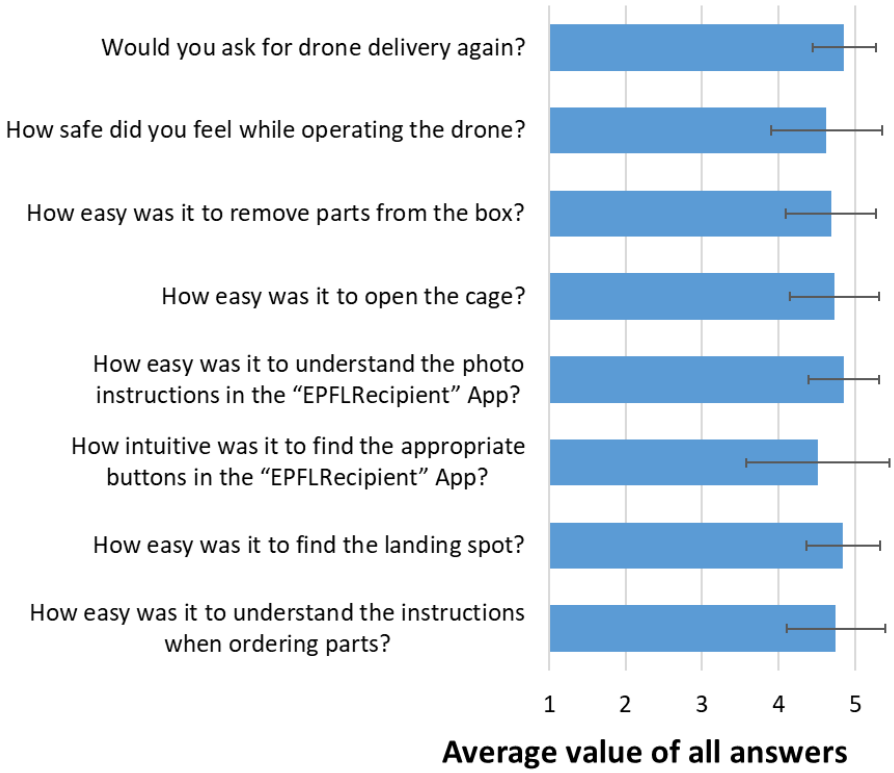

Figure 4.6 Survey questions and average numerical answers. Answers to Questions were graded on a five-level scale, where value 1 means *Hard/No* and value 5 means *Easy/Yes.* Whiskers represent the standard deviation. Two questions are not presented on the plot: one asking for the participant's age and an open question asking for "Additional comments" from the recipients. Answers to both questions are presented in the text below.

The majority of participants (92%) were aged 20 to 40 years and the remaining 8% between 40 and 60. The survey revealed a largely positive evaluation of Dronistics; the average answers to the questions were graded above four and half points on a five-point scale. Participants indicated that the procedure to order items and the recipient web application were easy to understand and use. They felt that handling the drone was not difficult and that the parcel was easy to retrieve. The majority of people felt safe next to the drone and would request drone delivery again.

The open question ("Additional comments") revealed the following comments and suggestions to improve the system:

1. Messages on the laptop display were hard to see due to sunlight reflection. Use of a smartphone was recommended (1 recipient)
2. The drone take off and turn during flight was too aggressive and scared participants. Use of a buzzer was proposed to signal the moment the drone takes off. Smoother change of direction during the flight should be implemented for less aggressive and frightening flight (3 recipients).
3. During parcel removal, the cage tended to close. Thus, a system to keep the cage open while removing a parcel was recommended (1 person)
4. It was hard to open the cage and hold the phone to watch the tutorial how to operate the drone (1 person).
5. Older smartphones had a problem to display the web app interface properly (1 person)

6. The Wifi signal was very weak at the recipient location (1 person). Not every portable device has enabled internet connection.

Furthermore, we received additional spoken comments from people who did not take part in the delivery tests. Three people from a nearby cafeteria and the library complained about the noise of the drone. The people from the cafeteria complained about the noise during take-off and landing. The students heard the noise through open roof vents in the library when the drone flew nearby.

4.4.3 Weather conditions

Wind speed was monitored with an anemometer installed on a building next to the recipient location. It was acquired at 1Hz between 9am and 4pm during the test period and over the following three months (Fig. 4.7).

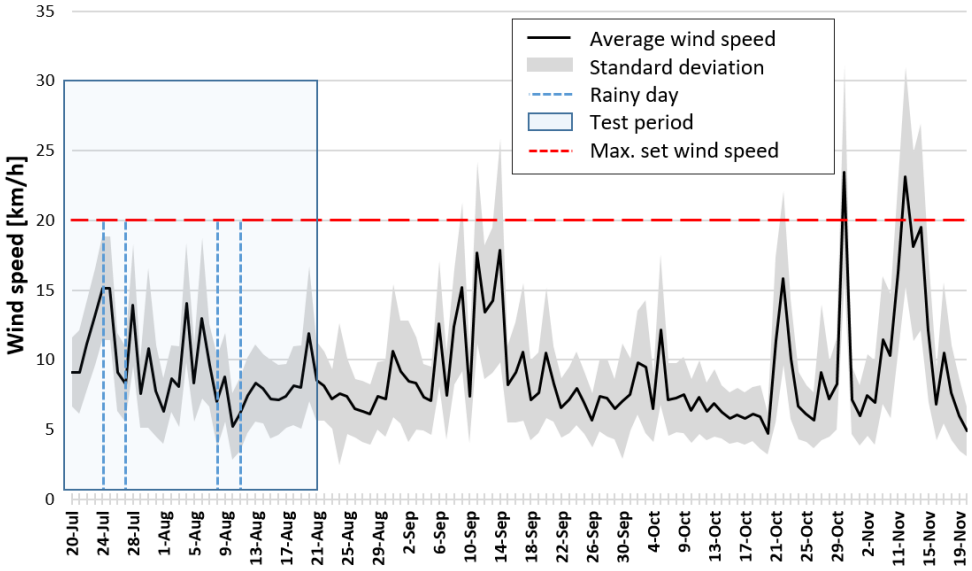

Figure 4.7 Wind speed average (black line) and standard deviation (grey area) measured for four months. The blue rectangle highlights the test period. The blue dashed lines show rainy days in the test period. The red dashed horizontal line shows the maximum value of the wind speed above which, flights were restricted. Over four months of wind measurements, 94% were flyable days.

As explained in Section 2.4 the speed of the drone was limited to 6 m/s. Thus, we set the maximum wind speed to 5.5 m/s (20 km/h) for drone delivery to withstand headwinds. Over the field test period, the wind never exceeded the maximum allowable speed. In the additional three months' monitoring period, we observed only two days when the average speed was above 20 km/h and five days when wind gusts exceeded this threshold. This accounts for 8% of the three-month period. Additionally, there were four days when we could not fly the drone due to heavy rainfall in the field test period.

Despite these precautions, undetected wind gusts at the recipient location led the drone to crash into a tree near the sender location on two occasions. These two incidents highlight the need for additional wind sensors placed close to landing sites or additional control algorithms to improve stability in wind gusts. Of note, however, the cage successfully protected the drone and its cargo during collision.

4.4.4 **Flight data**

Delivery in cluttered environments such as cities or university campuses requires high precision for landing to prevent accidental landing on pedestrians, cars, buildings or trees. In these experiments, the drone used GPS signals only to estimate its location. To determine the precision and accuracy of our drone, we measured the distance between the desired landing spot and the effective landing position at the sender and recipient locations. The recipient landing spot was located in an open area (maps in Fig. 4.4 and Fig. 4.5) more than 30 meters away from buildings. The sender landing spot was between two buildings, 8, 12 meters high respectively and 10 meters apart (maps in Fig. 4.4 and Fig. 4.5). Moreover, two trees with heights of 5 and 10 meters were located 10 meters away from the landing spot.

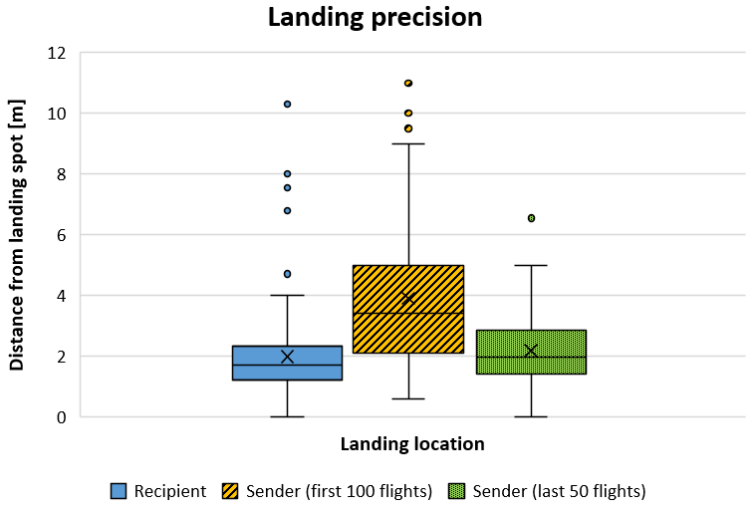

Figure 4.8 The plot shows measured distances between the desired and the effective landing position at sender and recipient locations. The first box plot presents the average landing error at the recipient location. The second box plot the average landing error at the sender location, measured over the first 100 deliveries and the third box plot presents the average landing error for the last 50 deliveries. During the last 50 deliveries, the coordinates of the landing position at the sender's location were fixed. Dots above box plots are outliers; horizontal black line in the box is the median and the black cross the mean value.

The drone had the coordinates of the recipient location, but used its own GPS estimates of sender coordinates at take-off for the return landing. The average landing error at the recipient location was 2 meters with a standard deviation of 2 meters (Fig. 4.8 – blue box plot). The average landing error measured at the sender location during the first 100 deliveries was 4 meters with a standard deviation of 5 meters (Fig. 4.8 – yellow box plot). We hypothesize that this higher error was caused by a poor estimation of the sender's coordinates from the on-board GPS at take-off time due to signal reflections between nearby buildings and further increased by the estimation error during the return landing. We thus fixed the coordinates of the landing spot in the sender location for the last 50 flights, which reduced the average landing error to 2.2 meters with a standard deviation of 2.2 meters (Fig. 4.8 – green box plot). Overall, these results show that GPS guidance may not be sufficient for reliable last-cm, person-to-person delivery in dense environments. For this type of operation, drones should be equipped with additional solutions for precise vertical take-off and landing, such as IR beacons placed on the ground, RTK GPS or vision-based navigation, which, unlike the first two solutions, requires no additional hardware on the ground.

We also analyzed the precision of the drone path. Here, we present flight path data from the last 50 flights with the hardcoded coordinates of the sender location. As shown in Fig. 4.9, the average flight path (blue dashed line) follows the ideal path (dotted green line), except for the geographical location where the drone performed a sharp 90-degree turn. The data indicates that the drone systematically overshot and corrected its trajectory, suggesting that its speed should be reduced ahead of sharp turns or the control parameters of the waypoint navigation algorithm should be better adapted to sharp turns.

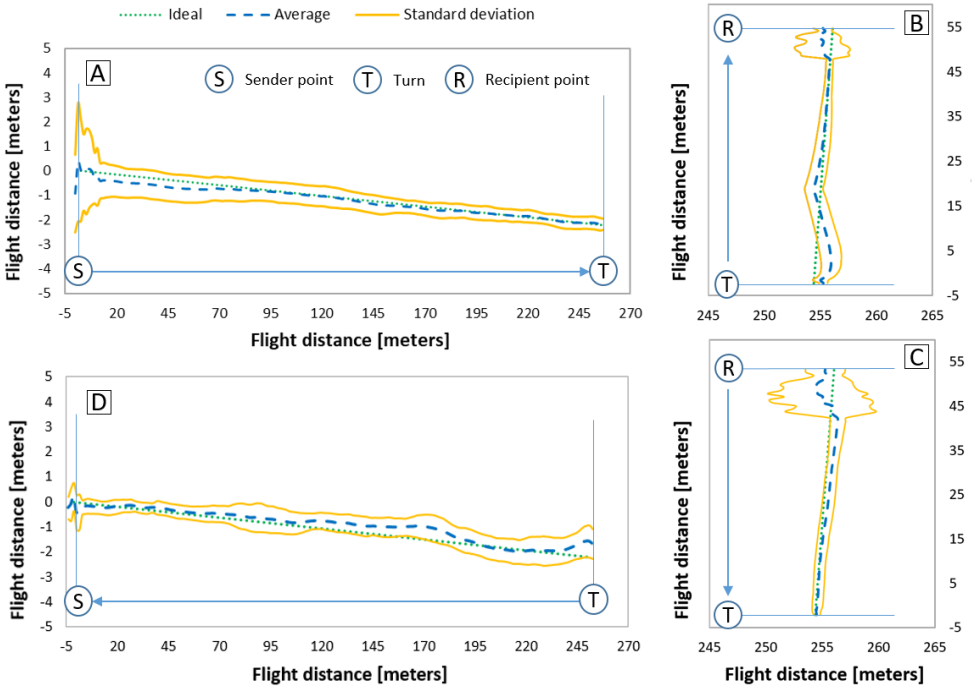

Figure 4.9 The mean flight paths of the drone. (A) From sender location to turning point, (B) from turning point to recipient location, (C) from recipient location to turning point, (D) from turning point to sender location. Green dotted lines represent the desired path between waypoints. Blue dashed lines represent averaged values (n=50). Yellow lines represent the standard deviation (n=50).

The standard deviation is a continuous yellow line and indicates small variations about the desired flight trajectory. Thus, we can conclude that GPS in flight is more accurate than for landing mode at both recipient and sender locations. Furthermore, we observed large deviations during take-off at the recipients' location. This behavior was caused by a malfunction of one of the electronic speed controllers (ESC), starting one of the four motors a few milliseconds later and causing the drone to deviate from the planned path. The malfunction occurred randomly and we solved it by replacing the hardware component.

During flight tests, we experienced two unexpected falls to the ground from 5 and 10 meters, respectively, after take-off, caused by disconnection of the battery power connectors. In both cases, the cage was fractured and the holder for the autopilot and companion computer were broken. Additionally, following the 10m fall, the 200g cargo damaged the box and fell out although the box remained attached to the cage. These experiments indicate a need to use reliable connectors and components and to reinforce the inner box.

4.5 Field tests – delivery of medications to a remote location

The goal of the second field test was to use the *Dronistics* system to investigate delivery of health care-related payloads such as medications, vaccines, blood and other samples to remote locations in rural environments. This investigation was conducted with a Non-Governmental Organization – *WeRobotics* that has representatives in 23 countries all over the world; representative units are called Flying Labs. The *Dronistics* system was tested with the *FlyingLab* from the Dominican Republic. The representatives of the *Dominican FlyingLab* had good relations with the local civil aviation authorities, which simplified the process of receiving authorization to fly in this region. The flight tests were performed in remote areas of the mountains of the Dominican Republic with the goal being to deliver health care-related items from local clinics, hospitals or pharmacies directly to health care workers who examine patients in the field. To understand further this use case, the flight ranges and challenges of the environment, we visited a few local clinics in the region to perform flight tests on site. The local exploration of the environment revealed that rural areas are no less challenging than urban locations. The high level of vegetation, inclined environments, small areas in front of houses requires high precision for take-off and landing. Due to this terrain, lack of and difficult roads, the health care workers cannot easily carry needed equipment and medications out into the field. They would like to be able to get only the items they need according to the requirements of the visiting patients at the examination clinic. Moreover, some medicines or samples require stable low-temperatures for storage and transportation and carrying bulky and heavy storage boxes for this is impractical. We selected one clinic in the most challenging mountainous environment, where after a rainfall, soil gathers on the only road making it slippery and hard to walk on, not mention driving a car or motorbike. Indeed, one of the main ways to transport items in these areas is local residents on motorbikes. However, lack of good roads reduces time of delivery and it becomes very dangerous after rainfall as mentioned. One of the patients visiting this local clinic is an elderly woman, who has heart and locomotion problems, requiring continuous administration of heart medication. During the rainy period, she has difficulty reaching the clinic. All these problems show that use of small delivery drones for short ranges would increase and improve health care services in these remote rural areas. At first, we were concerned that the curious local residents, inexperienced with drone technology may be not interested or even be against drones. However, we managed to instruct rapidly local representatives on how to operate the drone and unload the delivered parcels. Moreover, even small children were able to interact easily with the drone, as observed in Fig. 4.11.

Figure 4.10 (Top) The PackDrone flying over the mountains of the Dominican Republic. (Centre) Place of delivery marked with an orange circle. (Bottom) Logos of participants involved in the field tests in the Dominican Republic.

Figure 4.11 A PackDrone delivering medical supplies safely and directly examined by members of the Dominican Republic community. Top and bottom figures show that ease of use of the drone is simple enough for operation by those inexperienced with the technology, including children.

4.6 Field tests – delivery of temperature sensitive items in highly-populated environments

The goal of the third field test was to validate using Dronistics for person-to-person drone delivery of commercial goods, such as ice cream, in a highly populated environment. To achieve this goal, we joined up with Unilever and their ice cream brand, Ben & Jerry's. Unilever sponsored the ice cream, which was offered for free to test participants. To perform a high number of deliveries testing the system with many participants, the test was conducted during the Drone Days and Open Days of the EPFL in September 2019. Over the two days, we managed to perform 180 successful flights, delivering 180 ice creams to delighted ice cream lovers.

For the test of the highest number of ice cream delivery flights in two days, the flight path was reduced to 50 meters. To secure by-standers and random passers-by, the ground area below the flight path and landing spot was fenced off. The take-off spot was from the roof of the closest building to the landing spot.

According to Swiss law, autonomous flights of drones have to be performed at least 100 meters away from gatherings of more than 24 people and the safety pilot has to have the drone within the Visual Line of Sight (VLOS). In this case, to be able to fly during a public event with people closer than 100 meters, a special authorization from the Federal Office of Civil Aviation (FOCA) was needed. To get the authorization, a document known as the Specific Operations Risk Assessment (SORA) [114] had to be filled in and submitted to the FOCA for approval. The form describes and self-evaluates possible risks of collision of the drone in the air or with the ground. It contains a detailed description of, the area around the flight path, all software and hardware specifications used for operation, weather restrictions, procedure of all operations and the experience of each member of the team concerning how they were trained for the operation. One of the requirements of SORA was to provide calculations assessing possible effects of a ground impact. Calculations presented in Appendix A were used for this part of the authorization document.

For this field test, a new Graphic User Interface for the recipient WebApplication was designed to allow recipients to choose from a series of flavors of Ben & Jerry's ice cream (Fig. 4.2). This information was then sent to the senders WebApplication.

Additionally, to transport the temperature-sensitive payload required design and manufacture of a new box with thermal isolation (Fig. 4.x). The box had the shape of a cylinder instead of a cube to reduce drag effect during the flight. The top and bottom part of the box was made of 3D-printed parts. The wall of the cylinder was a 0.3 mm thick glass-fiber sheet, painted white. The temperature-isolating material was 5mm-thick PPT foam.

The test delivering ice cream was an excellent experience in learning how to deliver a temperature-sensitive payload. This will allow us to improve the system and the payload container for the delivery of more valuable items such as medicines, vaccines, blood and tissue samples that require also special temperature conditions. Moreover, preparing the SORA document taught us the special safety precautions and features that have to be performed for flights in populated environments delivering directly to inexperienced users. In the end, obtaining the authorization to fly autonomously and close to people showed our system was advanced enough to gain approval from FOCA.

During all field tests, we learned that high-temperature might not only be a problem for the delivered payload. In initial flight tests, a tablet used to operate the users Web Applications was exposed to sunlight for a few minutes (ambient temperature $\sim 30°C$) that resulted in shutting down all applications due to overheating. For the final flight, the tablet was used inside a tent, which solved the problem of overheating.

On fixed flight paths, it is very important to examine carefully the spots for take-off and landing. In initial flight tests, we observed strange behavior of the drone at take-off until the drone reached an altitude of 3 meters above the roof. The drone selected a different direction of flight than programmed. This behavior was due to affected magnetometer readings. In the building at the take-off point, one of the laboratories was using a machine that generates strong electro-magnetic fields. The problem was solved by moving the take-off spot further away.

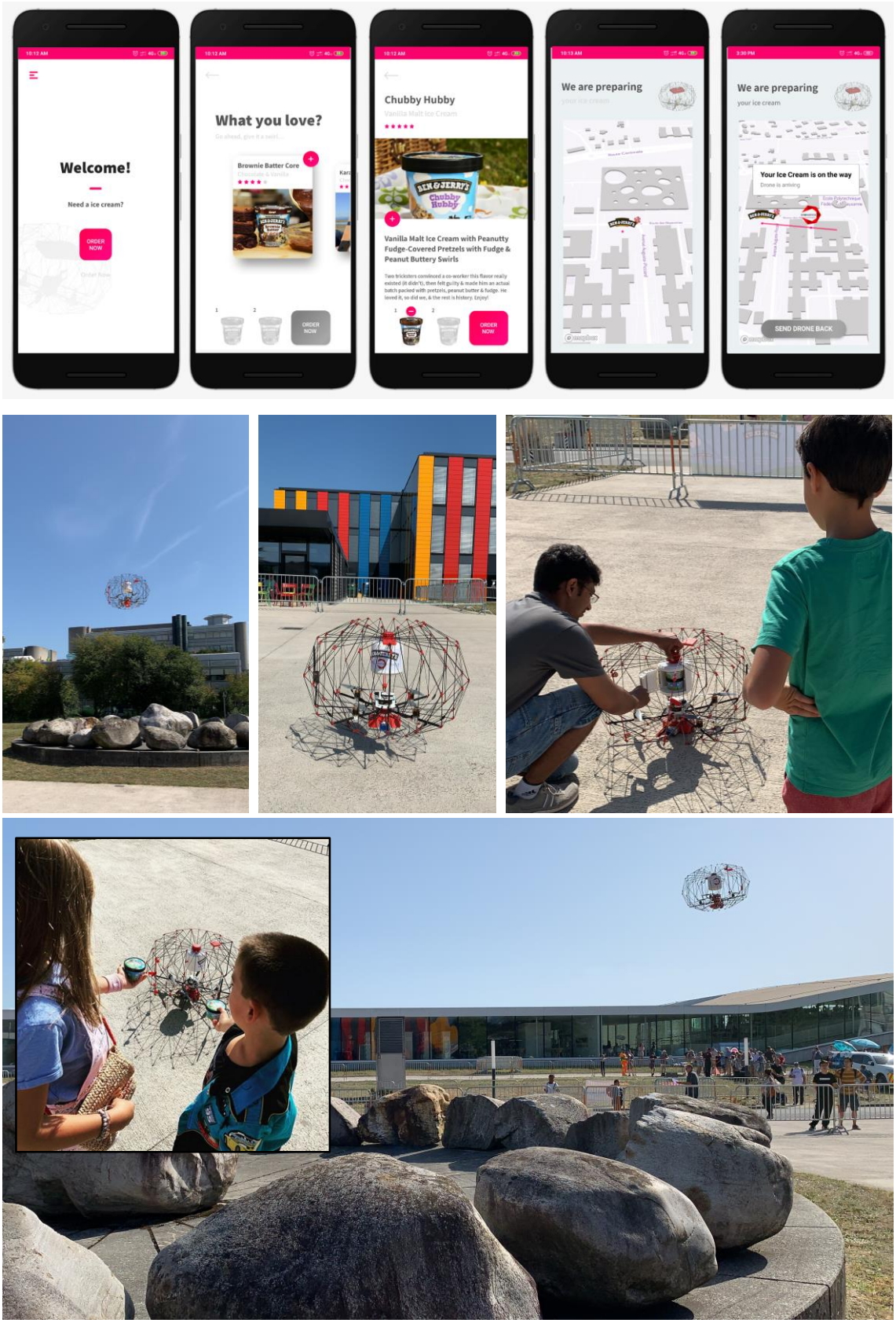

Figure 4.12 PackDrone delivering Ben & Jerry's ice creams on the EPFL campus. (Top) Recipient Web Application. (Below) Different phases of delivery.

4.7 Demos during public events

During last four years, I presented the *PackDrone* and *SimplyFly* systems at different events. These demos and discussions allowed improving the systems from received feedback of future users.

2016:

- Demonstration at Epeisse for Search and Rescue teams (DEZA), April 2016
- Demonstration at EPFL for opening of MED building, May 2016
- Demonstration at EPFL for Swiss SRF TV – programme Einstein, July 2016
- Demonstration in Neuchatel - MicroCity open day, September 2016
- Demonstration at EPFL for Cybathlon with live on TV, October 2016
- Demonstration at NCCR Industry Day (designed and build a bigger version of the foldable cage drone), November 2016
- Presentation for delegation of Polish start-ups accompanied with delegation of Polish president, November 2016
- Other small demos at the lab for visiting guests

2017:

- Presentation at EPFL for Fischer Connectors, January 2017
- Demonstration at EPFL for Swiss Post, January 2017 (built improved version of the foldable cage drone)
- Presentation for Polish journalists, March 2017
- Demonstration at Epeisse for Search and Rescue teams (DEZA), May 2017
- Flight tests – drone delivery of PCB and 3D printed parts on the EPFL campus, August 2017
- Demonstration during exhibition „Drone Days", EPFL, Lausanne, Switzerland, September 1-3, 2017
- Demonstration and interview at EPFL for Reuters – winter semester 2017
- Demonstration and interview at EPFL for Swiss SRF TV – winter semester 2017
- Demonstration and interview at EPFL for RTSun – winter semester 2017
- Demonstration at "NCCR Industry Day", November 2017
- Demonstration during the exhibition "Digital Days", Geneva, Switzerland, November 21, 2017
- Other small demos at the lab for visiting guests

2018:

- Presentation: "Last-centimetre drone delivery" during The European Robotics Forum 2018, Tampere, Finland, March 13-15, 2018
- Demonstration during "Salon International des Inventions de Genève", Palexpo, Geneva, Switzerland, April 11-15, 2018
- Demonstration - The World Economic Forum in Zurich, Switzerland, 26.07.2018
- Demonstration - SIR SA, 19.07.2018, Lausanne Switzerland
- Demonstration - Chamber of commerce - General Assembly, Fribourg, Switzerland, 03.09.2018
- Demonstration - Intel workshop in Munich, Germany, 4-5.09.2018

- Demonstration and presentation during meetup SwissAI, 15.10.2018

2019:

- Demonstration (drone show), Las Vegas, CES 3-7.01.2019
- Demonstration and presentation during workshop at European Robotics Forum -"Aerial Robotics Technologies & Applications with the new European UAS regulation" Bucharest, Romania, 21-22.03.2019
- Demonstration - Hannover Messe, Hannover, Germany, 1-5.04.2019
- Tests of the technology in the Dominican Republic, 23-29.05.2019
- Demonstration - Unilever, Lausanne, Switzerland, 14.06.2019
- Demonstration, TUV, Lausanne, Switzerland, 14.06.2019
- Demonstration, Canso event, Geneva, 18.06.2019
- Demonstration Drone/Open Days of EPFL, 14-15 September 2019
- Demonstration and presentation for AssaAbbloy, Lausanne, October 2019
- Other small demos in the lab for visiting guests

4.8 Conclusions

This chapter presents an integrated software and hardware system for last-centimeter drone delivery between people and for business-to-customer services. The results of the flight tests indicate the service's feasibility and its positive acceptance, at least among members of a technical research institution. The behavioral analysis of the user interaction, the analysis of the flight data and the few technical problems, point to areas for improvement presented below that could be useful for future improvements and other drone delivery services.

Future work will focus on enhancing user interaction and drone guidance. For instance, we are incorporating a small speaker for voice instructions as a complement to the photo tutorial. These will help recipients to operate the drone when bright sunlight makes it hard to see the screen and will free both hands for retrieving the package. A loud buzzer should be installed to signal the landing and taking-off of the drone. Once autonomous flight Beyond Visual Line of Sight (BVLOS) authorization is received [111][114], the flight altitude could be increased to reduce the noise perceived from the ground. Additionally, other techniques for noise reduction should be studied and implemented to improve user acceptance.

Furthermore, the guidance, control and navigation algorithms should be adjusted to achieve smoother flight during take-off and sharp turns. Additional guidance systems must also be considered for take-off and landing between tall structures. Multiple weather stations will be required to estimate more precisely local wind conditions between buildings where strong air tunnels can form and disturb the flight and additional research in wind-resilient control algorithms is warranted. Further tests of the sender's behavior could be conducted to verify the ease of deploying the cage.

Despite current autonomous BVLOS flight restrictions in public areas [111], it is easier to receive authorization for such flights in private and restricted areas such as campuses of universities or large companies. This study has been the first application of our last-centimeter aerial delivery service. Future implementations of the system may enable new delivery services between small businesses and customers (B2C) and directly between customers. Moreover, aerial deliveries over the short range could also cut emissions [115]. Finally, last-centimeter delivery may become an integral part of the "sharing economy" [116] where individuals borrow or rent assets owned by someone else.

Chapter 5
A morphing body as a solution for increased safety and efficiency

DELIVERY drones used by logistics companies today are equipped with unshielded propellers, which represent a major hurdle for in-hand parcel delivery. The exposed propeller blades are hazardous to unsuspecting bystanders, pets and untrained users. One solution to provide safety is to enclose the drone with an all-encompassing protective cage. However, the structures of existing cage designs have low density in order to minimize obstruction of propeller airflow, to avoid decreasing efficiency. The relatively large openings in the cage do not protect hands and fingers from fast rotating propellers.

This chapter presents a novel approach to safety and aerodynamic efficiency by means of a high-density cage and morphing arms loosely inspired from a box turtle. The drone cage is made of a dense and lightweight grid. When flying close to humans, the arms and propellers are retracted and fully sealed within the cage, making the drone safe and reducing the total footprint. When flying at cruising altitudes far from people and objects, the arms and propellers extend out of the protective grid, increasing aerodynamic efficiency by more than 20%.

The material presented in this chapter is adapted from:

[117] **P. M. Kornatowski,** M. Feroskhan, W. J. Stewart, and D. Floreano, "A morphing cargo drone for safe flight in proximity of humans," will be submitted to *Robotics and Automation Letters*, (2020).

The work presented in this chapter was submitted for patenting:

[118] **P. M. Kornatowski**, and D. Floreano. "A morphing cargo drone for safe flight in proximity of humans," patent pending, 2019.

5.1 Introduction

Drones are becoming an increasingly useful tool to deliver parcels faster [6], greener [115] and cheaper [1] to previously inaccessible places. As a result, several logistics companies [97] are considering using drones for e-commerce markets. However, most of these deliveries tend to employ bulky drone platforms designed for stable, long-range dispatch and require designated take-off and landing spaces. Additionally, user access to these spaces are restricted during operation to avoid harm posed to bystanders due to exposed propellers. Moreover, delivery to places where there is no space to land, e.g. a window or balcony, delivery to people stuck in a traffic jam or inclined environments is impossible for drones. Together, these three challenges remove the possibility of person-to-person and last-centimeter deliveries where packages can be safely delivered directly to the recipient's hands or hard-to-reach, cluttered locations.

In the context of ensuring safe handling for last-centimeter delivery, one approach is to encase the propellers in a protective cage [28]. A highly dense cage structure enhances safety [121] by preventing users from accessing the propellers. However, high-density cages incur a high drag penalty [81] and decrease available lift [78]. The alternative, a low-density cage structure would allow small external objects, such as fingers or hands, access to propellers, which could be dangerous for people and animals. Additionally, to reduce the added weight of the cage, the vehicle volume is kept low by shortening the arm length of the quadcopter. However, this reduces the drone's stability due to the lower mass moment of inertia [122], and decreases its efficiency since a larger change in thrust is required to tilt the drone. Therefore, a higher change in the rotation speed of propellers is needed and more power is consumed.

In this paper, we present a novel approach to safety and efficiency for delivery drone design. We propose to enclose a quadcopter (Fig. 5.1A-B) in a safe, densely gridded cage based on a tennis-racket stringing technique [123]. To overcome the drag penalty of such a cage, the quadcopter has a morphing capability inspired by the 'box turtle's' (Terrapene Carolina, T. ornata) limb retraction for protection (Fig. 5.1C-D) [124]. The quadcopter can retract its arms into the cage during take-off and landing to prevent access to its propellers, keeping people safe. In addition to preventing injury, the retractable arms strategy results in a smaller footprint of the quadcopter during take-off and landing, offering access to cluttered and hard-to-reach places. In the proposed solution, the parcel is strategically located on top of the drone. This approach, as suggested in [57], enables the propellers to be tightly packed into the cage together without the parcel blocking the slipstreams. This allows the volume of the cage structure to be designed at a minimum by overlapping the propellers as shown in Fig. 5.2C. The overall small vehicle volume provides better portability and storage with the arms fully retracted (Fig. 5.2). The cage structure also replaces the need for landing gears. During cruise flight, the arms of the quadcopter can be extended out of the cage, giving it the associated increase in efficiency and stability. Based on this proposed design, the mission profile of a drone, illustrated in Fig. 5.1E, consists of the propellers contained inside the cage during take-off and landing only (just a small portion of the whole mission) and deployed outside the cage during cruise to increase aerodynamic efficiency.

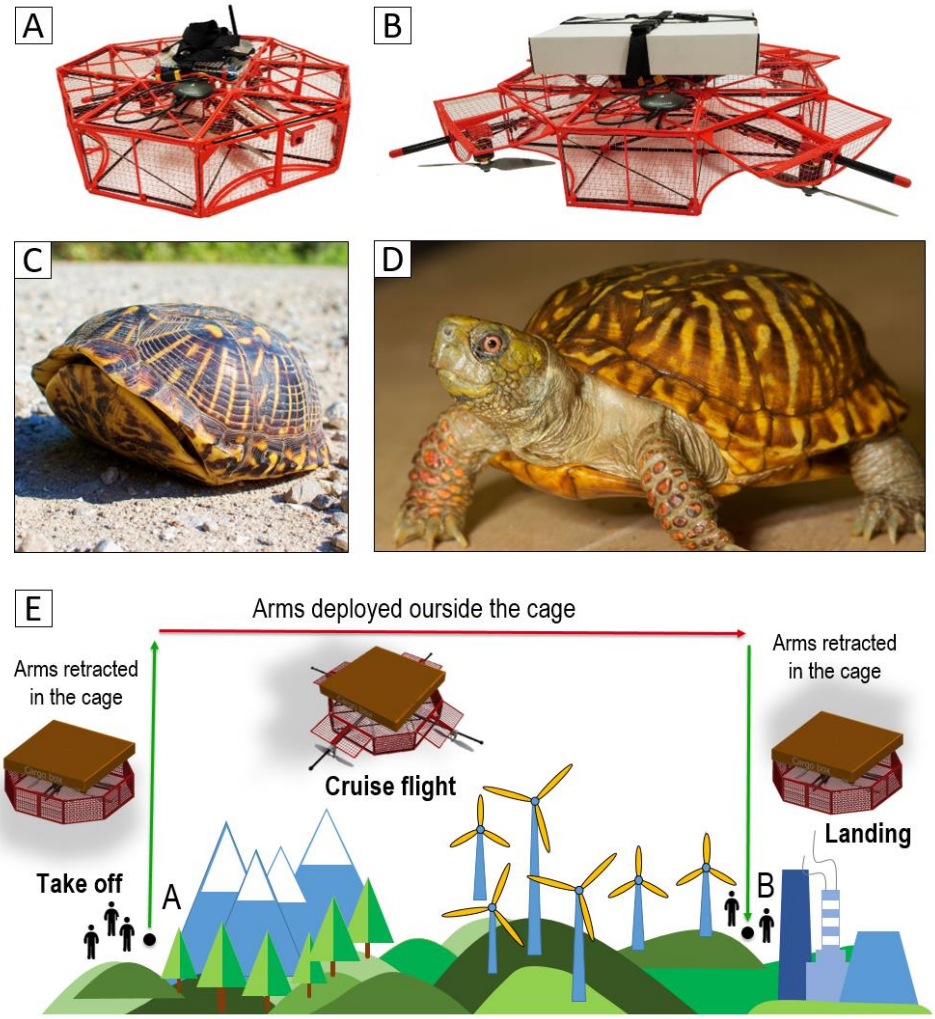

Figure 5.1 The morphing quadcopter fully enclosed in a cage enhancing safety for children and animals. (A) Photo of the retracted arms configuration inside the cage for take-off and landing. (B) Photo of the arms deployed outside the cage for the cruise mode with a parcel. (C) A 'box turtle' with retracted limbs and closed shell for protection [124]. (D) A box turtle with deployed limbs for locomotion [125]. (E) The concept of safe and efficient delivery by a quadcopter with retractable arms. (Green arrow) The arms retracted in the cage during take-off and landing mode – while close to people and animals. (Red arrow) The arms deployed out of the cage for efficient cruise mode – far away from people and obstacles.

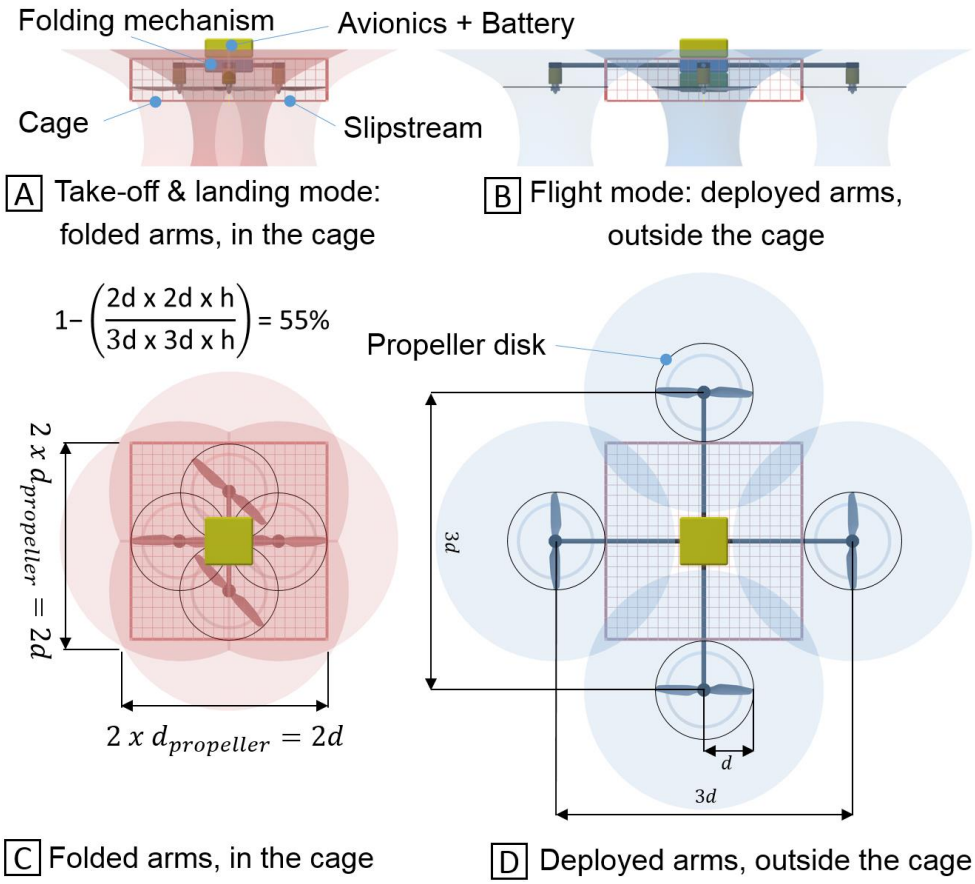

Figure 5.2 (A-B) Side cross-section of the quadcopter with the parcel and the cage. (C-D) Top view of the quadcopter without the parcel. (A, C) Retracted safe mode: arms inside the cage for take-off and landing. (B, D) Deployed mode for the cruise flight: arms deployed outside the cage. Increased efficiency, not affected by the grid of the cage.

5.2 Cage design

The design of a safety cage that simultaneously protects humans and does not obstruct the propeller airflow requires addressing multiple conflicting design challenges. The first is that the cage should be dense enough to prevent even small children's fingers from passing through and touching the fast moving propellers. The second is that the cage should be stiff enough to prevent deformation resulting in contact with the propellers when people grab it. The third challenge is to disturb minimally the airflow through the propellers.

To little affect the airflow from the propellers and reduce drag during take-off and landing, thickness of the grid strings should be minimized. Multicopters typically fly in a variety of orientations and inclinations within a single mission. Thus, the strings should have a symmetrical cross-section to keep the same drag coefficient regardless of the pitch angle. To fulfill this requirement, a circular cross-section was selected. To reduce the drag, the thickness of cylinders should be minimized, but thinner cylinders are more flexible and may allow the cage to deform and enter in contact with the spinning propellers. Therefore, this tradeoff requires a study of the appropriate thickness and choice of materials. To do that, the forces applied on the cage while the drone is flying close to people and during in-hand landing need to be defined.

To fulfill the above-mentioned requirements, we designed a stringed cage inspired by a tennis racket that consists of a rigid frame and stretched strings that provide rigidity with very small deformation to the stiffness of the tensioned strings.

5.2.1 Density of a grid

The density of the cage was designed such that the gaps in the cage were small enough that a child could not put his fingers into the cage. As a reference, statistical data of a three-year-old children's smallest finger was selected [127] and the diameter of the fingertips (distal phalanges) used. The diameters ranged from 9 to 10 mm. Moreover, to enhance safety, one millimeter was subtracted from this diameter. The resulting maximal open space in the grid is 8 mm. This density ensures that the drone is safe when used near children.

5.2.2 Stiffness of the cage and grid

The hallmark of multicopter safety is being safe enough for the user to catch the vehicle in flight. For this paper, we therefore used the scenario of in-hand landing as a goal for user safety. As a pair of outstretched hands can withstand a load of up to 20 kg without risk of injury [128], the user should be able to bear the weight of the proposed drone (2.5 kg), which is eight times lighter. We focused on three possible in-hand landing situations (Fig. 5.3).

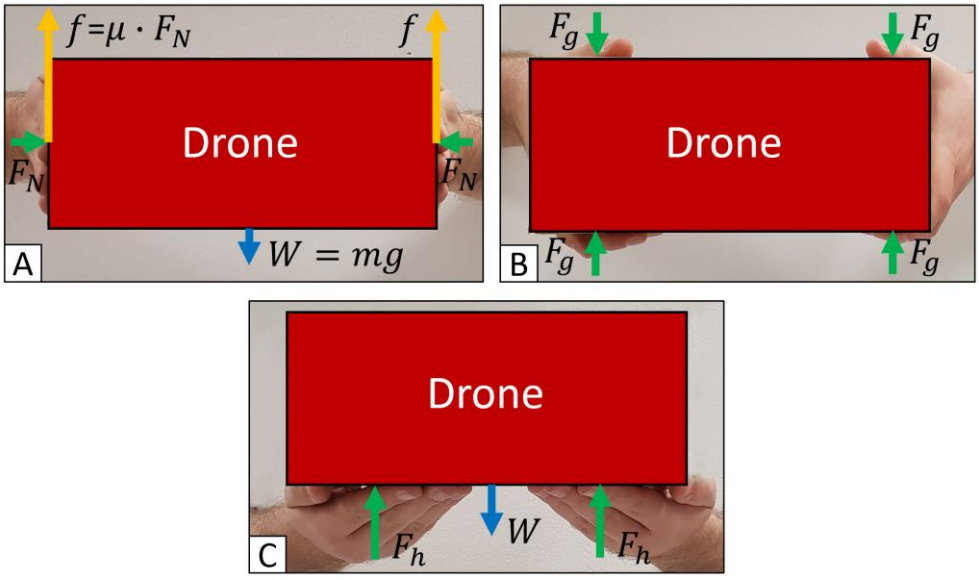

Figure 5.3 Free body diagrams of the drone cage held by the user (side view). (A) Drone held between a user's open palms. (B) Drone gripped by a user's palms. F_h is holding force, W is the drone weight, m is the drone mass, g is gravitational acceleration, f is friction force, F_N is the normal contact force, μ is the friction coefficient between the cage material (plastic) and human skin (0.7 [130]), F_g is the gripping force. (C) Drone held on top of a user's palms.

In situation A, the drone is caught from the sides, between the user's open palms flushed against the drone (Fig. 5.3A). Here, the friction forces f generated between the palms and the cage bear the drone weight, W. Therefore, the required contact normal force F_N applied by the user's palms is $W/(2\mu)$ and is independent of the surface area of the palms. For a 2.5 kg drone and a friction

coefficient μ of 0.7 [130], the required normal force F_N is 17.5 N. Therefore, as two hands hold the cage, the maximum force that the cage needs to withstand without being deformed is 35 N.

In situation B, the user grasps the drone with both palms, mainly the fingers (Fig. 5.3B). To determine the gripping forces acting on the cage as the user grasps the drone, we assume that the weight of the drone is borne by the user's arm muscles. A study from [128] indicated the maximum average gripping force applied by one's palms when gripping an object between 3.5 and 9.5 cm thick. At 9.5 cm thickness, the average gripping force applied is 270 N. The magnitude of the gripping force also depicts a downward trend as the thickness increases. Therefore, the drone, 14.5 cm thick would experience a smaller gripping force during in-hand landing. Thus, 270 N ($2 \cdot F_g$) would be a conservative approximation of the force that a user would apply when grasping a landing multicopter.

In situation C, the drone lands on top of the user's outstretched palms, perpendicular to his body (Fig. 5.3C). Here, the drone structure should be able to bear its own W weight force of approximately 25 N, which is much lower than in situation B. Since situation C is comparable to situation B when the force is applied to the cage frame and is the least demanding in terms of the force applied, only situations A and B are tested in the experimental validation for in-hand landing in Section 5.5.

5.2.3 Drag calculations of a grid

The drag generated by the grid in the propeller slipstream and in the incident airflow during cruise flight can be calculated using the drag coefficient for obstructions in a wake, called the wake loss factor [132]. The wake loss factor for cylindrical shaped obstructions can be written as:

$$C_{dw} = \beta \cdot C_d \tag{5.1}$$

Where, β is the blockage factor:

$$\beta = \frac{projected\ area\ of\ obstructing\ cylinders}{total\ area\ of\ the\ wake} \tag{5.2}$$

C_d is the drag coefficient of the cylinders [133], which is a function of their local Reynolds numbers.

The projected area of obstructing cylinders can be calculated knowing the space between strings and the diameter of the strings.

The Reynolds number can be calculated from:

$$Re = \frac{\rho \cdot u \cdot L}{\mu} \tag{5.3}$$

Where, ρ is the density of the air (1.225 kg/m^3), u is the velocity of the air with respect to the object obstructing the flow [m/s], L is a characteristic linear dimension [m], and μ is the dynamic viscosity of the air (18.5 μPa·s). For small diameters of cylinders (0.1-1 mm) and low airspeeds ($\sim 25\ m/s$), the local drag coefficient will typically range between 0.95 and 1.65 [134].

Because of the uniform grid density, the blockage factor is simply the grid density. This means that it is independent of wake area. Combining this with the drag coefficient, C_d gives the wake loss factor. In the case where the wake loss factor is too high, the string diameter should be reduced and stronger material found to provide enough strength. The lift reduction equations presented here will be validated experimentally in Section 5.4.

5.3 Implementation

To validate the proposed concept, we designed and characterized a morphing, densely caged quadcopter, codenamed *GearQuad*, capable of carrying 500 g payload.

5.3.1 Cage

The cage is composed of two elements: external grid modules of different sizes and shapes (Fig. 5.4A) and an internal carbon truss (Fig. 5.4B). The grid modules are attached to the outside of the carbon truss (Fig. 5.4C). The truss is composed of 6 x 1 mm carbon fiber beams glued together with 3D printed joints. Thus, the carbon truss provides rigidity to the cage.

The grid module was designed following the procedure presented in Section 5.2 and validated experimentally in Section 5.4. The grid modules (Fig. 5.4A) consist of tensioned string (0.3 mm diameter Dyneema string, 336.5 N at the break (tensile strength)) threaded through 3D printed, stiff and lightweight plastic frames (PLA). The string was threaded into an 8 mm by 8 mm grid through 1 mm diameter holes drilled into the frame. The strings were glued to each other using cyanoacrylate glue to prevent them from sliding if a finger is placed between them. The added glue increased the string diameter to 0.35 mm. The plastic module was attached with M2 screws to the plastic joints of the truss. The bottom part of the cage has semi-circular cutouts as presented in Fig. 5.4E. The semi-circular cutouts ensure that the grid does not impede the propeller slipstreams when the propellers extend fully. In addition, these cutouts reduce the time required to deploy and retract the arms by decreasing the distance the propellers must travel to reach clean air. Therefore, a shorter arm length is implemented, which reduces weight and drag.

The vehicle has the dimensions 52 x 52 x 14.5 cm with the arms retracted and 86 x 86 x 14.5 cm with the arms deployed. The dimensions of the drone are the result of two design decisions: (i) the propellers should provide sufficient thrust to lift the drone with a 500-gram payload; (ii) the maximum size of the drone with its arms retracted should fit within a person's arms (with his hands outstretched, perpendicular to his body). For a small British adult (44 kg body weight), the length between the outstretched palm and chest is 34.5 cm [128], which is more than half of the length of the drone. This allows the drone to be grabbed by the recipient when landing.

The cage was designed intentionally in octagon shape instead of a square to reduce the total mass of the material. Four doors are located at the four perpendicular sides of the cage. The doors are pushed open by the arms of the quadcopter on deployment (Fig. 5.4E) and are automatically closed by springs when the arms are retracted into the cage.

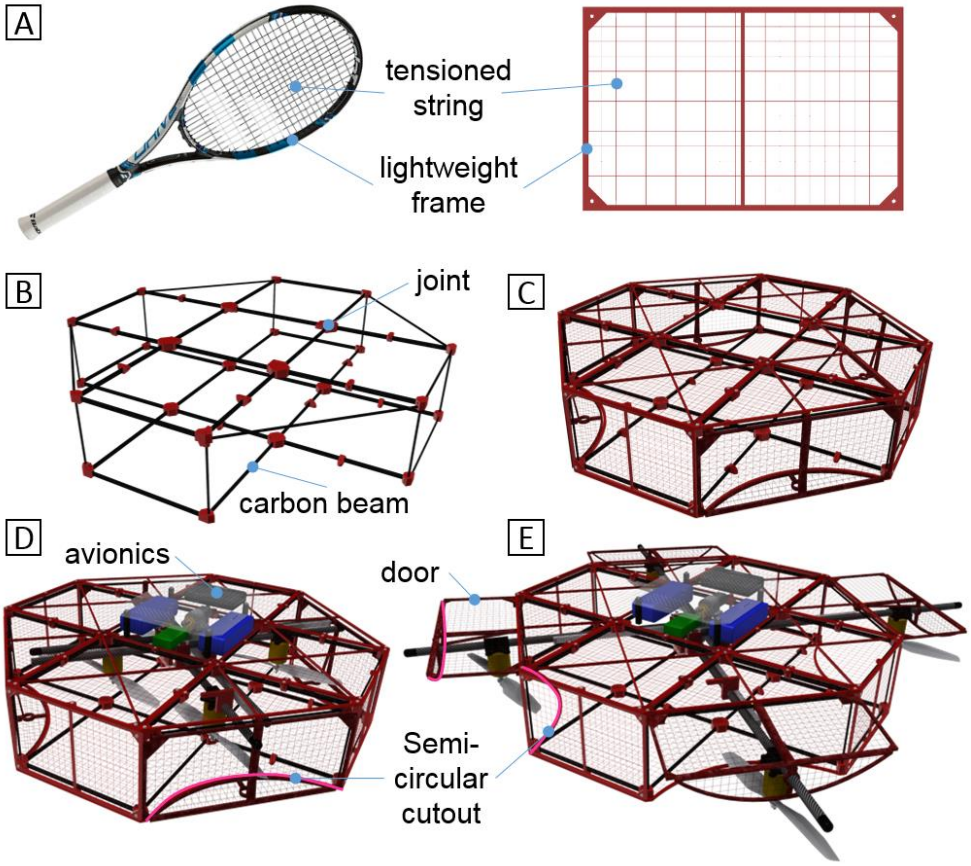

Figure 5.4. Elements of the *GearQuad* (A) Comparison between a tennis racket and a drone grid module. (B) Truss structure of the cage composed of pultruded carbon fibre beams connected by plastic joints. (C) Truss structure with grid modules installed. (D) The cage with integrated rotor arms and avionics payload. The arms are retracted inside the cage. (E) The drone with deployed arms and opened doors.

5.3.2 **Morphing drone**

To minimize the size of the cage, and thus its weight and drag, the propeller disks were vertically offset by 12 mm, as shown in Fig. 5.5A, which allows overlapping between the propellers (Fig. 5.2C). This is a key design feature to reduce the quadcopter cage footprint to a minimum. One of the challenges of designing the morphing technique is to limit the number of actuators deploying the arms of the quadcopter without compromising the mechanical strength of the arms. As a result, we designed a new, innovative mechanism that deploys the four arms symmetrically and simultaneously (Fig. 5.5B-C).

The main body of the mechanism (Fig. 5.5B) is made out of 5 mm-thick laser cut acrylic plates. The arms consist of 10 mm carbon fiber tubes with a wall thickness of 1 mm. Each arm was inserted into a plastic, 3D printed (ABS) lubricated slider that allows the arms to deploy and retract freely (Fig. 5.5C). To move the arms, a plastic rack was glued to each arm using cyanacrylate glue. The rack is engaged by a single main gear placed in the center of the drone between the arms (Fig. 5.5B-C). Thus, when the gear rotates, all four arms simultaneously deploy or retract (Fig. 5.5C). To rotate the main gear, a DC motor (Pololu 154:1 Metal Gearmotor 20D x 44L mm) was used. To ensure a compact design, the motor is mounted perpendicular to the main gear of

the mechanism deploying the arms. Two conical gears (Fig. 5.5B-C) connect the motor and the main.

An electronic controller (Pololu Simple High-Power Motor Controller 24v12) to control the speed and direction of rotation of the motor is connected to the autopilot's PWM output. Moreover, two end switches are connected to the controller. The switches are responsible for turning off the DC motor when the limit position is reached.

As shown in Tables 5.1 and 5.2, the elements that allow extension of the arms amount to 6.5% of the gross weight of the drone.

TABLE 5.1 MASS DISTRIBUTION OF THE MORPHING MECHANISM OF THE QUADCOPTER.

Component	Mass [g]
4 x racks	39
gears + shaft + bearings	21
longer arms to open the doors	53
2 x switch	4
motor	45
controller	8
TOTAL MASS OF MORPHING MECHANISM	**169**

TABLE 5.2 MASS DISTRIBUTION OF THE PROTOTYPE.

Component	Mass [g]
folding mechanism	169
quadcopter	1193
battery	344
cage	377
payload	500
TOTAL MASS OF QUADCOPTER	**2583**

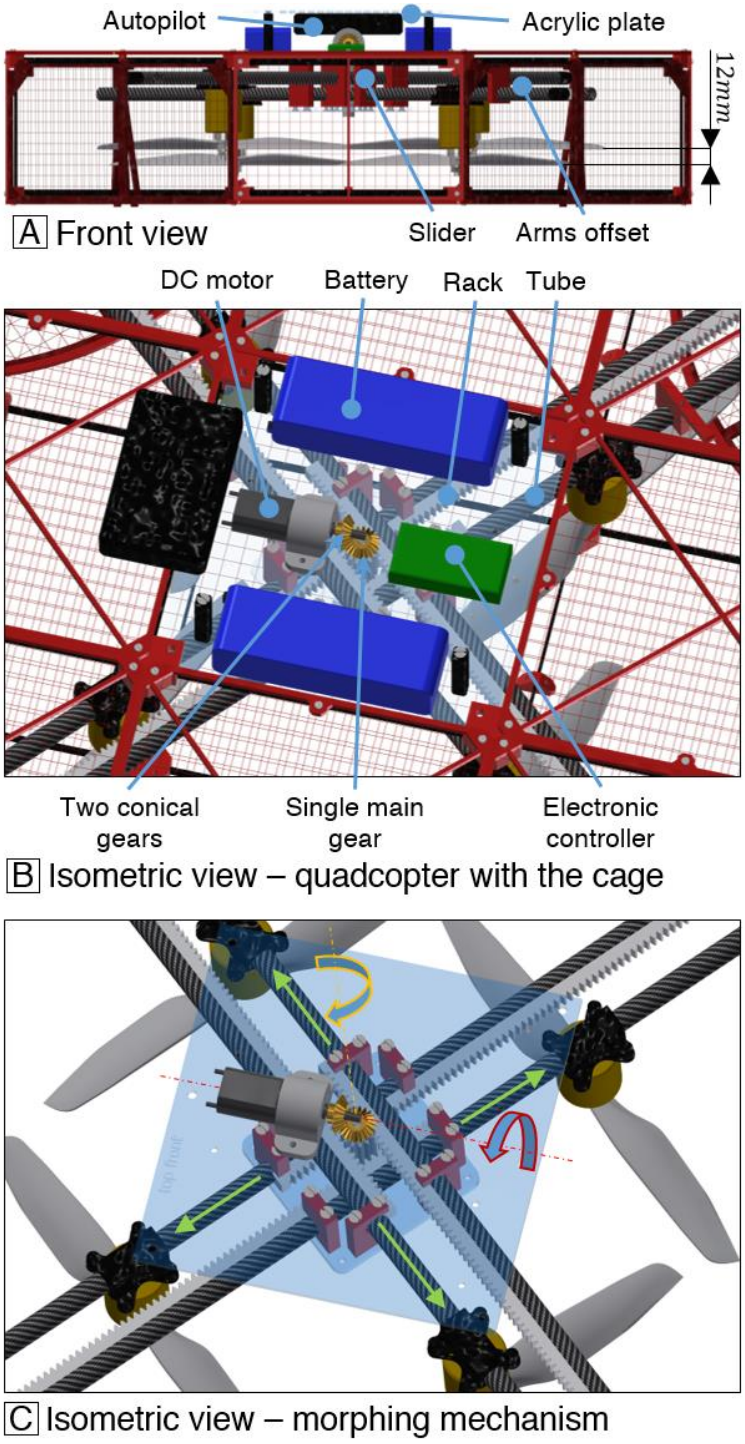

Figure 5.5. Details of the propulsion mechanisms and morphing mechanism of the drone. (A) Side view of the drone presenting the offset of the arms placed in the plastic sliders. (B) Magnified isometric view of the drone showing the morphing arms mechanism and avionics. (C) The morphing mechanism of the arms shown without the cage and avionics. The blue arrows show the direction of rotation of the conical gears about the motor axis (red dashed line) and gear axis (yellow dashed line). The green arrows show the direction of arm deployment. Reversing the direction of rotation of the motor will change the direction of translational movement of the arms.

5.4 Experimental characterization

A series of experiments was performed to validate the influence of the grid and of the entire cage (including reinforcing elements) on lifting capabilities of the drone as predicted by the calculations described in Section 5.2.3.

In the experiments, lift was measured at varying distances (d) between a grid and a single propeller in two configurations (Fig. 5.6). In the first configuration, the grid is downstream of the propeller (Fig. 5.6A). To test this configuration, the grid was installed below the propeller as shown in Fig. 5.6A and the setup shown in Fig. 5.6D was implemented. In the second configuration, the grid is upstream of the propeller (Fig. 5.6B). This represents the case where the grid modules are positioned above the propellers on the quadcopter. To test both configurations, the characterization bench shown in Fig. 5.6D was used, however, the propeller orientation was changed (flipped 180 degrees around the horizontal axis) and direction of rotation was reversed. This allows the grid in the setup to remain in the position below the propeller, as shown in Fig. 5.6B. In addition, for distance between the propeller and grid, studies on the dependency of rotation speed and propeller size were also performed by repeating the experiment at various rotation speeds and propeller sizes.

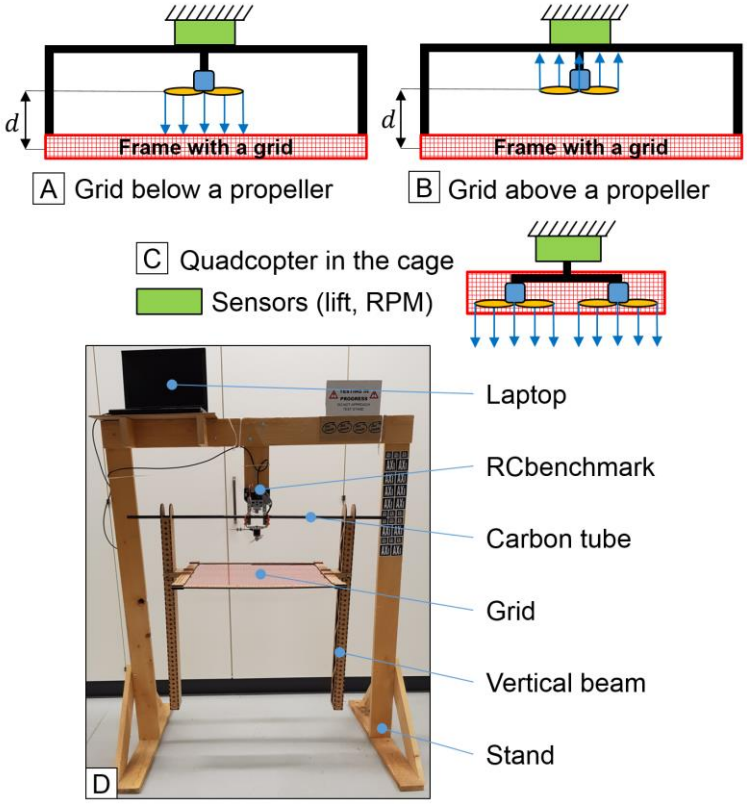

Figure 5.6 Experimental setup for lift measurements. Blue arrows represent the direction of the airflow. (A) A schematic representation of the setup with the grid placed downstream of a single propeller. (B) A schematic representation of the setup with the grid placed upstream of a single propeller. (C) A schematic representation of the setup with the arms retracted quadcopter with a cage. (D) Photo of the experimental setup with a grid attached to 60x60 cm square wooden frame.

The measurements were conducted using the RC Benchmark 1580 Series dynamometer sensor, which gives values in kg [74], attached to a custom stand (Fig. 5.6D). During the experiment, an AXI 2217-16 V2 (1380KV) motor with 40A ESC was used. The voltage was set to 12.6V with a power supply (Keithley 2260B-30-72) corresponding to the equivalent of a fully charged 3S battery. The grid is stretched into a square frame with external dimensions of 60 cm and internal dimensions of 54 cm. The grid is composed of 0.3 mm strings (after gluing 0.35 mm) with 8 mm spacing in between. The frame is connected to the RC benchmark sensor by a 10 mm carbon tube and two vertical beams (Fig. 5.6D). The sensor is attached by screws to the stand at the center. The grid is moved from a distance of 2 cm to 50 cm from the propeller, with measurements taken at thirteen different steps in between. The values of distances are presented on the x-axis of the plot in Fig. 5.7. The experiment was conducted for the two specified configurations (grid positioned upstream and downstream of propeller) and for the case without the grid.

As shown in Fig. 5.7, the grid placed at the aforementioned distances upstream of an 8x4.5MR propeller reduces the lift by an average value of 6.5 g or 0.6% of the measured for a single propeller rotating at 13200 RPM upstream of the grid. On the other hand, the grid placed downstream of the single propeller rotating at 13200 RPM, decreases the lift by an average value of 78 g or 6.3%. The value of decrement for both configurations is constant for varying distances between the grid and propeller. Therefore, varying the distance between the grid and the propeller does not have a measurable influence on the electric power consumed by the motor.

For the downstream configuration, the wake loss factor can be calculated using equation (5.1) and then compared with the experimental results. Based on the string diameter and spacing, the blockage factor β calculated using (2) is 0.070. The Reynolds number, calculated from (3), is approximately 477, which corresponds to a local drag coefficient of 1.1 [133]. The air speed (24 m/s) used in the calculation of the Reynolds number was measured using a hot wire anemometer sensor. The sensor was placed 2 cm below the propeller without the grid and at a distance equal to half of the propeller radius from the axis of rotation of the motor. Using these values, the wake loss factor calculated with (1) gives a value of 0.0776.

This value of the wake loss factor can be compared to an experimentally determined value by comparing the motor thrust with and without the grid using the formula:

$$C_{dw\ eperimental} = 1 - \frac{thrust_{with\ grid}}{thrust_{without\ grid}} \tag{5.4}$$

This experimentally determined value is approximately 0.0777. Thus, calculations (0.0776) match well with experimental validation (0.0777).

For the setup where the grid is upstream of the propeller (Fig. 5.6B), the airflow is pressing on the load cell, which creates an additional force on the load cell. This force must be accounted for to compare measurements to those obtained when the grid is downstream of the propeller. Thus, the drag value generated by the setup was measured and added to the values of lift measured in the upstream grid configuration. Wake loss factor was not calculated for the upstream configuration, as the grid is not in the wake of the propeller for this configuration.

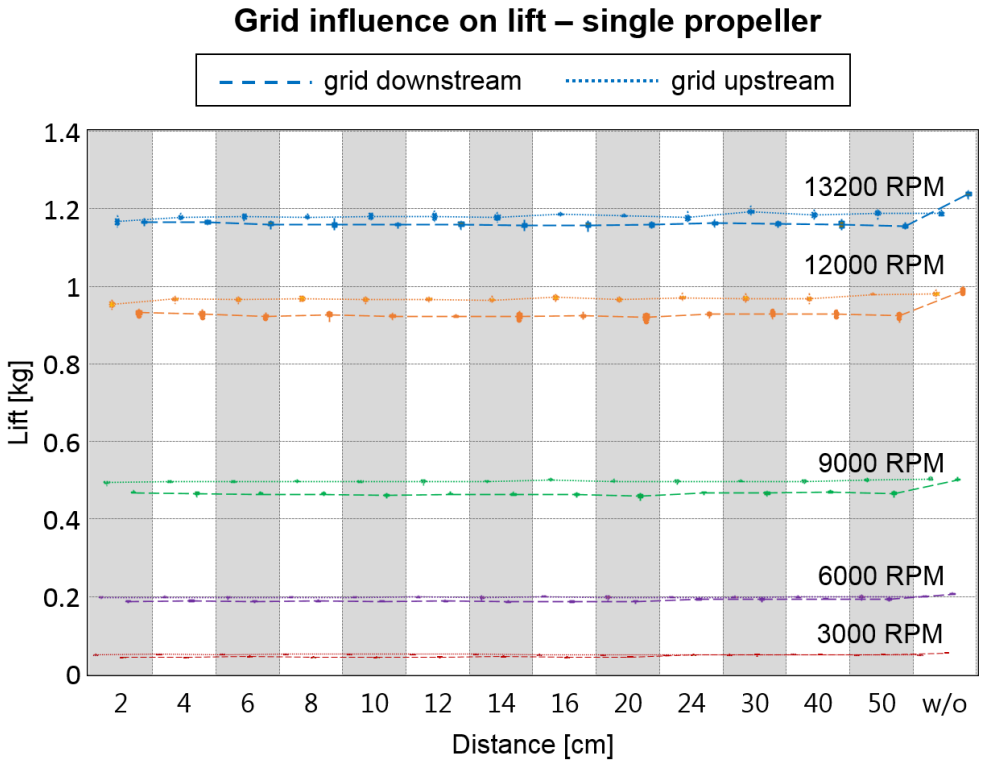

Figure 5.7. Influence on lift when a grid is placed downstream (dotted line) and upstream (solid line) of a single propeller - APC8x4.5MR. Measurements are made for different rotation speeds of the motor. The grid is placed at different distances from the propeller.

5.4.1 Lift savings with deployed arms of quadcopter

The grid placed below and above a propeller has minimal impact on lift (<10%). However, the cage placed around the quadcopter and the truss carbon structure with overlapping propellers generate additional drag and turbulence that reduce lift.

Two experiments were performed to understand the impact of the entire cage (Fig. 5.6C), one with the quadcopter equipped with the cage and the second with the same quadcopter without the cage. Both quadcopters were attached to the RC benchmark test stand used in the previous experiments. The lift was measured in different states of the arm deployment and with different motor speeds. The arm deployment distance was measured from the yaw axis of the drone to the axis of rotation of the propeller. In cruise flight, multicopters fly at a maximum of 80% of full throttle for maneuverability and energy efficiency. Measurements were therefore performed at 10400 RPM, which is 79% of full throttle. As observed in Fig. 5.8, the lift of the drone without the cage (dotted lines) is only affected at its smallest configuration with completely retracted arms (distance 12-16 cm), where the neighboring propellers overlap and tips of the propellers are close to each other. As soon as the propellers move away from each other, the lift value increases and becomes constant. The difference in lift between fully retracted arms and fully deployed arms is 12% for the quadcopter without cage and 21% with the cage. This shows that as expected, the cage decreases the lift of the drone. In addition, these experiments showed that the lift has the

same value when the propellers are outside the cage and with propellers placed at the same position but without the cage (plots converge). This result demonstrates that deploying the arms outside the cage provides unobstructed airflow and avoids negative impact on the lift.

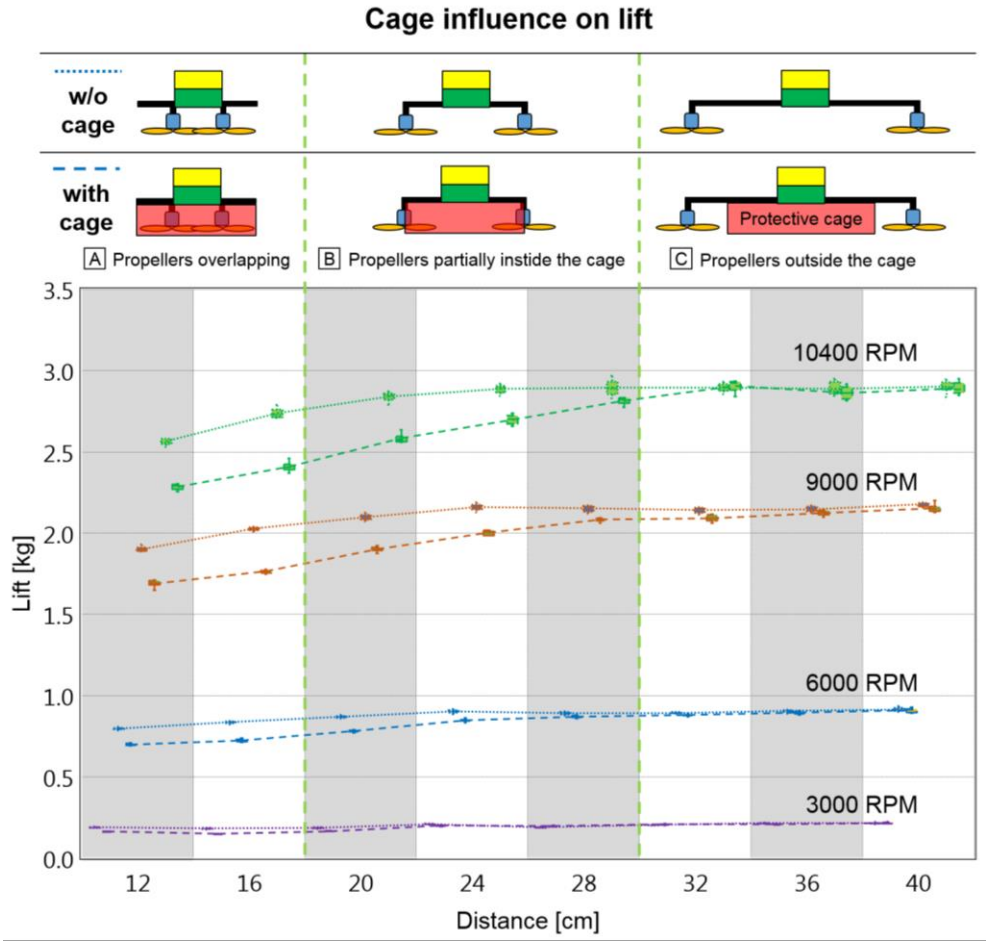

Figure 5.8. Influence on lift for a quadcopter with and without the cage in different arms deployment configurations. At the top of the figure are quadcopters in different phases of arms deployment, indicating graphically the state of the quadcopter corresponding to the plot below. Images above the plot show three phases of deployment, (A) propellers overlapping and fully in the cage, (B) propellers partially in the cage, (C) propellers outside the cage. Distance of deployment was measured from the yaw axis of the drone to the rotation axis of a propeller. On the graph, the solid lines present plots for the drone without the cage. The dashed lines refer to the plots with the cage.

5.4.2 Grid strength for finger pressure

To validate the safety of the grid while a finger is pushed on the grid, an experiment with an artificial finger was performed. Of interest is how much force is required to deflect the grid 35 mm (the distance to the propeller tip) and how that compares with the force applied by an adult of 22 to30 years-old when catching the vehicle, which is 30N [138].

To imitate a soft finger, a flexible cylinder with rounded edges, made of TPE (NinjaFlex) was 3D printed (Fig. 5.9). The size of the finger (19 mm in diameter) was selected from a population of British adults [30]. The artificial finger was mounted onto an Instron 5965 machine (with 500 N load cell), as shown in Fig. 5.10. The force required to break the single string used for the grid

according to string manufacturer is 336.5 N, which is almost twelve times higher than the force applied by a male subject's index finger [137]. This means that the string used has a high safety factor and could be the last breaking point. Thus, other breaking points of the grid should be considered, which could be: (i) reaching a grid deflection of 35 mm; (ii) cracking of the plastic frame holding the grid; and (iii) separation of strings at grid vertices due to failure of the glue used to bind the strings. For characterizing those additional breaking points, an experiment was performed. The artificial finger was placed between the strings so that the force applied by the Instron machine would press the strings apart. For the test, 5 x 10 cm square modules, which correspond to the size of the modules used on the vehicle, were 3D printed and threaded. The module was attached to a square wooden frame at the corners and at the middle of each side, the same way, as attached to the vehicle (Fig. 5.10).

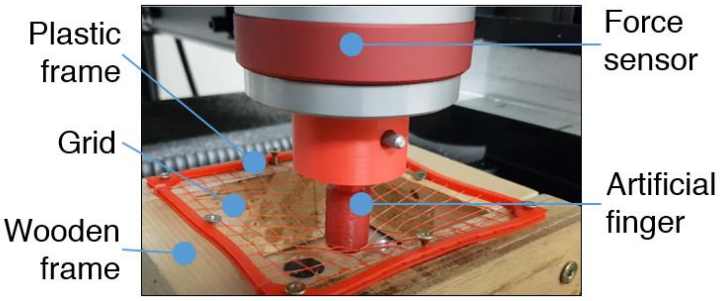

Figure 5.9 Experimental setup installed in Instron machine for testing a grid module. During the tests, an artificial 3D printed finger of the 19 mm diameter was used. The finger was applied between the strings of the grid.

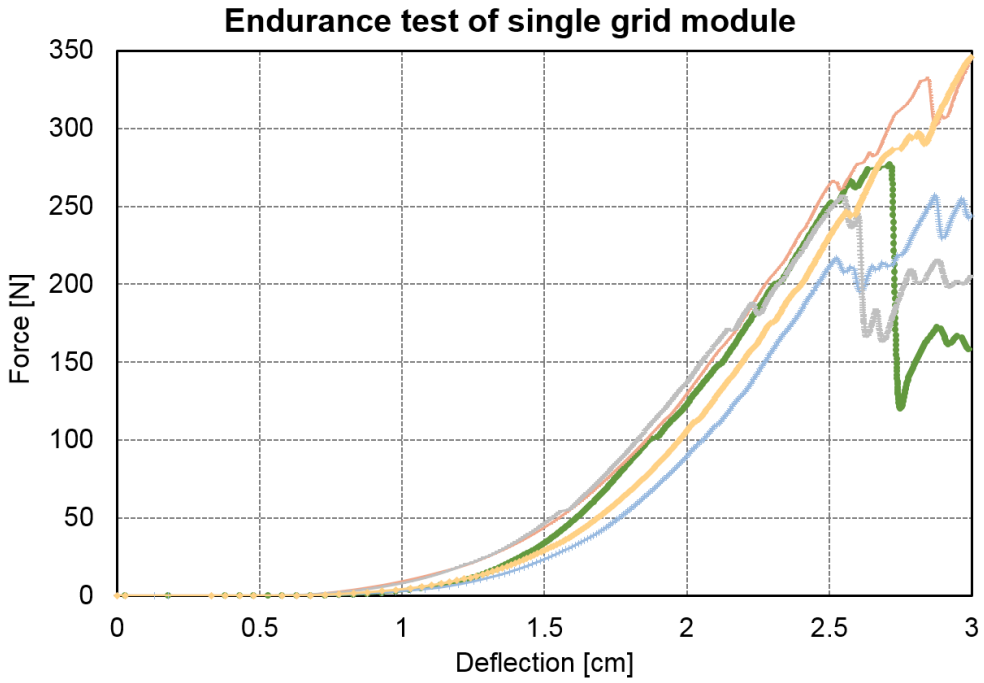

Figure 5.10. Plot shows results of the experiment, which tests strength of the grid module when a finger presses between strings of the grid. The force is measured until the module breaks which occurs after 2.5 cm and reaching an average value of 297N.

Fig. 5.10 presents the results of the strength tests of five grid modules. Each color represents a single test. The average value of maximum load at breaking point is 297 N with standard deviation 46 N. Samples started to fail reaching average extension of 28 mm with standard deviation 2 mm. This number fulfils the previously presented required force of 30 N that can be applied by an index finger of adults between 22 and 30 years old [138]. Under a load of 30 N, the deflection is smaller than 1.5 cm, which is smaller than the 35 mm that separate the grid from the tip of the rotating propeller. During the test, the plastic frame broke three times and the glue broke two times.

5.4.3 Cage frame strength while landing in hands

To enable in-hand delivery, the cage has to be rigid enough to prevent deformation and access to the propellers. To measure the maximum force applicable without bringing the cage in contact with the propellers, the two situations A and B in Section 5.2 were considered: (A) the drone is caught from the sides, between the user's open palms flushed against the drone (Fig. 5.3A); (B) drone is gripped at the sides by two palms, mainly the fingers (Fig. 5.3B).

For situation A, the drone platform was placed between two wooden plates and installed vertically in the Instron machine (Fig. 5.11A-B). The Instron applied a force from 0 N to 350 N. The experiment revealed that the structure of the cage can withstand on average 312 N (10 tests, standard deviation 8.1 N) before it experiences a deformation of at least 5 mm (distance between the propeller tips and the cage is 35 mm in the prototype), which is nine times greater than the 35 N force approximated in Section 5.2. The experiment was stopped after reaching 5 mm to prevent damaging the prototype.

For situation B, where the drone is gripped between two palms while landing, the drone platform was placed horizontally in the Instron machine (Fig. 5.11C) between a plate and a force sensor, mimicking four fingers from the bottom and a thumb at the top. The cage deformation was measured at two locations. In the first location, the thumb was placed at the center of the sidewall of the drone (Fig. 5.11C). An applied force from the Instron machine of 300 N (rounded up from the 270 N force approximated in Section 5.2) deformed the cage by 9.5 mm (10 tests, standard deviation 0.6 mm). In the second location at the connection of two walls, the cage under the load of 300 N deformed by only 1.9 mm (10 tests, standard deviation 0.75 mm). Both tests revealed that the drone could be safely gripped because the minimum distance between the cage and a propeller in this direction is 2.5 cm.

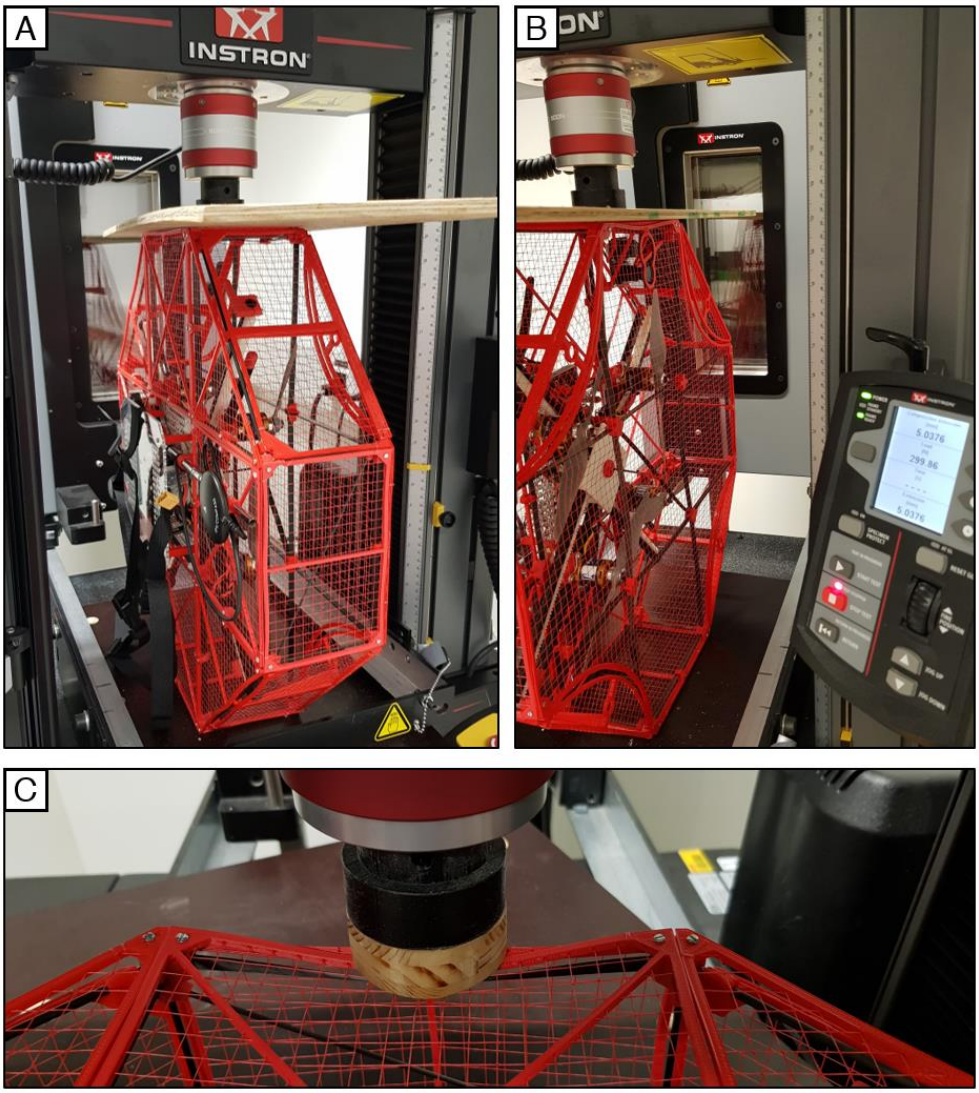

Figure 5.11. The drone installed in the Instron machine to test deformation during in-hand landing. (A-B) The drone placed on its sides (vertical orientation) for the cage deformation test where the cage is held between two open palms. (A) Top view of the drone. (B) Bottom view of the drone. (C) The drone placed in the horizontal orientation for the cage deformation test where the cage is gripped by two palms – four fingers and thumb.

5.4.4 Flight stability during morphing

In order to measure the stability of the drone during morphing, a series of deployment tests was performed in an OptiTrack motion capture system. The drone was commanded to hover in position at 0.7 meters altitude. During hover, the arms were retracted and deployed. Default autopilot settings were taken from the PX4 flight stack controller for an X shaped quadcopter. Fig. 5.12 shows the position of the drone in x, y, z and roll, pitch, and yaw angles as a function of time. As the arms deploy and retract, the drone remains in position in the x-y horizontal plane, but deviated by approximately 0.3 m along the vertical axis z (Fig. 5.12A). This altitude variation is generated by the influence of the cage on the lift force as the arms extend and retract. Fig. 5.12B shows the small oscillation around the pitch (y) and roll (x) axis (maximum 1.9 degrees). During morphing, the drone slowly rotates around its yaw axis to a maximum value of 3.25 degrees and subsequently

returns to its original position. These experiments showed that the drone remains stable both in its position and in orientation during morphing. The test was repeated five times, producing similar results. These results, including the 0.3 meters variation in altitude and small yaw oscillations, could be further improved by tuning the gains of the PID controller (rather than using the default values) to ensure that thrust can be adjusted quickly to maintain the altitude and orientation of the quadcopter.

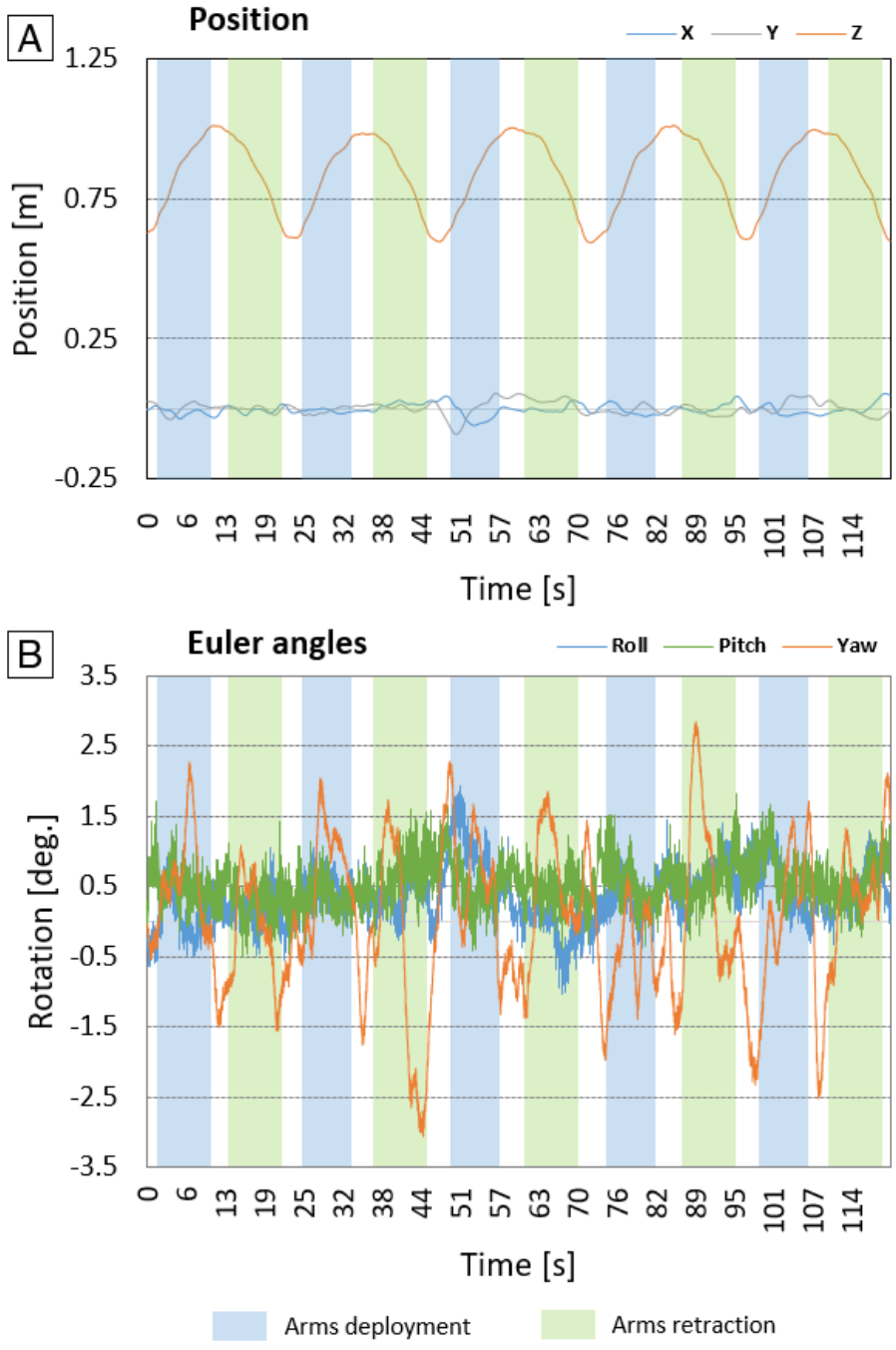

Figure 5.12. Plots showing the stability of the drone's attitude and altitude during arms morphing. Colored areas show the different phases of morphing: the blue area – arm deployment, the green area -arm retraction, the white area – stable hover state between morphing. (A) Plot shows the position profile of the drone. (B) Plot shows the attitude profile of the drone.

5.4.5 Hovering time

To show the difference in flight endurance between the retracted and deployed arm configurations, a test was conducted where the vehicle with a fully charged battery was commanded to keep a constant position and altitude of 1 m above the ground until the battery level reaches 15% of full charge. The hovering time was measured five times in two different conditions: (i) fully retracted arms in the cage (average: 5 minutes 34 seconds, standard deviation: 4 seconds); (ii) deployed arms outside the cage (average: 8 minutes 3 seconds, standard deviation: 7 seconds). The experiment revealed that the drone with arms deployed outside the cage could hover 31% longer before the battery reaches a 15% charge level.

5.5 Conclusions

We have described a novel approach to increase the safety and aerodynamic efficiency of an aerial delivery multicopter by using a compact, dense cage and morphing arms. The cage is made of a dense grid, which prevents fingers from accessing rotating propellers. During the short period of take-off and landing, the propellers are retracted into the cage to provide safety for people and the drone. During cruise flight at high altitude, the quadcopters arms deploy from the cage to increase aerodynamic efficiency. Arms deployed outside the cage increase lift by 0.606 kg, which is a 21% enhancement when compared with inside the cage. The mass of the components used to enable the arm deployment is 0.169 kg, which is 6% of the gross mass of the drone. This leads to a net lift saving of 15% or 0.437 kg compared to when the arms are retracted. This additional lift can be used to carry larger batteries or heavier payload. Moreover, placing the propellers and motors further apart from each other increases the stability of the quadcopter and decreases the control effort to maneuver the drone, which in turn leads to further energy savings. The storage volume of the drone is reduced by 55% when the arms are retracted into the cage, which facilitates storage and transportation of the drone to the place of deployment.

Further weight reduction is possible by replacing the small plastic grids with larger modules. In addition, the frame holding the strings could be further strengthened by using carbon, aluminum alloy or titanium, similarly to the frame of tennis rackets. Moreover, the mixer and PID gains should be further optimized by testing the drone in a wind tunnel. Future development will also contain a controller that should allow adapting the gains during morphing for different external conditions, e.g. wind gusts.

Chapter 6 **Concluding remarks**

THE final chapter summarizes the main contributions of the thesis, namely creating a single delivery solution to the limitations of parcel delivery from person-to-person over a short range. The chapter also presents possible applications for the drone delivery system created from the described solutions. The real-life demonstrations and flights delivering directly to inexperienced users prompted additional questions and challenges on how drone systems for last centimeter delivery can be improved, directing at topics for further research and developments, which are discussed here.

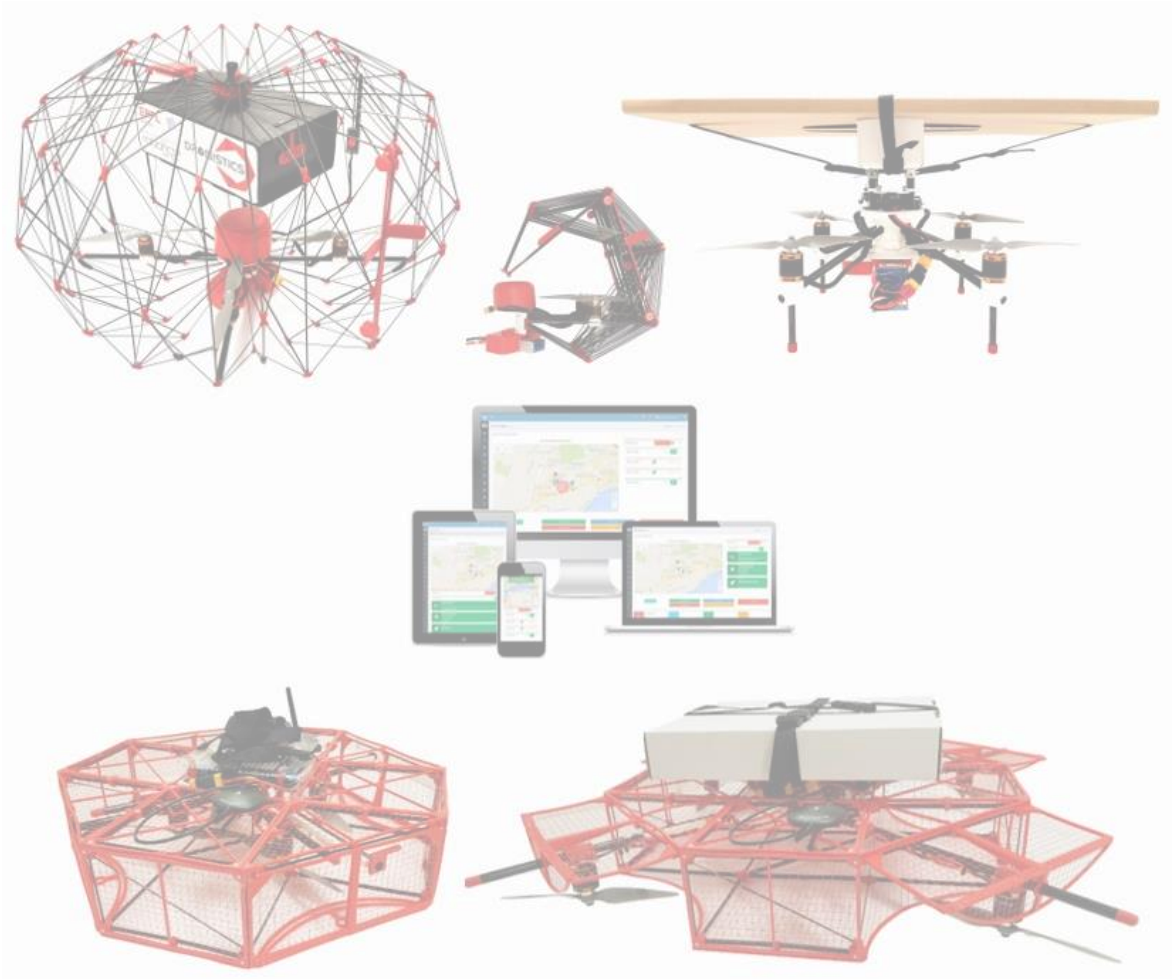

6.1 Main accomplishments

This thesis describes the design process of an integrated parcel delivery solution developed to address the current limitations of drone delivery systems for last-mile delivery. Specifically, the developed solutions together, created a next generation drone delivery system for last-centimeter delivery, transporting payloads directly from person-to-person. The system is composed of hardware and software components that enables the following features: adaptable to different payload dimensions, safe for people, the drone and its cargo, easy to store and transport, easy to use and efficient. Moreover, the system is uncomplicated for inexperienced users. The goals were achieved through four main developments.

Firstly, a new approach of placing the parcel above the propellers was done to enable delivery of parcels of variable sizes. Particularly super-sized parcels, which exceed the footprint of the multicopter. The study of this new design approach, presented in chapter 2, showed various benefits, which include the capability of using a small multicopter airframe that leads to a significant reduction in drag and weight. As such, the design framework of the new, safe and efficient drone delivery solutions, as presented in Chapters 3 and 5, centers on the proposed parcel placement approach. We believe this design will inspire other designers and engineers to find solutions for existing limitations in other drone applications.

The second major contribution of this thesis is the development of the method to design and manufacturing foldable protective structures for multicopters, based on origami technique. The novel method transforms a flat origami pattern into a spatial cage structure that can be simultaneously used as protection for people, the drone and the transported payload without significantly affecting the aerodynamic efficiency of the quadcopter. The new cage truss structure is composed of a combination of rigid and soft components in order to obtain an easy transition from the deployed drone configuration to a storable one for easy transportation and storage. The foldable feature enables reducing storage volume of the drone by 92%. The concept of a folding protective cage could be used to encapsulate other commercially available flying vehicles.

Thirdly, the software *SimplyFly* was developed to provide autonomous delivery drone service from person-to-person. The intuitive Graphical User Interface and integrated photo tutorial in the Web Application, guides a recipient to operate intuitively the drone to receive a parcel delivery. The flight path between the sender and recipient of the drone is generated automatically. The software is compatible with Unmanned Traffic Management Systems (UTMS) that will automatically provide authorization for the drone to fly according to the available air space at the deployment location. The sender has to select a recipient from the recipients registered in the system to send a parcel. The software takes into account of all the steps required for the drone to fly which include controlling and navigating the drone. Therefore, even inexperienced users can use the software and hardware. Furthermore, the software may be used by all drones equipped with a flight stack controller that uses the MavLink protocol, making the software available to a wide variety of platforms.

The assessment of hardware and software functionality was performed in several demonstration and field tests. This allowed us to observe software-human-drone interaction as well as gather feedback directly from the users. The lessons learned are currently being used for future system improvements.

Finally, the fourth development was to improve safety and aerodynamic efficiency. The arms of the quadcopter can retract into a very dense cage serving to separate the propellers from the external environment for take-off and landing. The dense cage allows delivery in the proximity of children, in-hand landing and landing in cluttered environments or on inclined surfaces. The decreased aerodynamic efficiency and increased power consumption from the drag caused by the very dense cage lasts only a short time, which is during the take-off and landing.

6.2 Potential applications

The last-mile delivery of parcels costs transportation companies more than 53% of the total delivery cost [7]. Fast delivery of items in cluttered urban environments with congested ground traffic is starting to be problematic for delivery companies. The problem is even bigger during rush hours. Likewise, delivery in a short range may be challenging, for example, from one side of a river to the other could take a lot of time if the bridge you have to cross is far from the point of dispatch. Also, ground delivery capacity for small samples on campuses and in clinics or hospitals is limited to the available paths, corridors and elevators that may be already fully-occupied by doctors, nurses and patients who have priority when moving or being transported to the treatment place. Besides, delivery of letters, samples or small items manufactured in workshops on site in large universities or companies is usually minimum one-day delivery by internal mail. In less congested environments, the problem of rapid delivery is no less problematic. Remote locations in developing countries suffer from a lack of good road infrastructure and often-harsh environments that decrease the speed of moving from point-to-point.

In this regard, the easy-to-use, person-to-person drone delivery system for last-centimeter delivery is able to solve these ground delivery limitations. Firstly, the electric power consumption of delivery drones is very low [1].The system can be stored easily in an office and deployed outside of a building without the need to create special landing stations. Moreover, thanks to in-hand landing possibility, a drone can deliver directly through windows or onto balconies and the easy-to-use software permits launching a drone from any mobile device.

In the introduction and in Chapter 5, examples of other drone delivery applications indicate the real interest of different stakeholders for using drones for last-cm delivery. A respected Swiss security company recognized the benefits of easy and fast air delivery of valuable items. They would like to acquire the Dronistics drone delivery system. The company's interest is in transportation of one-time high-value objects from one location to another. Due to the complexity of flight paths in urban environments and the proximity of international airports, use of a small drone with a safe cage for landing in crowded environments is critical. Trial flights are planned with this company for spring 2020. A further application was seen by the Non-Governmental Organization – *WeRobotics*, who would like to use *Dronistics* system for delivery of health care-related items found in hospitals, clinics or pharmacies directly to health care workers working in villages in remote locations. Lack of good roads slows down the worker's movements and they cannot always know in advance the equipment and medications they may require. In addition, some medications require special storage conditions such as low temperature for delivery.

6.3 Future development

This section proposes future development to improve and extend the drone delivery possibilities. The proposed future work is organized into groups according to the challenges for drone delivery defined in the thesis.

A surrounding protective structure presented in this thesis greatly improves safety, but increases the overall surface area of a drone, which makes them more sensitive to wind. When wind gust appears, the drone is destabilized or even flipped over, which could cause a crash. In that respect, algorithms to withstand winds, especially when transporting super-sized parcels would be a very important part of future studies. A promising candidate is the Incremental Nonlinear Dynamic Inversion (INDI) controller. Another solution can be use of ESCs and motors that could quickly revert rotation direction or variable pitch propellers. They would allow quickly changing direction of thrust vectors of each propeller, which would allow stabilizing the drone to the initial efficient flight orientation even if the drone were upside down. In addition, algorithms that can dynamically plan flight paths according to information from ground sensors detecting high wind speeds are essential. These algorithms could extend to users to change delivery points during flights to adapt to difficult wind situations. Dynamic path planning would be very helpful in situations where dynamic obstacle avoidance must be triggered based on information from sensor readings. Indeed, alongside further drone development, position and location of sensors should be taken into consideration, which can be challenging when working with morphing structures such as folding cages.

The impact of different cage structures and parcel size on the propulsion system of the drone was studied in this thesis. Several solutions were presented to curb the reduction of aerodynamic efficiency. However, this work mainly dealt with the hover mode that allows the drone to stay in the air. Further investigation should be focused on the impact of the cage and the payload during cruise flight. Wind tunnel tests should be performed to measure the influence of the cage and parcel on the endurance of the drone. Aerodynamic efficiency of standard configurations of multicopters are available. However, combining propellers with different configurations and the influence of one airflow on another could be an interesting direction of study. For example, new configurations may allow decreasing the footprint of multicopters used to land in cluttered environments, providing redundancy in the system and at the same time maintaining high aerodynamic efficiency.

All-around cages separate propellers from the environment when flying close to people and allow in-hand landing. However, energy absorption capabilities are still limited. Further studies should test use of new lightweight materials. Advanced manufacturing techniques could help create structures with existing materials that absorb more energy and possibly reduce the mass of the protective structures to increase the range and payload of drones. These studies should be accompanied by investigation of manufacturing techniques that would allow faster production of protective grids and assembling of cages.

To simplify use of hardware and software, further studies of software-human-drone interaction will have to be performed in various user scenarios. The software Graphic User Interface can be further simplified to reduce the number of steps that the user has to follow. Implementation of voice instructions to assist users at every step when operating the system could reduce time of operation and may increase comfort and acceptability of drone use for personal deliveries.

Appendix A

Energy absorption capabilities of the cage at the moment of impact with the ground

A.1 Introduction

Delivery of high value and fragile payloads that are sensitive to shocks or vibrations requires providing additional protection. This is particularly true in the event of a crash caused by a malfunction in the propulsion system or unexpected contact with an obstacle. To protect a drone and payload from high altitude falls, the most adopted and efficient solution is a parachute. However, additional protection should be provided for low altitude flights where a parachute will not have enough time to open and decrease the speed before the hitting the ground. The problem is worse when the parcel is located below the vehicle, as it could be crushed. On the other hand, when the parcel is placed inside the cage and attached to the top of the cage, the cage can act as a damper absorbing energy of the impact with the ground after a fall from low altitude. In this Appendix, an improvement to the cage is proposed that increases the energy that can be absorbed during impact with the ground in the case of a vertical fall. The idea is to increase cage stiffness without significantly increasing the weight.

A.2 Concept and calculations

During impact with the ground, the cage can act as a damper absorbing impact energy by displacing the parcel attached at the top of the cage. This reduces the overall energy transferred to the ground or object during the collision.

The energy absorbed by the cage (E_{cage}) can be calculated using the equation:

$$E_{cage} = F \cdot S = m \cdot g \cdot S \tag{A.1}$$

Where S, is the maximum possible displacement of the parcel on impact (distance between the bottom of the parcel and the top of the electronic lid), F, the weight of the parcel, m, the mass of the parcel and g, the gravitational acceleration. A free-body diagram is presented in Figure A.1.

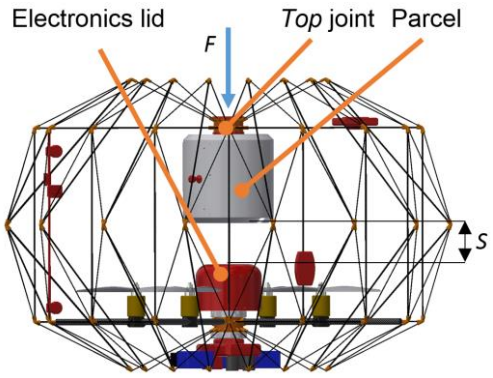

Figure A.1 Schematic representation of components, forces and dimensions of PackDrone required for study in this Appendix.

The experiment performed in Section 3.5.1 measured the vertical displacement of the top central joint of the cage under different cargo loads. In Figure 3.8A, we can see results of the experiment where the top joint displaces 0.15 m under a load of 1.35kg. Thus, the energy absorbed calculated from equation (A.1) is$1.99J$.

On impact after free fall, the parcel travels vertically down deforming first the flexible joint and second, the rods in each module of the cage marked by dashed yellow curved lines in Figure 3.8B. To increase the stiffness of the cage and energy absorption capabilities, rods of larger diameter that can withstand a higher critical force $F_{cr,}$ before buckling replace the old rods. The critical force $F_{cr,}$ can be calculated from equation 3.5 in Section 3.5.1. The goal is to increase the energy absorption capacity with minimal increase in the weight of the rods and overall mass of the cage using commercially available components, such as those in Fig. A.2.

The rods used in the prototype presented in chapter 3 are pultruded carbon fiber rods of diameter 1.5 mm and length 0.3 meter. Results of the calculations of the critical force before buckling are set out in Figure A.2.

A.3 Experimental results

After replacing the rods (1.5 mm in diameter) described in the previous section by tubes (2.5 mm external diameter, internal diameter 1.5 mm), the experiment in Section 3.5.1 was repeated to calculate the new energy absorption capability. The results are presented in Figure A.3. In this experiment, the top joint displaces 0.15 m under a load of 8.21 kg. Thus, the energy absorbed by the cage, calculated from equation A.1, is 12.15 J, which is six-fold increase in energy absorption compared to the cage with rods of diameter 1.5 mm.

To maximize absorbed energy, the distance S should be maximized, meaning that the height of the parcel must be minimized to maximize energy absorption.

The increment of stiffness of the cage after replacing the rods can be defined by calculating the value of the safety factor $s_{f,}$ from equation 3.7. The safety factor for 1.5 mm diameter rods is 2.4, and for 2.5 mm diameter tubes 15.2. Thus, the stiffness is increased 6.3 fold.

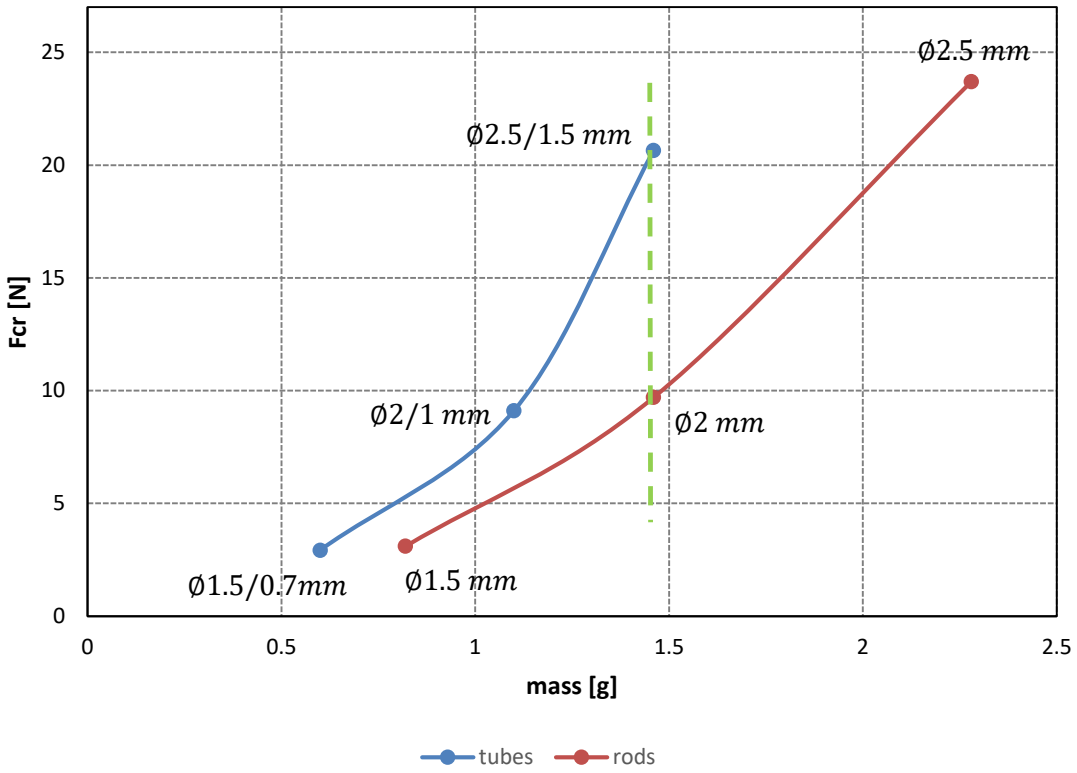

Figure A.2. The plot presents critical force as a function of mass for several commercially available rods and tubes (o external diameter /internal diameter of tubes).

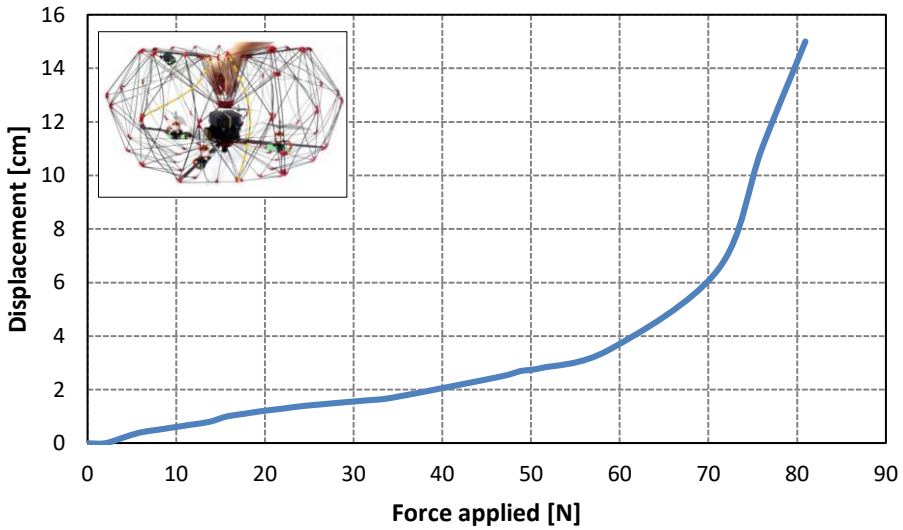

Figure A.3. The plot presents experimentally measured displacement of the top joint of the cage under different parcel loads (continuous blue line). The tubes of the cage start to buckle significantly under a load of 60N.

Appendix B PackDrone V2, Enhanced endurance/payload, and safety of the propulsion system

This Appendix presents work in progress and future steps to produce increased endurance/payload and enhanced safety of the propulsion system in the *PackDrone* platform.

C.1 Introduction

The standard approach to increase payload or endurance of multicopters is to increase the size or number of propellers and increase capacity of the battery. The most aerodynamically efficient configuration is when the propellers are placed in the same plane, next to each other. However, this method increases the drone's footprint, which makes it hard to fly among obstacles or land in cluttered environments. One approach to reduce the footprint of a drone is to place the motors and propellers in close proximity one above another, e.g., placing two motors and propellers onto one arm of the multicopter - coaxial configuration. This allows limiting additional weight added to the platform because motors use a common airframe. However, the airflows generated by propellers placed in close proximity interact directly with one another, reducing aerodynamic efficiency by 10-20%. This is because the bottom motor rotates in air already speed-up by the top propeller. Thus, the difference in air pressure for the bottom propeller is smaller, which causes a reduction in lift, so the drone loses efficiency. State-of-the-art data presents only results of experiments where propellers are placed in close proximity. Therefore, the solution to avoid reduced efficiency could be to increase the distance between the propellers. However, this solution has never been studied, as this idea requires additional structural components of the airframe to maintain distance between the propellers, which would increase the weight of the platform to overcome the 20% loss. In *PackDrone*, additional propellers can be just integrated into the top part of the cage, which would give a configuration of a co-axial quadcopter (Figure B.1). This proposed design would increase the distance between the propellers and no additional components are required to connect both quadcopters. Validation of this concept by aerodynamic tests is an interesting topic and will be performed in future studies.

The second goal of the new design of *PackDrone* is to enhance the safety of the propulsion system by a procedure allowing the drone stay in the air even if some components of the propulsion system are damaged, such as one of the motors, the Electronic Speed Controller, a propeller or a battery. Different solutions to withstand malfunction of motors were presented in Section 1.2.2. However, they require special control algorithms that require optimizing each time the inertia of the drone is changed due to different weighs of payload. In that way, selection of an approach that increases the number of motors to provide a redundant system is a simple and safe solution.

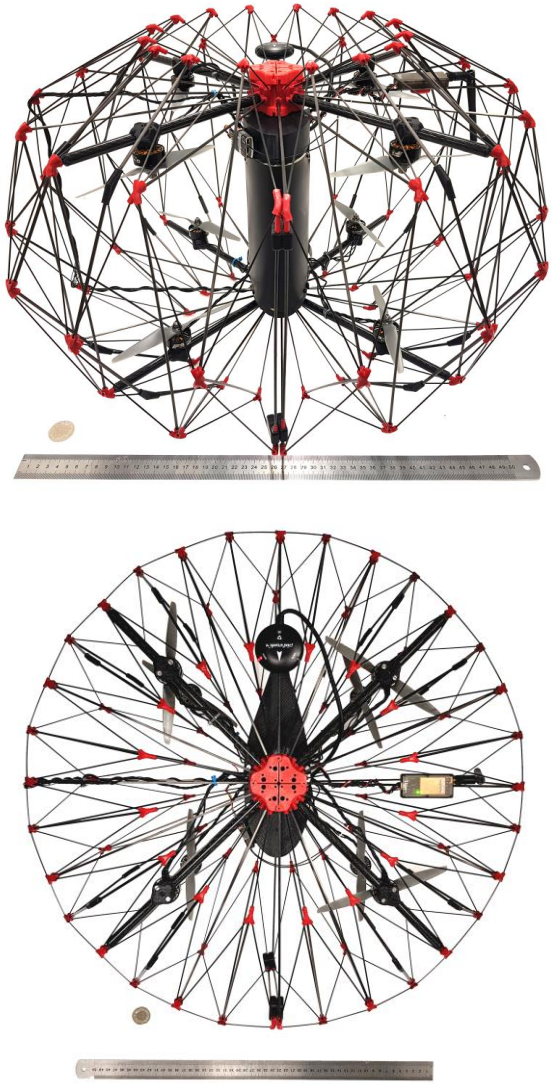

Figure B.1 Photograph of the first version of the prototype of PackDrone V2. (Top) Isometric view. (Bottom) Top view shows the airfoil shape of the battery case.

In this Appendix, we propose a design of *PackDrone* with an integrated quadcopter in a co-axial configuration (eight motors), which, based on initial calculations compared to *PackDrone* version 1, should increase the payload two fold, endurance three fold and provide a redundant propulsion system. This creates a system in which even if four motors fail, the drone can still balance in the air and land safely. Challenges to integrate this particular configuration of propulsion system into *PackDrone* are: (i) defining the position of the batteries and payload, (ii) connecting redundant batteries to the propulsion system, (iii) distributing power and signal between the top and bottom layers of the motors, the autopilot and batteries, (iii) reducing drag created by big-sized batteries, (iv) folding the cage with a second set of arms, (v) programming a co-axial quadcopter when the distance between the propellers is increased.

C.2 Prototype

This section presents the first version of *PackDrone* prototype V2, which addresses a few of the challenges presented.

In the configuration of a co-axial quadcopter, four motors are integrated into the top and four the bottom part of the cage (Figure B.1 and B.2), creating two layers at a distance of less than the radius of the cage. Two motors placed above each other have to run in opposite directions (Figure B.3), but each layer has a configuration of the quadcopter. Thus, the drone could still fly if the second layer is turned off. This feature provides redundancy of the power source, where two batteries can be used, and each quadcopter (layer of motors) can be powered from a single battery. This allows the drone to stay in the air and land safely even if one battery malfunctions. To reduce the length of the cables to power the quadcopters, the batteries were placed inside the cage between the quadcopters. Cables of each battery are facing up or down to power accordingly each quadcopter. The large size of the batteries increases drag and reduces the range of flight or payload. Thus, to reduce drag during a fast cruise flight, the batteries were encapsulated into an airfoil-shaped case (Figure B.2). Two 4-in-1 ESCs are placed at the center, above and below the arms of both quadcopters and are connected directly to the batteries. The autopilot is situated at the top part of the drone to reduce the GPS' cable length, which is placed on the top of the cage. The PWM signal from the autopilot to the bottom of the 4-in-1 ESC is distributed via five thin lightweight cables tangled around the rods of the cage. The battery case was designed as a compartment for small-sized payloads. Bigger-sized payloads can be placed above the cage. However, further investigation of the distribution of the CG should be considered, taking into account malfunctions of the different motors. For the autopilot, PixHawk4 with PX4 flight stack software was used. Initial flight tests (without the payload), revealed that using a standard flight stack for co-axial quadcopters allows the drone to fly stably.

Appendix C presents two versions of *PackDrone* V2.

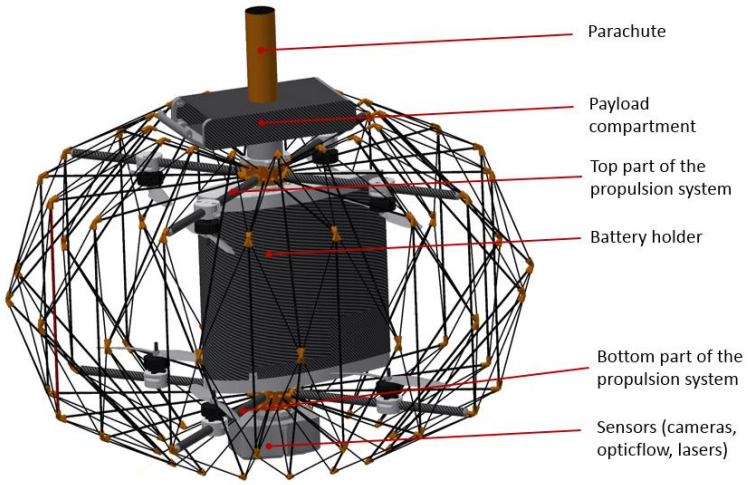

Figure B.2 CAD design of the PackDrone V2 prototype with the first approach of positioning components.

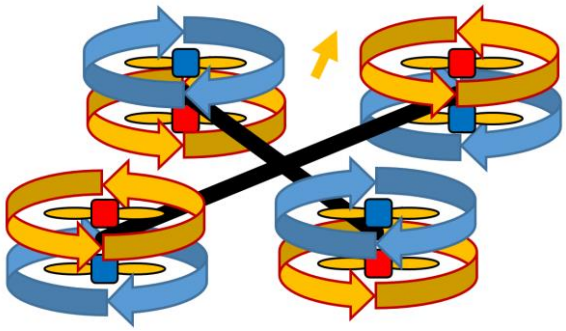

Figure B.3 Symbolic representation of directions of rotation of each propeller in the configuration of a co-axial quadcopter.

C.3 Conclusions and future work

Despite the possible loss of efficiency, *PackDrone* with co-axial quadcopter configuration will increase safety by using redundant components, increase the payload/range from sharing the air-frame between the increased numbers of motors. Additional motors will provide more lift, thus, a battery with higher capacity can be used. The co-axial quadcopter configuration will maintain the small footprint of the drone, thereby allowing delivery to cluttered environments.

In a future investigation of the position of the CG, the case of malfunction of the different components should be taken into consideration. Aerodynamic experiments to verify the concept of reduced loss of power efficiency due to increased space between the propellers should be performed. Wind tunnel tests should be done to verify use of the airfoil-shaped casing of the battery. Moreover, flight tests should be performed to validate calculations of the range of flight without and with different payload weights. Additional tests should be done to verify the drone's behavior when simulating malfunction of the different components.

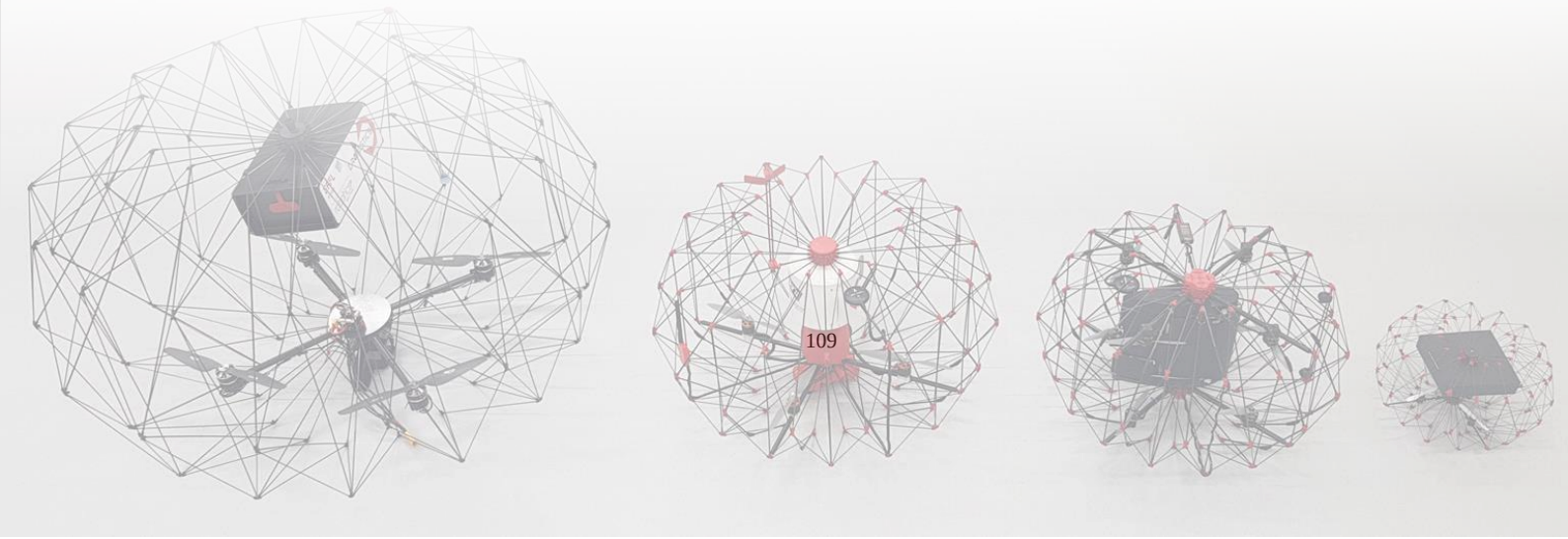

Appendix C Evolution of the PackDrone

In this thesis, different types and sizes of the *PackDrone* platform were designed and manufactured. The purpose and improvement for each version are described in this Appendix. The evolution of the *PackDrone* platform led to the final design of *PackDrone V2*.

C.1 PackDrone v1.0

Proof of concept prototype

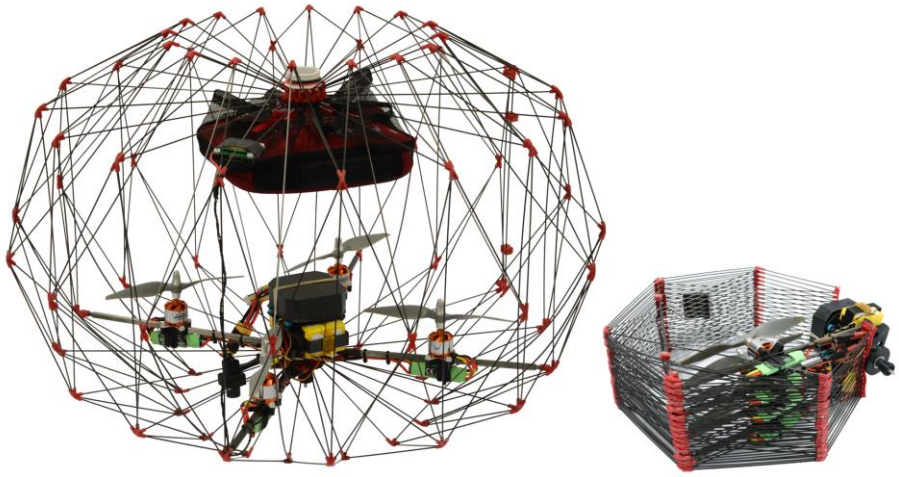

The goal for this prototype was to validate the concept of a foldable protective cage. In this version of the *PackDrone*, the cage was made out of 1.5 mm rods. The bottom locking mechanism was designed to unlock the arms in case of collision with the ground, preventing damaging the propulsion mechanism and other components of the drone. Two batteries were located inside the cage. The main limitations of this platform were related to the propulsion system. Cheap components caused different problems, preventing performing extensive flight experiments. For example, motors overheated reducing rotation speed, which lead to a sudden reduction in thrust on a random motor, causing a crash. The software of ESCs were designed to restart themselves as soon as PWM signal was lost for a fraction of a second, which lead to unexpected stopping of a motor.

Payload: 0.5 kg
Time of hover: 10 min.
Weight: 1.5 kg
Deployed dimensions: Ø65 x 43 cm (D x H)
Folded dimensions: 31 x 38 x 12 cm (W x L x H)
Interface for the parcel: net

C.2 PackDrone v1.0S

Two-times smaller version of the *PackDrone* v1.0 - designed for wind tunnel tests

This prototype was built to test the effect of drag generated by the cage during cruise flight. The dimensions of this prototype were scaled down two times to fit the prototype into a small available wind tunnel. The prototype was used to perform the aerodynamic experiments in Chapter 3.

When scaling down the cage, the biggest challenge appeared the manufacturing process of the flexible joints. Using FDM technology to 3D-print small and complex shapes of the joints did not give the expected results. To obtain accurate shapes and angles, the flexible joints had to be re-designed to achieve simpler shapes, which required adjusting the lengths of the rods used in the cage.

Payload: nd
Time of hover: nd
Mass (without battery and payload): 107 g
Deployed dimensions: Ø33 x 20 cm
Folded dimensions: 31 x 38 x 12 cm (W x L x H)
Interface for the parcel: paper box (44g)

C.3 PackDrone v1.1

Reinforced stiffness of the cage according to the calculation from Appendix A.

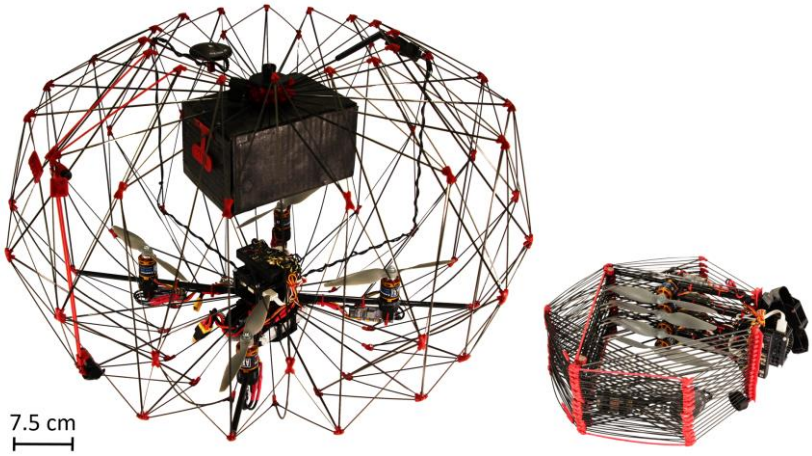

The goal of this version of the prototype was to address two challenges:

- Increase the capability of the cage to absorb energy from the parcel during free-fall to the ground
- Increase the stiffness of the cage to prevent deformation of the cage with payload during dynamic changes of flight direction.

As presented in Appendix A, to improve cage stiffness the long rods of the cage were replaced by tubes of larger diameter to increase the critical force under which the rods start to buckle. Replaced rods reinforced cage stiffness on the sides also to prevent deforming the cage during side collision. The previous locking mechanism required the user to position precisely the arms of the propulsion system before locking the bottom joint. Thus, the joint was redesigned using a slider that allowed the arms to self-align. Unfortunately, on folding, the bottom joint would block itself, which was unexpected for inexperienced users who might have broken it when using higher force. In this version, the batteries were placed below the drone to bring the position of the CG closer to the plane of the propellers. The batteries were secured with Velcro tape, which proved difficult for laypeople to secure them in the correct position. Moreover, the new *PackDrone* was equipped with an external on-board computer, Odroid used as an interface to connect a 4G modem and connect the drone to the *SimplyFly* software via the Internet, as this version *PackDrone* was equipped with a safety switch to disengage the propulsion system when the user opens the cage. To solve the problem of overheating in the previous version, new motors were installed after a series of extensive tests performed with temperature sensors on a test bench. This version was used for the test flights on the EPFL campus to deliver 3D-printed parts or PCB.

Payload: 0.5 kg
Time of hover: 10 minutes
Weight w/o payload: 1950 g
Deployed dimensions: ∅70 x 46 cm
Folded dimensions: 38 x 37 x 14 cm (W x L x H)
Interface for the parcel: paper box

C.4 PackDrone v1.2

A larger version for extended range and payload**.**

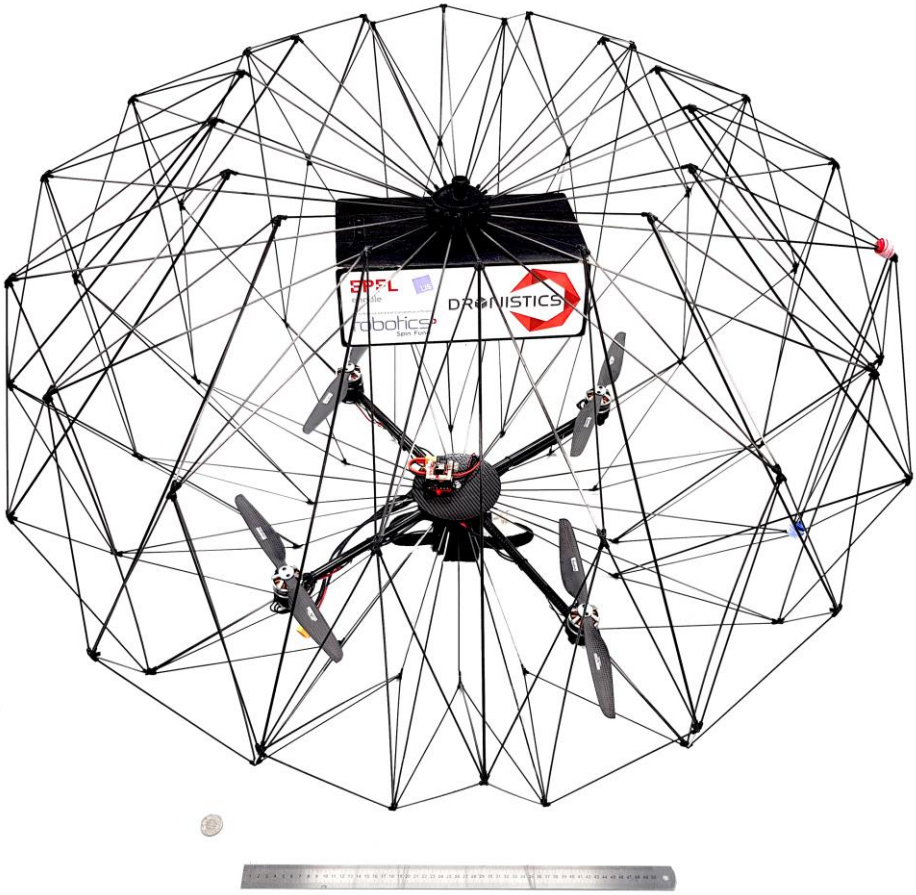

The two main goals of this prototype were to: (i) increase payload and range of delivery by using bigger 12-inch propellers and a higher capacity battery, (ii) verify the usability of such a large platform. Unfortunately, the scaled-up cage significantly increased the space between the rods that we attempted to fill in by attaching a denser grid to the rods. However, the attached grid entangled around other components of the drone and itself when folding and deploying the cage. Therefore, the cage was hard to operate, especially for inexperienced users. Due to these limitations, the avionics were never installed on the drone. Thus, this platform has not been tested in flying.

Payload: 1 kg
Time of hover: nd
Expected range: 4 km
Weight w/o payload: (cage + 4 x motors + propellers): 1173g
Deployed dimensions: Ø112 x 72 cm
Folded dimensions: 54 x 58 x 12 cm
Interface for the parcel: paper box

C.5 PackDrone v1.4

Demonstration kit

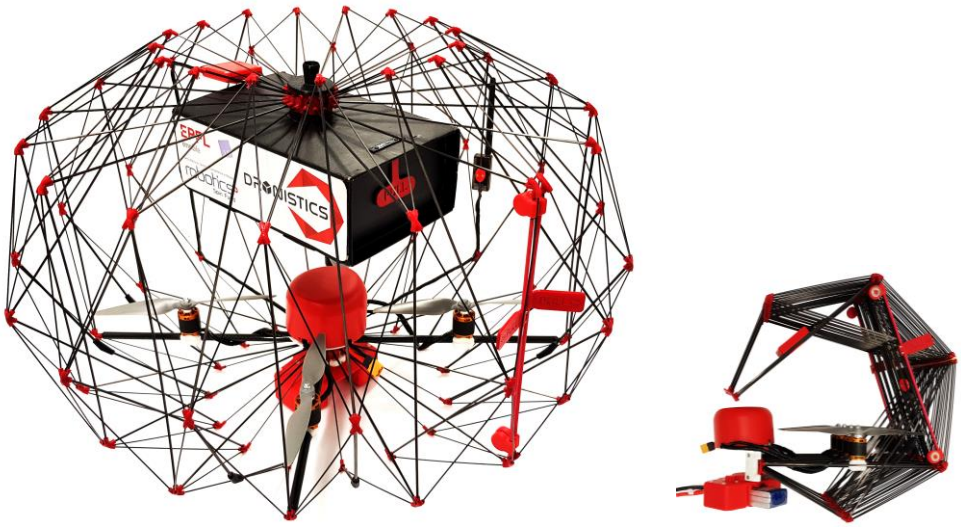

This version of *PackDrone* had a series of improvements. Compared to *PackDrone* version 1.1, the mass of this version was reduced by 300 g. This was achieved by: (i) replacing the four separate ESCs with one 4-in-1 ESC, (ii) reducing the length of the power and signal cables coming from the motors and ESCs, (iii) replacing the big external computer Odroid with a smaller and lighter version, called RaspberryPi0. The reduction in mass allowed installing additional sensors: (i) a camera, installed to verify the recipient; (ii) a laser altitude sensor – Lidar v3 and for XY positioning PX4flow to increase precision during take-off and landing; (iii) a second GPS module. The first module connected to three satellite constellations to increase precision and time to receive "GPS fix". The second GPS module is an RTK GPS to increase the drone's navigation precision at take-off and landing by centimeters. All the electronics are placed under a lid that protects them in flight and transportation. A new joint was designed, composed of hinges that allows users to easily fold and deploy the drone without needing to lock the bottom joint. Due to the reduced weight, a larger battery was used. A new holder for the battery was designed that allows the battery to slide in to the specially prepared slot. The battery is secured from sliding out during flight by small neodymium magnets. The larger 9-inch propellers were used to decrease noise and increase efficiency.

Payload: 0.5 kg
Time of hover: 10 minutes
Range: 2km
Weight w/o payload: 1.6 kg
Deployed dimensions: Ø70 x 46 cm
Folded dimensions: 38 x 37 x 14 cm (W x L x H)
Interface for the parcel: paper box

D.6 PackDrone v2.0

Extended range and enhaced safety of the propulsion system

The first goal of this prototype was to increase the range of the drone by decreasing the size of the platform and decreasing the drag during fast cruise flight.
To increase the range, smaller 6-inch propellers powered by a 4S 2 x 10Ah battery were used to achieve high speed of the platform, which theoretically should reach a range of 4km. Two batteries placed inside the cage were encapsulated into the airfoil-shaped casing to decrease the drag force during high-speed flight.
The battery case has a compartment for small-sized payloads. The bigger-sized payloads may be located just above the cage. Additional sensors for precise landing are located below the drone.
Future work will require tests in wind tunnel to measure the drag generated by the cage, the influence of the propellers on each other and the airfoil-shaped battery casing when the drone flies at high-cruise speeds.
The second goal was to increase safety in the case of a malfunction of one of the components of the propulsion system. More details are presented in Appendix C.

Payload: 0.5 kg
Time of hover: x minutes
Expected range: 4 km
Weight without payload: 1.6 kg
Battery capacity: 2 x 4S 10Ah
Deployed dimensions: Ø60 x 39 cm
Folded dimensions: 30 x 28 x 14 cm (W x L x H)
Interface for the payload: container above the cage or inside the battery compartment

D.7 PackDrone v2.1

Extended range and increased payload

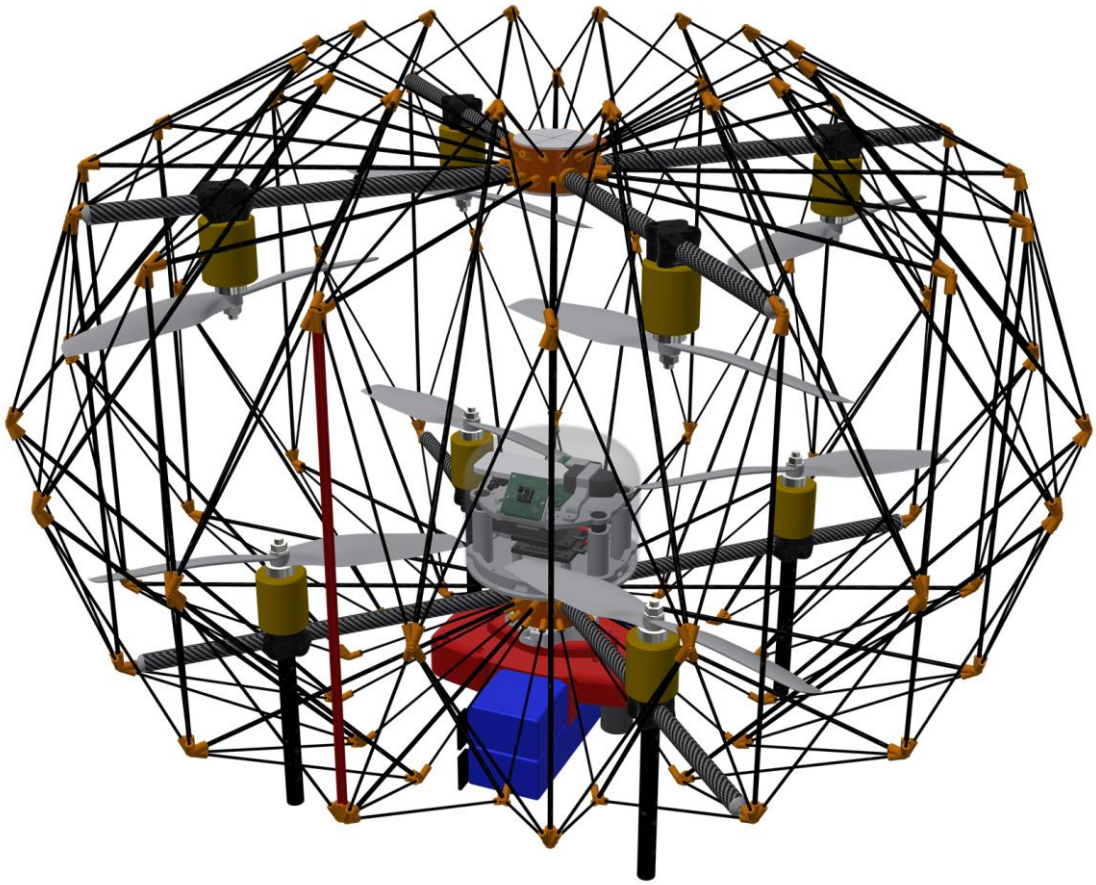

The goal of this version was to increase the payload and range of the platform compared to *PackDrone* v2.0. Use of bigger 9-inch propellers allows increasing lift, thus the payload and using a battery with higher capacity. This version is still in the design process, but based on the initial calculations, it should allow transport of 1kg payloads over 4km or 0.5 kg payloads over 6km. The figure above presents a CAD design of the drone.

Payload: 0.5-1 kg
Theoretical time of hover: 23 minutes (0.5kg) or 19 minutes (1 kg).
Expected range:
0.5kg payload – 6 km
1 kg – 4 km
Weight without payload: 2.8 kg
Battery capacity: 2 x 3S 10Ah
Deployed dimensions: Ø70 x 46 cm
Folded dimensions: 38 x 37 x 14 cm (W x L x H)
Interface for the payload: container inside the battery holder or above the cage

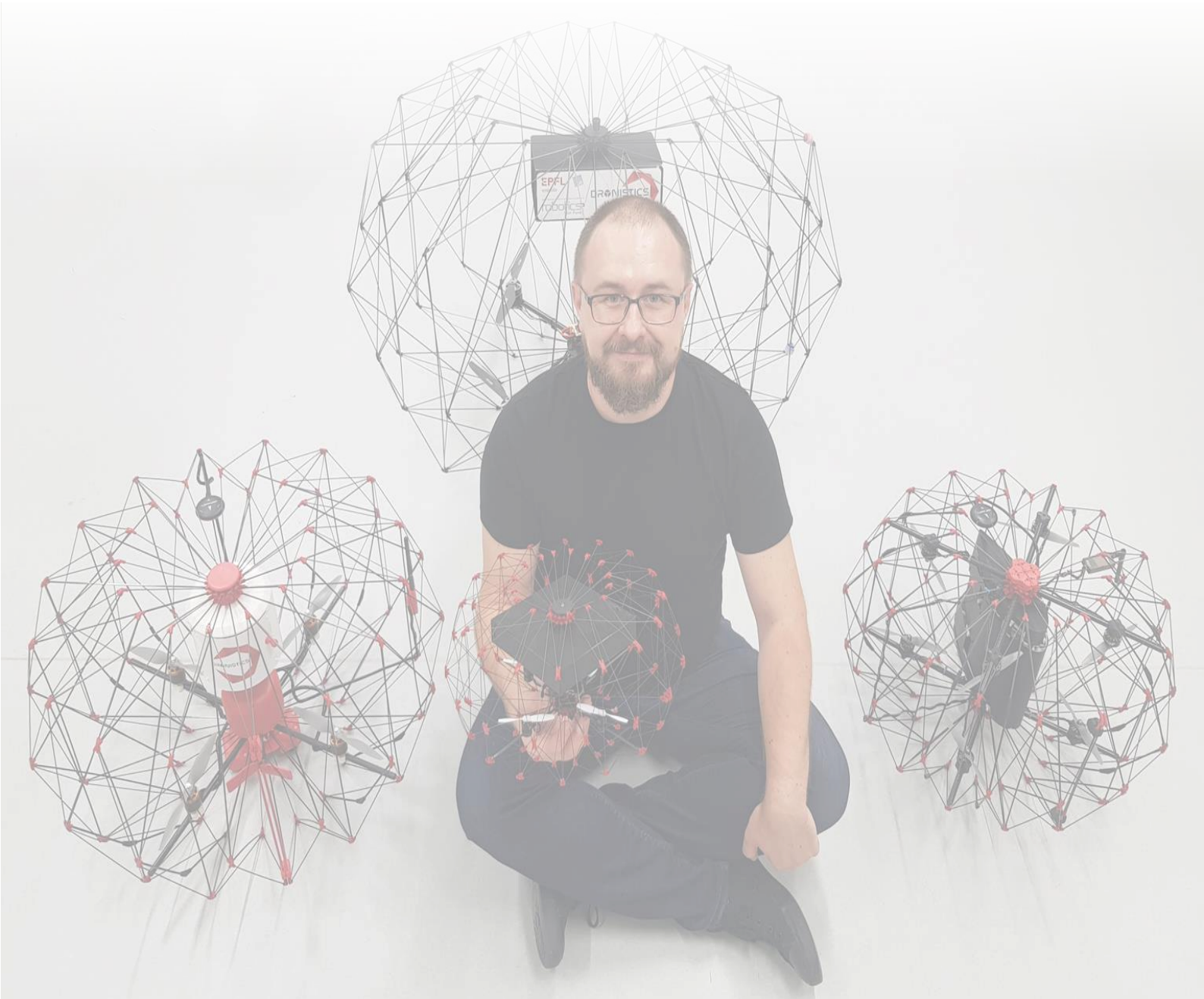
EPFL
DRONISTICS

Appendix D Publications

Manuscripts under review in peer-reviewed scientific journals:

P. M. Kornatowski, M. Feroskhan, W. J. Stewart, and D. Floreano, "Morphing delivery drone for safe flight in proximity of humans". *Robotics and Automation Letters* **in review** (2019).

P. M. Kornatowski, M. Feroskhan, W. J. Stewart, and D. Floreano, "Downside Up: Rethinking parcel position for aerial delivery". *Robotics and Automation Letters* **in review** (2019).

Manuscripts published in peer-reviewed scientific journals and conferences:

P. M. Kornatowski, A. Bhaskaran, G. M. Heitz, S. Mintchev, and D. Floreano, "Last-Centimeter Personal Drone Delivery: Field Deployment and User Interaction," *IEEE Robotics and Automation. Letters*, 2018.

P. M. Kornatowski, S. Mintchev, and D. Floreano, "An origami-inspired cargo drone," in *IEEE International Conference on Intelligent Robots and Systems*, 2017.

P. Bai, B. Guerreiro, R. Cunha, **P. Kornatowski**, D. Floreano, and C. Silvestre, "Wall-contact sliding control strategy for a 2D caged quadrotor," in *International Conference on Control, Automation and Systems*, 2018.

Other publications not related to the topic of the thesis:

J. E. Auerbach, A. Concordel, **P. M. Kornatowski**, and D. Floreano, "Inquiry-Based Learning with RoboGen: An Open-Source Software and Hardware Platform for Robotics and Artificial Intelligence," *IEEE Transactions on Learning Technologies*, 2018.

J. E. Auerbach, G. Heitz, **P. M. Kornatowski**, and D. Floreano, "Rapid evolution of robot gaits," in *GECCO 2015 - Companion Publication of the 2015 Genetic and Evolutionary Computation Conference*, 2015.

J. Auerbach, D. Aydin, A. Maesani, **P. Kornatowski** and T. Cieslewski et al. „RoboGen: Robot Generation through Artificial Evolution," *Artificial Life 14: International Conference on the Synthesis and Simulation of Living Systems*, New York, NY, USA, July 30-August 2, 2014.

Previous work - published publications not related to the topic of the thesis:

A. Briod, **P. Kornatowski**, J. C. Zufferey, and D. Floreano, "A collision-resilient flying Robot," *J. F. Robot.*, 2014.

A. Briod, **P. M. Kornatowski**, A. Klaptocz, A. Garnier and M. Pagnamenta et al. "Contact-based navigation for an autonomous flying robot". *Proceedings of the IEEE International Conference on Intelligent Robots and Systems (IROS 2013)*, Tokyo, Japan, November 3-7, 2013.

Patents:

P. M. Kornatowski, and D. Floreano. *"*A morphing cargo drone for safe flight in proximity of humans*,"* patent pending, 2019.

P. M. Kornatowski, Mir Feroskhan, and D. Floreano. "Downside Up: Rethinking parcel position for aerial delivery," patent pending, 2019.

P. Kornatowski, S. Mintchev, and D. Floreano, "*Foldable aircraft with protective cage for transportation and transportability*, (US10252795, PCT/IB2017/052034).

A. Briod, **P. Kornatowski**, A. Klaptocz, J.-C. Zufferey, and D. Floreano, *A vertical take-off and landing aerial vehicle*, (*EP 13171364.6*, 2013).

References

[1] R. D'Andrea, "Guest editorial can drones deliver?" IEEE Transactions on Autom. Science and Engineering, vol. 11, no. 3, pp. 647–648, 2014.

[2] Murray, C. C., & Chu, A. G. (2015). The flying sidekick traveling salesman problem: Optimization of drone-assisted parcel delivery. Transportation Research Part C: Emerging Technologies, 54, 86-109.

[3] IEEESpectrum (2016, November 28). The Economics of Drone Delivery [Online]. Retrieved from http://spectrum.ieee.org/automaton/robotics/drones/.Vo1QM-VPpPU.twitter

[4] Bamburry, D. (2015). Drones: Designed for Product Delivery. Design Management Review, 26(1), 40-48.

[5] Thiels, C. A., Aho, J. M., Zietlow, S. P., & Jenkins, D. H. (2015). Use of unmanned aerial vehicles for medical product transport. Air medical journal, 34(2), 104-108.

[6] Floreano, D., & Wood, R. J. (2015). Science, technology and the future of small autonomous drones. Nature, 521(7553), 460-466.

[7] OC&C Strategy Consultants (2019, September 10) Reinventing the Last Mile. [Online] Retrieved from https://www.occstrategy.com/en/about-occ/news-and-media/article/id/3276/2016/03/reinventing-the-last-mile

[8] Business Insider (2019, September 10) The challenges of last mile logistics & delivery technology solutions. [Online] Retrieved from https://www.businessinsider.com/last-mile-delivery-shipping-explained?r=US&IR=T

[9] OveBlog (2016, November 28) Protégeons nos mains, voir beaucoup plus ! Images choquantes, vidéos!! [Online]. Retrieved from http://chrismeme11.over-blog.com/article-36258812.html

[10] Clarke, R., & Moses, L. B. (2014). The regulation of civilian drones' impacts on public safety. *Computer Law & Security Review*, *30*(3), 263-285.

[11] The Verge (2019, September 28) *Here's Amazon's new transforming Prime Air delivery drone* . [Online]. Retrieved from https://www.theverge.com/2019/6/5/18654044/amazon-prime-air-delivery-drone-new-design-safety-transforming-flight-video

[12] D. Bamburry, "Drones: Designed for Product Delivery," Des. Manag. Rev., vol. 26, no. 1, pp. 40–48, 2015. R.

[13] Benito, J. A., Glez-de-Rivera, G., Garrido, J., & Ponticelli, R. (2014, November). Design considerations of a small UAV platform carrying medium payloads. In *Design of Circuits and Integrated Circuits (DCIS), 2014 Conference on* (pp. 1-6). IEEE.

[14] Forbes [Online]. Retrieved from: https://www.forbes.com/sites/jonbird1/2018/07/29/what-a-waste-online-retails-big-packaging-problem/#701084ac371d, 13 April 2019.

[15] Interspot. (2015, September 2) Robots Will Soon Deliver Both Medicine And Mail. [Online]. Retrieved from http://inventorspot.com/articles/robots_will_soon_deliver_both_medicine_and_mail

[16] TechCrunch [Online]. Retrieved from: https://techcrunch.com/2016/10/13/a-test-flight-with-zipline-makers-of-humanitarian-delivery-drones/, 13 April 2018.

[17] Amazon. (2015, September 2) Amazon PrimeAir. [Online]. Retrieved from http://www.amazon.com/b?node=8037720011

[18] Matternet (2016, November 28) *Matternet One* [Online]. Retrieved from https://mttr.net/

[19] The Verge. (2016, February 16) Drones could make Amazon's dream of free delivery profitable. [Online]. Retrieved from http://www.theverge.com/2015/6/3/8719659/amazon-prime-air-drone-delivery-profit-free-shipping-small-items

[20] DPDHL (201, October 28) *DHL launches its first regular fully-automated and intelligent urban drone delivery service* [Online]. Retrieved from https://www.dpdhl.com/en/media-relations/press-releases/2019/dhl-launches-its-first-regular-fully-automated-and-intelligent-urban-drone-delivery-service.html

[21] Project Wing (2016, November 28) *Transforming the way goods are transported* [Online]. Retrieved from https://x.company/projects/wing/

[22] FlyTrex (2016, November 28) [Online]. Retrieved from https://www.flytrex.com/#project-detail https://www.rigi.tech/

[23] BrandSynario (2019, September 28) *Domino's Pizza Starts Drone Delivery in Pakistan.* [Online]. Retrieved from https://www.brandsynario.com/dominos-pizza-starts-drone-delivery-in-pakistan/ https://dronedeliverycanada.com/resources/drone-delivery-canada-announces-commercial-agreement-with-edmonton-international-airport/

[24] RigiTech (2019, September 28) [Online]. Retrieved from https://www.rigi.tech/

[25] Drone Delivery Canada (2019, November 7) [Online]. Retrieved from https://dronedeliverycanada.com/resources/drone-delivery-canada-announces-commercial-agreement-with-edmonton-international-airport/

[26] Parrot. (2019, September 2) AR Drone 2.0. [Online]. Retrieved from https://www.parrot.com/global/drones/parrot-ardrone-20-elite-edition]

[27] DJI. (2019, September 2) AR Drone 2.0. [Online]. Retrieved from https://www.dji.com/

[28] Klaptocz, A.; Briod, A.; Daler, L.; Zufferey, J.-C.; Floreano, D., "Euler spring collision protection for flying robots," in Intelligent Robots and Systems (IROS), 2013 IEEE/RSJ International Conference on, vol., no., pp.1886-1892, 3-7 Nov. 2013.

[29] A.Kalantari and M. Spenko, "Design and experimental validation of HyTAQ, a hybrid terrestrial and aerial quadrotor," in IEEE International Conference on Robotics and Automation, ICRA, 2013.

[30] Briod, A., Kornatowski, P., Zufferey, J. C., & Floreano, D. (2014). A Collision-resilient Flying Robot. Journal of Field Robotics, 31(4), 496-509.

[31] C. J. Salaan, K. Tadakuma, Y. Okada, Y. Sakai, K. Ohno, and S. Tadokoro, "Development and Experi-mental Validation of Aerial Vehicle with Passive Rotating Shell on Each Rotor," IEEE Robot. Autom. Lett., 2019.

[32] FlyAbility (2019, September 28) [Online]. Retrieved from https://flyabilit.com

[33] C. J. Salaan, K. Tadakuma, Y. Okada, E. Takane, K. Ohno, and S. Tadokoro, "UAV with two passive rotating hemispherical shells for physical interaction and power tethering in a complex environment," in Proceedings - IEEE International Conference on Robotics and Automation, 2017.

[34] Taamallah, S. (2015). *Small-Scale Helicopter Automatic Autorotation: Modeling, Guidance, and Control* (Doctoral dissertation, TU Delft, Delft University of Technology).

[35] Rotorcraft Flying Handbook, H. (2000). U.S. DEPARTMENT OF TRANSPORTATION FEDERALAVIATION ADMINISTRATION Flight Standards Service. FAA-H-8083-21.

[36] Mueller, M. W., & D'Andrea, R. (2014, May). Stability and control of a quadrocopter despite the complete loss of one, two, or three propellers. In *Robotics and Automation (ICRA), 2014 IEEE International Conference on* (pp. 45-52). IEEE.

[37] Wyllie, T. (2001). Parachute recovery for UAV systems. Aircraft Engineering and Aerospace Technology, 73(6), 542-551.

[38] De Temmerman, N. (2007). Design and analysis of deployable bar structures for mobile architectural applications. *Vrije Universiteit Brussel*.

[39] Wever, T. (2008). Tensairity: The effect of internal stiffeness on the buckling behaviour of an inflatable column (Doctoral dissertation, TU Delft, Delft University of Technology).

[40] Shaker, J. F., & Acquaviva, T. H. (1995). Static stability of the Space Station solar array FASTMast structure.

[41] Quagli, C. P., Ballard, Z. C., & Thrall, A. P. (2014). Parametric modelling of an air-liftable origami-inspired deployable shelter with a novel erection strategy. Mobile and Rapidly Assembled Structures IV, 136, 23.

[42] Konings, R. (2005). Foldable containers to reduce the costs of empty transport? A cost-benefit analysis from a chain and multi-actor perspective. Maritime Economics and Logistics, 7(3), 223.

[43] Buhl, T. Jensen, F. V., & Pellegrino, S. (2004). Shape optimization of cover plates for retractable roof structures. *Computers & Structures*, *82*(15), 1227-1236.

[44] Pellegrino, S. (2001). Deployable structures in engineering. In Deployable Structures (pp. 1-35). Springer Vienna.

[45] Hanaor, & Levy. (2001). Evaluation of deployable structures for space enclosures. International Journal of Space Structures, 16(4), 211-229.

[46] Quinn, G., & Gengnagel, C. (2014). A review of elastic grid shells, their erection methods and the potential use of pneumatic formwork. Mob Rapidly Assem Struct IV, 136, 129.

[47] Pellegrino, S., & Vincent, J. F. (2002). HOW TO FOLD A MEMBRANE1. CISM COURSES AND LECTURES, 59.

[48] SunSpiral, V., Gorospe, G., Bruce, J., Iscen, A., Korbel, G., Milam, S., ... & Atkinson, D. (2013). Tensegrity based probes for planetary exploration: Entry, descent and landing (EDL) and surface mobility analysis. International Journal of Planetary Probes.

[49] Buri, H., & Weinand, Y. (2008, June). ORIGAMI—Folded Plate Structures, Architecture. In 10th World Conference on Timber Engineering. Parrot. (2015, September 2) AR Drone 2.0. [Online]. Retrieved from http://ardrone2.parrot.com/

[50] A multi-modal hovering and terrestrial robot with adaptive morphology S. Mintchev and D. Floreano

[51] Gizmag. (2015, September 2) Sub-$500 Pocket Drone folds for transport and carries a GoPro. [Online]. Retrieved from http://www.gizmag.com/pocket-drone-folding-tricopter/30457/pictures#1

[52] Mintchev, S., Floreano, D. (2018). *A multi-modal hovering and terrestrial robot with adaptive morphology* (Proceedings of the 2nd International Symposium on Aerial Robotics).

[53] S. Mintchev and D. Floreano, “A pocket sized foldable quadcopter for situational awareness and reconnaissance,” in SSRR 2016 - International Symposium on Safety, Security and Rescue Robotics, 2016, pp. 396–401.

[54] Mintchev, S., Daler, L., Saint-Raymond, L., & Floreano, D. (2015). *Foldable and Self-Deployable Pocket Sized Quadrotor*. In 2015 IEEE International Conference on Robotics and Automation (ICRA 2015) (No. EPFL-CONF-207879).

[55] QGround Control (2019, September 28) [Online]. Retrieved from http://qgroundcontrol.com/

[56] Ardupilot (2019, September 28) *Mission Planner* [Online]. Retrieved from http://qgroundcontrol.com/

[57] P. M. Kornatowski, M. Feroskhan, W. J. Stewart, and D. Floreano, Senior Member, IEEE, "Downside Up: Rethinking parcel position for aerial delivery". *Robotics and Automation Letters* in review (2019).

[58] P. M. Kornatowski, and D. Floreano. *Downside Up: Rethinking parcel position for aerial delivery*, patent pending, 2019.

[59] S. Mintchev and D. Floreano, "Adaptive morphology: A design principle for multimodal and multifunctional robots," *IEEE Robot. Autom. Mag.*, vol. 23, no. 3, pp. 42–54, 2016.

[60] N. Zhao, Y. Luo, H. Deng, and Y. Shen, "The deformable quad-rotor: Design, kinematics and dynamics charact., and flight performance validation," in IEEE International Conference on Intelligent Robots and Systems, 2017, vol. 2017–September, pp. 2391–2396.

[61] D. Falanga, K. Kleber, S. Mintchev, D. Floreano, and D. Scaramuzza, "The Foldable Drone: A Morphing Quadrotor That Can Squeeze and Fly," *IEEE Robot. Autom. Lett.*, vol. 4, no. 2, pp. 209–216, 2019.

[62] M. Bernard, K. Kondak, I. Maza, and A. Ollero, "Autonomous transportation and deployment with aerial robots for search and rescue missions," J. F. Robot., vol. 28, no. 6, pp. 914–931, 2011.

[63] Maza, K. Kondak, M. Bernard, and A. Ollero, "Multi-UAV cooperation and control for load transportation and deployment," J. Intell. Robot. Syst. Theory Appl., vol. 57, no. 1–4, pp. 417–449, 2010.

[64] K. Sreenath, N. Michael, and V. Kumar, "Trajectory generation and control of a quadrotor with a cable-suspended load - A differentially-flat hybrid system," in Proceedings - IEEE International Conference on Robotics and Automation, 2013, pp. 4888–4895.

[65] K. Sreenath, T. Lee, and V. Kumar, "Geometric control and differential flatness of a quadrotor UAV with a cable-suspended load," in Proceed-ings of the IEEE Conf. on Decision and Control, 2013, pp. 2269–2274.

[66] S. Tang, V. Wuest, and V. Kumar, "Aggressive Flight With Suspended Payloads Using Vision-Based Control," IEEE Robot. Autom. Letters., vol. 3, no. 2, pp. 1152–1159, 2018.

[67] P. M. Kornatowski, S. Mintchev, and D. Floreano, "An origami-inspired cargo drone," in IEEE International Conference on Intelligent Robots and Systems, 2017, vol. 2017–September, pp. 6855–6862.

[68] NASA CRgis, Helicopter Test Tower, Films section: Visualization of Vertical Flows Over Propellers [Online]. Retrieved from: https://crgis.ndc.nasa.gov/historic/1231A, 10 February 2019.

[69] E._L._Houghton, *Aerodyn. for Eng. Students*. 2016. Page 527-528.

[70] P. Pounds, R. Mahony, J. Gresham, P. Corke, and J. Roberts, "Towards Dynamically-Favourable Quad-Rotor Aerial Robots," *Robot.*, 2004. 21

[71] P. Pounds, R. Mahony, and P. Corke, "Modelling and control of a large quadrotor robot," *Control Eng. Pract.*, vol. 18, no. 7, pp. 691–699, 2010.

[72] Q. Quan, Introduction to multicopter design and control, 2017.24

[73] P. E. I. Pounds, D. R. Bersak, and A. M. Dollar, "Stability of small-scale UAV helicopters and quadrotors with added payload mass under PID control," *Auton. Robots*, 2012. 22

[74] RCbenchmark.com [Online]. Retrieved from https://www.rcbenchmark.com/pages/series-1580-thrust-stand-dynamometer, 24 March 2019.

[75] Y. H. Hsiao and P. Chirarattananon, "Ceiling Effects for Surface Locomotion of Small Rotorcraft," 2019, pp. 6214–6219.

[76] R.W. Prouty, Helicopter performance, Stability, and Control. Malabar, Florida, 2006.

[77] P. M. Kornatowski, M. Feroskhan, W. J. Stewart, and D. Floreano, Senior Member, IEEE, "Safe and efficient morphing delivery drone for in-hand landing" -to be submitted to Robotics and Automation Letters.

[78] P. M. Kornatowski, S. Mintchev, and D. Floreano, "An origami-inspired cargo drone," in IEEE International Conference on Intelligent Robots and Systems, 2017, vol. 2017–September, pp. 6855–6862.

[79] Patent "Foldable aircraft with protective cage for transportation and transportability" (US10252795, PCT/IB2017/052034).

[80] The Economic Times. "Switzerland begins postal delivery by drone," [Online]. Retrieved from http://economictimes.indiatimes.com/slideshows/nation-world/switzerland-begins-postal-delivery-by-drone/slideshow/47998181.cms, 2 September 2015.

[81] J. Salaan, Y. Okada, K. Hozumi, K. Ohno, and S. Tadokoro, "Improvement of UAV's flight performance by reducing the drag force of spherical shell," in IEEE International Conference on Intelligent Robots and Systems, vol. 2016–November, pp. 1708–171, 2016.

[82] S. S. Tolman, I. L. Delimont, L. L. Howell, and D. T. Fullwood, "Material selection for elastic energy absorption in origami-inspired compliant corrugations," Smart Mater. Struct., vol. 23, no. 9, p. 94010, 2014.

[83] M. Schenk and S. D. Guest, "Origami folding: A structural engineering approach," Origami 5 Fifth Int. Meet. Origami Sci. Math. Educ., pp. 1–16, 2011.

[84] E. A. Peraza-Hernandez, D. J. Hartl, R. J. Malak Jr, and D. C. Lagoudas, "Origami-inspired active structures: a synthesis and review," Smart Mater. Struct., vol. 23, no. 9, p. 94001, 2014.

[85] L. Dufour, K. Owen, S. Mintchev, and D. Floreano, "A drone with insect-inspired folding wings," in IEEE International Conference on Intelligent Robots and Systems, 2016, vol. 2016–November, pp. 1576–1581.

[86] R. J. Lang, Origami 4, vol. 10, 2009.

[87] Serjbumatay Blogspot. Retrieved from http://serjbumatay.blogspot.ch/2011/04/how-to-make-origami-paper-lantern.html, 2 August 2016.

[88] De Temmerman, I.A.N., Mollaert, M., Van Mele, I.A.T. and De Laet, I.A.L., 2007. "Design and analysis of a foldable mobile shelter system." International Journal of Space Structures, 22(3), pp.161-168.

[89] D.-Y. Lee, J.-S. Kim, S.-R. Kim, J.-S. Koh, and K. Cho, "The deformable wheel robot using magic-ball origami structure," Proc. ASME 2013 Int. Des. Eng. Tech. Conf. Comput. Inf. Eng. Conf. IDETC/CIE 2013, pp. 1–9, 2013.

[90] Le, P.H., Molina, J. and Hirai, S., "Application of Japanese Origami Ball for Floating Multirotor Aerial Robot," World Academy of Science, Engineering and Technology, International

Journal of Mechanical, Aerospace, Industrial, Mechatronic and Manufacturing Engineering, 8(10), pp.1740-1743, 2014.

[91] Roberts, J., "Enabling Collective Operation of Indoor Flying Robots,"PhD Thesis, Ecole Polytechnique Federale de Lausanne, 2011.

[92] S. Driessens and P. E. I. Pounds, "Towards a more efficient quadrotor configuration," in 2013 IEEE/RSJ International Conference on Intelligent Robots and Systems, 2013, pp. 1386–1392.

[93] W. C. Young and R. G. Budynas, Roark's Formulas for Stress and Strain, vol. 7, no. 7th Edition. 2002.

[94] Russell, C.R., Jung, J., Willink, G. and Glasner, B., "Wind Tunnel and Hover Performance Test Results for Multicopter UAS Vehicles," 2016.

[95] K. Cooper, "Bluff-body Blockage Corrections in Closed- and Open-Test-Section Wind Tunnels," *Agard Ag-336*, vol. 6, 1998.

[96] P. M. Kornatowski, A. Bhaskaran, G. M. Heitz, S. Mintchev, and D. Floreano, "Last-Centimetre Personal Drone Delivery: Field Deployment and User Interaction," *IEEE Robot. Autom. Letters*, 2018.

[97] Air, Amazon Prime. "Revising the airspace model for the safe integration of small unmanned aircraft systems." Amazon Prime Air (2015).

[98] Moormann, Dieter. "DHL parcelcopter research flight campaign 2014 for emergency delivery of medication." Proceedings of the ICAO RPAS Symposium. 2015.

[99] The Verge. Alphabet's Project Wing drones will deliver burritos to Australian homes [Online]. Retrieved from https://www.theverge.com/2017/10/16/16486208/alphbet-google-project-wing-drone-delivery-testing-australia, 05 January 2018.

[100] Swiss Post drone to fly laboratory samples for Ticino hospitals. [Online]. Retrieved from https://www.post.ch/en/about-us/company/media/press-releases/2017/swiss-post-drone-to-fly-laboratory-samples-for-ticino-hospitals, 25 December 2017.

[101] D. O'Driscoll, "UAVs in humanitarian relief and wider development contexts," K4D Helpdesk Report. Brighton, UK: Institute of Development Studies.

[102] S. Brar, R. Rabbat, and Runcie George, "Drones for Deliveries," Berkeley, Sutardja Cent. Entrep. Technol., 2015.

[103] B. Rao, A. G. Gopi, and R. Maione, "The societal impact of commercial drones," Technol. Soc., vol. 45, pp. 83–90, 2016.

[104] R. Luppicini and A. So, "A technoethical review of commercial drone use in the context of governance, ethics, and privacy," Technol. Soc., vol. 46, pp. 109–119, 2016.

[105] A. J. Lohn, "What's the Buzz? The City-Scale Impacts of Drone Delivery," The RAND Corporation, December 2017.

[106] Xu, Jia, "Design Perspectives on Delivery Drones," RAND Corporation [Online]. March 2018.

[107] C. C. Murray and A. G. Chu, "The flying sidekick traveling salesman problem: Optimization of drone-assisted parcel delivery," Transp. Res. Part C Emerg. Technol., vol. 54, pp. 86–109, 2015.

[108] A. V. Shelley, "A model of human harm from a falling unmanned aircraft: implications for UAS regulation," International Journal of Aviation, Aeronautics, and Aerospace 3.3 (2016): 1.

[109] X. Liu, J. Heo and L. Sha, "Modeling 3-tiered Web applications," 13th IEEE International Symposium on Modeling, Analysis, and Simulation of Computer and Telecommunication Systems, 2005, pp. 307-310.

[110] S. Atoev, K.-R. Kwon, S.-H. Lee, and K.-S. Moon, “Data analysis of the MAVLink communication protocol,” in 2017 International Conference on Information Science and Communications Technologies (ICISCT), 2017, pp. 1–3.

[111] “Regulations and general questions relating to drones,” Federal Office of Civil Aviation FOCA, [Online]. Retrieved from https://www.bazl.admin.ch/bazl/en/home/good-to-know/drones-and-aircraft-models/allgemeine-fragen-zu-drohnen.html, December 2017.

[112] “Drone flights above EPFL,” École Polytechnique Fédérale de Lausanne [Online]. Retrieved from https://securite.epfl.ch/drones-en, 10 December 2017.

[113] L. A. Streeter, D. Vitello, and S. A. Wonsiewicz, “How to tell people where to go: comparing navigational aids,” Int. J. Man. Mach. Stud., vol. 22, no. 5, pp. 549–562, 1985.

[114] Federal Office of Civil Aviation FOCA, [Online], Permits for the operation of drones, Retrieved from https://www.bazl.admin.ch/bazl/en/home/good-to-know/drones-and-aircraft-models/permits-drones.html, December 2017.

[115] J. K. Stolaroff, C. Samaras, E. R. O’Neill, A. Lubers, A. S. Mitchell, and D. Ceperley, “Energy use and life cycle greenhouse gas emissions of drones for commercial package delivery,” Nat. Commun., vol. 9, no. 1, 2018.

[116] L. Richardson, “Performing the sharing economy,” Geoforum, vol. 67, pp. 121–129, 2015.

[117] **P. M. Kornatowski,** M. Feroskhan, W. J. Stewart, and D. Floreano, Senior Member, IEEE, "A morphing cargo drone for safe flight in proximity of humans," will be submitted to *Robotics and Automation Letters* (2020).

[118] **P. M. Kornatowski**, and D. Floreano. "GearQuad, a morphing cargo drone for safe flight in proximity of humans," patent pending, 2019.

[119] Swiss Post drone to fly laboratory samples for Ticino hospitals. [Online]. Retrieved from https://www.post.ch/en/about-us/company/media/press-releases/2017/swiss-post-drone-to-fly-laboratory-samples-for-ticino-hospitals, 25 December 2017.

[120] Moormann, Dieter. "DHL parcelcopter research flight campaign 2014 for emergency delivery of medication." Proceedings of the ICAO RPAS Symposium. 2015.

[121] P. Abtahi, D. Y. Zhao, L. E. Jane, and J. A. Landay, “Drone Near Me: Exploring Touch-Based Human-Drone Interaction,” Proc. ACM Interact. Mob. Wearable Ubiquitous Technol., 2017.

[122] Mahony, V. Kumar, and P. Corke, “Multirotor aerial vehicles: Modeling, estimation, and control of quadrotor,” *IEEE Robot. Autom. Mag.*, vol. 19, no. 3, pp. 20–32, 2012.

[123] Maeda, H., Okauchi, M., & Shimada, Y. A, “Model for analysis of the impact between a tennis racket and a ball”.

[124] ZooMed. North American Box Turtle [Online]. Retrieved from https://zoomed.com/north-american-box-turtle/, 30 July 2019.

[125] Project Noah. Ornate Box Turtle [Online]. Retrieved from https://www.projectnoah.org/spottings/12040375, 30 July 2019.

[126] D. M. Bramble, “Emydid Shell Kinesis: Biomechanics and Evolution,” Copeia, 2006.

[127] B. Hohendorff, C. Weidermann, K. J. Burkhart, P. M. Rommens, K. J. Prommersberger, and M. A. Konerding, “Lengths, girths, and diameters of children’s fingers from 3 to 10 years of age,” Ann. Anat., 2010.

[128] S. Pheasent, and C. M. Haslegrave. “Bodyspace: Anthropometry, ergonomics and the design of work,” CRC Press, 2018.

[129] R. G. Snyder, "Physical characteristics of children as related to death and injury for consumer product safety design: May 1975, 241 pp; abstr in Government Reports Announcements (Report No PB-242 221/0GA)." Applied Ergonomics 7.2 (1976): 112.

[130] L. Vilhena and A. Ramalho, “Friction of human skin against different fabrics for medical use,” Lubricants, vol. 4, no. 1, 2016.G.

[131] T. Kulkarni and R. Uddanwadiker, “Modeling of Muscle Force at Varied Joint Angles of the Human Arm and Estimation of Gripping Force Using Surface EMG,”Molecural Cell. Biomech., 2016.

[132] J. Leishman, “Principles of helicopter aerodynamics with CD extra,” Cambridge university press, 2006.

[133] W. F. Lindsey, “Drag of cylinders of simple shapes,” NACA Annu. Rep. 619, 1938.

[134] M. Mallick, a Kumar, N. Tamboli, and A. Kulkarni, “Study on Drag Coefficient for the Flow Past a Cylinder,” Ripublication.Com, 2014.

[135] D. J. Leith and W. E. Leithead, “Survey of gain-scheduling analysis and design,” International Journal of Control, vol. 73, no. 11. pp. 1001–1025, 2000.

[136] RCbenchmark.com [Online]. Retrieved from https://www.rcbenchmark.com/pages/series-1580-thrust-stand-dynamometer, 24 March 2019.

[137] C.Y. Gooderson, D.J. Knowles, P.M. Gooderson, “The hand anthropometry of male and female military personnel,”. APRE Memorandum 82M510, Army Personnel Research Establishment, Farnborough, Hants. 1982.

[138] E. Romero, R. Callupe and D. Elias, "Implementation of a finger force detection platform with a graphical user interface," 2017 IEEE XXIV International Conference on Electronics, Electrical Engineering and Computing (INTERCON), Cusco, 2017, pp. 1-4.

[139] P. Bai, B. Guerreiro, R. Cunha, **P. Kornatowski**, D. Floreano, and C. Silvestre, “Wall-contact sliding control strategy for a 2D caged quadrotor,” in *International Conference on Control, Automation and Systems*, 2018.

Curriculum Vitae

Przemysław Mariusz Kornatowski

LIS-IMT-STI, MED1 1612,
1015 Lausanne, Switzerland

E-mail: p.kornatowski@dronisitcs.ch

Work experience:

May 2012 - February 2015	**École Polytechnique Fédérale de Lausanne**, Lausanne, Switzerland Mechanical engineer – Laboratory of Intelligent Systems at EPFL **Project GimBall**: http://lis.epfl.ch/gimball
January - February 2012:	Internship - Engineering Design Center, Warsaw, Poland (a part of **General Electric** and **Warsaw Institute of Aviation**), Warsaw, Poland
March - May 2011:	Internship - **Industrial Research Institute for Automation and Measurements,** Warsaw, Poland
December 2010 - February 2011:	Internship - **European University College Association (EUCA)**, Brussels, Belgium
July 2007:	Internship - **Industrial Research Institute for Automation and Measurements,** Warsaw, Poland

Education:

2015 - …	**École Polytechnique Fédérale de Lausanne**, Lausanne, Switzerland Ph.D. student in EDRS Robotics, Control and Intelligent Systems
2003 - 2011:	**Warsaw University of Technology**, Warsaw, Poland Faculty - Mechatronics, Department - Mechanical Engineering,

	Specialization – Micromechanics; Master's thesis: 'The project of the ball rolling in the direction selected by the operator'
2009 - 2010:	**European Academy of Diplomacy**, Specialization: international institutions, Warsaw, Poland

Awards and contests:

June 2015:	Winner of the Polish edition of the competition **"Innovators Under 35"** organized by **MIT Technology Review**
2018/2019:	**IMD Start-up Competition,** Lausanne
April 2018:	My drone *PackDrone* received three awards during **46th International Inventions Fair**, Geneva, Palexpo:
	Audience Award,
	Special Award of the President of the Patent Office of the Republic of Poland,
	Award of the President of the Association of Portuguese Inventors.
June 2015:	Winner of the Polish edition of the competition **"Innovators Under 35"** organized by **MIT Technology Review**
November 2015:	Featured in the second edition of the statement **New Europe 100** – lists of the greatest innovators in the areas of business, politics, culture, science and social activities

Training, summer schools, programs:

2019:	**CTI: Business concept**, Lausanne, Switzerland
2019:	**CTI: Business Creation ENGINEERING**, Lausanne, Switzerland
2019:	**Mass Challenge - start-up acceleration program**, Lausanne, Switzerland
2016:	**Venture Kick - start-up acceleration program**, Lausanne, Switzerland

2016:	**CTI: Business concept**, Lausanne, Switzerland
2016:	**MINTT: Management of Innovation and Technology Transfer,** Lausanne, Switzerland
June 2016:	**“SHERPA Summer School on Field Robotics”,** Passo Pordoi, Italy
April 2015:	**SMART-E & RoboSoft Joint School:"Applications and Frontiers of Soft Robotics",** The BioRobotics Institute, Scuola Superiore Sant’Anna, Livorno, Italy
2012:	**VentureLab - Venture challenge**, Lausanne, Switzerland

Teaching and supervision:

Winter 2019	**TransformTech Pretotyping** (assistant)
Spring 2019	**MTE Mentoring Program** (mentor)
	TransformTech Pretotyping (assistant)
	One semester student project (Ist assistant)
	One intern and two engineers* (supervision)
Winter 2018	**Two semester student projects** (Ist assistant)
	Two semester student projects (IInd assistant)
	One Master's student project (I assistant)
	Three interns and one engineer (supervision)
Summer 2018	**Three interns** (supervision)
Spring 2018	**TransformTech Pretotyping** (assistant)
	Aerial Robots course - B. cases (assistant)
	Four semester student projects (Ist assistant)
	Four semester student projects (IInd assistant)
	One Master's student project (Ist assistant)
	One Master's student project (IInd assistant)
	One intern and three engineers (supervision)
Winter 2017	**Two semester student projects** (I assistant)
	Four semester student projects (IInd assistant)

	Written exam observer (linear algebra)
	One intern and one engineer (supervision)
Spring 2017	**“Projet d'ingénierie simultanée 2017”**, Section: GÉNIE MÉCANIQUE (6 students)
	Evolutionary robotics: Robogen project (responsible for hardware, and grading)
	Oral exam observer (BioMEMS)
	Written exam observer (linear algebra)
	Journée des gymnasiens
	Supervision of two engineers
Winter 2016	**Two semester student projects** (I assistant)
	Two Master's student projects (I assistant)
	One intern (supervision)
Spring 2016	**STI Student Robot Competition** (assistant)
	Two semester student projects (I assistant)
	Two Master's student projects (I assistant)
	Two interns (supervision)
Winter 2015	**Two semester student projects** (I assistant)

Grants:

2019	**Enable grant**, 50k CHF
2018/2019	**NCCR Spin Fund Grant**, 100k CHF

Experience, student activities:

April 2010 – April 2011:	Regulations Committee of WUT*
January 2008 - January 2010:	President of International Cooperation Committee at WUT*
January 2008 - January 2010:	Senator of the WUT* (member of University Senate)
January 2008 - January 2010:	Member of the Student's Parliament at WUT*
February 2007 - January 2008:	The Chairman of The Council of Research Interest Groups of WUT*
June 2006 - May 2008:	The President of ’The Club Film & Photography Focus’
2006 - 2011:	Member of the Sailing Club **”**Wimpel”

*WUT - Warsaw University of Technology, Poland

Computer programs:	
Operation systems:	Windows; Unix/Linux, Android
Office programs:	Microsoft Office, Open Office,
Programming languages:	C/C++
Graphic programs:	Adobe Photoshop, Illustrator, Premiere Pro
Engineering programs:	Autodesk Inventor Professional, Unigraphics, AutoCAD, MATLAB/Simulink, ANSYS, ANSYS Workbench, MD ADAMS, EAGLE PCB, Eclipse
Engineering skills:	
Manufacturing devices:	Laser cutter, vacuum former, CNC mill and lathe, CNC Foam Cutter, Composites oven, soldering
Additive Manufacturing:	SLS, FDM, SLA, Polyjet
Carbon composite manufacturing:	Wet layup, pre-preg, resin infusion, vacuum bagging, bladder molding
Other:	The ability to pilot UAVs - Unmanned Aerial Vehicles
Languages:	
English:	Fluent
Russian:	Advanced
German, French:	Basic
Polish:	Native speaker

Publications:

P. M. Kornatowski, M. Feroskhan, W. J. Stewart, and D. Floreano, Senior Member, IEEE, “GearQuad, a morphing cargo drone for safe flight in proximity of humans,” *Robotics and Automation Letters* in review (2019).

P. M. Kornatowski, M. Feroskhan, W. J. Stewart, and D. Floreano, Senior Member, IEEE, “Downside Up: Rethinking parcel position for aerial delivery”. *Robotics and Automation Letters* in review (2019).

P. M. Kornatowski, A. Bhaskaran, G. Heitz, S. Mintchev, and D. Floreano, “Last-Centimetre Personal Drone Delivery: field deployment and user interaction,” *IEEE Robotics and Automation Letters*, pp. 1–1, 2018.

P. M. Kornatowski, S. Mintchev, and D. Floreano, “An origami-inspired cargo drone,” in IEEE International Conference on Intelligent Robots and Systems, 2017, vol. 2017–September, pp. 6855–6862.

P. Bai, B. Guerreiro, R. Cunha, **P. Kornatowski**, D. Floreano, and C. Silvestre, “Wall-contact sliding control strategy for a 2D caged quadrotor,” in *International Conference on Control, Automation and Systems*, 2018.

J. E. Auerbach, A. Concordel, **P. M. Kornatowski**, and D. Floreano, “Inquiry-Based Learning with RoboGen: An Open-Source Software and Hardware Platform for Robotics and Artificial Intelligence,” *IEEE Transactions on Learning Technologies*, 2018.

J. E. Auerbach, G. H. M. Heitz, **P. M. Kornatowski** and D. Floreano. "Rapid Evolution of Robot Gaits," GECCO '15, Madrid, Spain, July 11-15, 2015.

J. Auerbach, D. Aydin, A. Maesani, **P. Kornatowski** and T. Cieslewski et al. "RoboGen: Robot Generation through Artificial Evolution," Artificial Life 14: International Conference on the Synthesis and Simulation of Living Systems, New York, NY, USA, July 30-August 2, 2014.

A. Briod, **P. M. Kornatowski**, J.-C. Zufferey and D. Floreano. "A Collision Resilient Flying Robot, in Journal of Field Robotics, vol. 31, num. 4, p. 469-509, 2014.

A. Briod, **P. M. Kornatowski**, A. Klaptocz, A. Garnier and M. Pagnamenta et al. "Contact-based navigation for an autonomous flying robot," International Conference on Intelligent Robots and Systems (IROS), Tokyo, Japan, November 3-7, 2013.

Patents:

P. M. Kornatowski, and D. Floreano. “GearQuad, a morphing cargo drone for safe flight in proximity of humans,” - patent pending, 2019.

P. M. Kornatowski, and D. Floreano. "Downside Up: Rethinking parcel position for aerial delivery," - patent pending, 2019.

P. M. Kornatowski, S. Mintchev and D. Floreano. "Foldable aircraft with protective cage for transportation and transportability," PCT/IB2017/052034.

A. Briod, **P. M. Kornatowski**, A. Klaptocz, J.-C. Zufferey and D. Floreano. "A vertical take-off and landing aerial vehicle," EP13171364.6, 2013.

Interests and hobbies:

Playing the piano and guitar, swimming, photography, rock climbing, skiing, traveling, sailing, darts, project management